1991

Calculation of the metal temperature distribution within a two- pass counter-crossflow tubular air preheater

Ali Yilmaz
Lehigh University

AUTHOR:
Yilmaz, Ali

TITLE:Calculation of the Matal Temperature Distribution Within a Two-Pass Counter-Crossflow Tubular Air Preheater

DATE:January 1992

CALCULATION OF THE METAL TEMPERATURE DISTRIBUTION WITHIN A TWO-PASS COUNTER-CROSSFLOW TUBULAR AIR PREHEATER

by

Ali Yilmaz

A Thesis

Presented to the Graduate Committee

of Lehigh University

in Candidacy for the Degree of

Master of Science

in

Mechanical Engineering

Lehigh University

December, 1991

CERTIFICATE OF APPROVAL

This thesis is accepted and approved in partial fulfillment of the requirements for the degree of Master of Science.

Date: November 25, 1991

Professor in Charge: ______________________

(Edward K. Levy)

Chairman of Department: ______________________

(Robert P. Wei)

ACKNOWLEDGEMENTS

I am very grateful to my parents and fiancee for their love, support and understanding during my study at Lehigh. I would also like to thank my advisor, Dr. Edward K. Levy, for his guidance and support throughout my work.

The work in this thesis was funded by Allegheny Power Company as part of a project. I would like to express my appreciation to the sponsors for their support.

I am also grateful to Dr. Nenad Sarunac for his help and encouragement during my research.

Finally, I would like to thank my friends Ahmet Pinarbasi, Murat Ozturk, Patrick Coston, Ridvan A. Sahan, and Hasan Gunes for their support and help.

TABLE OF CONTENTS

LIST OF TABLES

LIST OF FIGURES

NOMENCLATURE

a	The relative transverse pitch, S_T/D
A	Exchanger total heat transfer area on one side, m^2
A_w	Total solid area for longitudinal conduction along a tube, $A_w=\pi(r_a{}^2-r_g{}^2)$, m^2
b	The relative longitudinal pitch, S_L/D
b_1, b_2, b_3	Coefficients in Equation 2.27
c	The relative diagonal pitch, S_D/D
c_1, c_2, c_3	Coefficients in Equation 2.26
c_p	Specific heat at constant pressure, J/kg K
C	Constant in Equation 3.6; Constant in Equation 3.14
C_a, C_g	Capacity rates of air and gas streams, W/K
C_{min}, C_{max}	Minumum and maximum capacity rates, W/K
C_R	Capacity rate ratio, $C_R=C_{min}/C_{max}$
D	Diameter of a circular tube, m
D_h	Hydraulic diameter of any internal passage, m
f	Friction factor, $f=\tau_w/(\frac{1}{8}\rho u_m{}^2)$
f_s	Friction factor for smooth tube surfaces
h	Convective heat transfer coefficient, W/m^2 K
k	Thermal conductivity of working fluids, W/m K
k_w	Thermal conductivity of the tube metal, W/m K
L	Tube length, m

m_a, m_g — Mass flow rates of air and gas, respectively, kg/s

m — Constant in Equation 3.14

$m^e{}_{ai1}$ — External mass flow rate of air at the inlet of *Pass I*, kg/s

$m^i{}_{a1}$ — Internal mass flow rate of air in *Pass I*, kg/s

m_{apass} — Passage mass flow rate of air, kg/s

$m^i{}_{a2}$ — Internal mass flow rate of air in *Pass II*, kg/s

m_{ao2} — Mass flow rate of air at the outlet of *Pass II*, kg/s

$m^e{}_{gi2}$ — External mass flow rate of gas at the inlet of *Pass II*, kg/s

$m^i{}_{g2}$ — Internal mass flow rate of gas in *Pass II*, kg/s

m_{gpass} — Passage mass flow rate of gas, kg/s

$m^i{}_{g1}$ — Internal mass flow rate of gas in *Pass I*, kg/s

$m^e{}_{go1}$ — External mass flow rate of gas at the outlet of *Pass I*, kg/s

$m_{L,cei}$ — Air leakage mass flow rate through gas-in section in the cold end of either pass, kg/s

$m_{L,ceo}$ — Air leakage mass flow rate through gas-out section in the cold end of either pass, kg/s

$m_{L,hei}$ — Air leakage mass flow rate through gas-in section in the hot end of either pass, kg/s

$m_{L,heo}$ — Air leakage mass flow rate through gas-out section in the hot end of either pass, kg/s

$m_{L,CE}$ — Cold end air leakage mass flow rate on either pass, kg/s

$m_{L,HE}$ — Hot end air leakage mass flow rate on either pass, kg/s

m_{L1}, m_{L2} — Air leakage mass flow rates of *Pass I* and *Pass II*, respectively, kg/s

m_L — Total air leakage flow rate of the air preheater, kg/s

M	Index
N	Index
n	Constant in Equation 3.6
NTU	Number of heat transfer units, Eqn. 2.6
Nu	Nusselt number
Nu_{fd}	Nusselt number for fully developed flow and heat transfer
Nu_m	Mean Nusselt number
Nu_s	Nusselt number for smooth surfaces
Nu_x	Local Nusselt number
$Nu_{m\ 1\text{-}2}$	Average Nusselt number between any arbitrary two points
Pr	Prandtl number
Pr_s	Prandtl number based on the tube wall temperature
q_a, q_g	Heat transfer rates on air side and gas side, respectively, W
q''_w	Heat flux, $q''_w=\frac{dq}{dA}$, W/m^2
Q	Total heat transfer rate of the air preheater, W
r_a, r_g	Outside and Inside radius of a circular tube, m
r_m	Average tube radius as $r_m=\frac{r_a+r_g}{2}$, m
r_1, r_2, r_3	The roots of the Equation 2.29
Re	Reynolds number
Re_{crit}	Critical Reynolds number
Re_D	Reynolds number, $Re_D=\frac{\rho VD}{\mu}$
Re_{Dmax}	Reynolds number based on the maximum flow velocity in a tube bank, $Re_{Dmax}=\frac{\rho V_{max} D}{\mu}$
R_{CE}	Leakage ratio parameter, $R_{CE}=\frac{m_{L,cco}}{m_{L,cci}}$

R_{HE}	Leakage ratio parameter, $R_{HE}=\frac{m_{L,heo}}{m_{L,hei}}$
R_δ	Leakage ratio parameter, $R_\delta=\frac{\delta_{L,CE}}{\delta_{L,HE}}$.
S_D, S_L, S_T	Diagonal, longitudinal, and transverse pitch of a tube bank, m
T	Temperature, K
T_{ai1}	Air inlet temperature of *Pass I*, K
T_{apass}	Passage air temperature, K
T_{ao2}	Air outlet temperature of *Pass II*, K
$T^e{}_{gi2}$	External gas temperature at the inlet of *Pass II*, K
$T^i{}_{gi2}$	Internal gas temperature at the inlet of *Pass II*, K
T_{gpass}	Passage gas temperature, K
$T^i{}_{gi1}$	Internal gas temperature at the inlet of *Pass I*, K
$T^i{}_{go1}$	Internal gas temperature at the outlet of *Pass I*, K
$T^e{}_{go1}$	External gas temperature at the outlet of *Pass I*, K
U	Overall heat transfer coefficient, W/m^2 K
u_m	Mean flow velocity in a circular tube, m/s
V_{max}	Maximum flow velocity in a tube bank, m/s
x, y, z	Cartesian coordinates, m
X	The criteria defined in Eqn. 4.12
x_{fd}	Entry length of a simultaneously developing flow in a tube, m
x^*	Dimensionless distance in a tube, $x^*=\frac{RePr}{(x/D_h)}$
z	Nondimensional coordinate, $z=Z/L$
Z	Coordinate of a tube in the gas flow direction, m

α	Number of heat transfer units on gas side, $\alpha = \frac{\xi L}{C_g}$;
	Thermal diffusivity, m^2/s
β	Number of heat transfer units on air side, $\beta = \frac{\zeta L}{C_g}$
δ_L	Total air leakage coefficient of the air preheater
δ_{L1}, δ_{L2}	Leakage coefficients of *Pass I* and *Pass II*, respectively
$\delta_{L,CE}$	Cold end leakage coefficient
$\delta_{L,HE}$	Hot end leakage coefficient
ϵ	Exchanger effectiveness
ϵ_a, ϵ_g	Heat transfer effectiveness of the tubular air preheater based on the rate of heat transfer to air and from gas, respectively
θ_a, θ_g, θ_m	Dimensionless temperature of air, gas, and tube metal, respectively
λ_g	Longitudinal conduction parameter defined by Eqn. 2.17
μ	Viscosity, kg/s m
ν	Kinematic viscosity, m^2/s
ρ	Mass density, kg/m^3
τ_w	Shear stress, N/m^2

ABSTRACT

A large number of tubular air preheaters in coal fired power plants have been experiencing difficulty with plugging and corrosion. When a flue gas containing sulfur trioxide and water vapor contacts a cold heat transfer surface in the air preheater, sulfuric acid will precipitate and fly ash will impact the liquid forming a sticky, adherent deposit. If the fly ash is not sufficiently alkaline to neutralize the precipitated sulfuric acid, in the long term the tubes will suffer from corrosion. In order to protect the tubes from acid deposition and corrosion, we need to keep the metal temperature field of the air preheater above the acid dewpoint temperature. This requires that the metal temperature field of the air preheater be known as a function of operating parameters of the air preheater. Since measurements of metal temperatures are not practical except for research purposes, a numerical simulation of the heat transfer problem is the only alternative.

A computer program named TPHMT (Tubular Air Preheater Metal Temperature) has been developed for a two-pass counter-crossflow tubular air preheater for computing the metal temperature field within the air preheater as a function of design and operating parameters. The mathematical model, based on the ϵ-NTU theory, uses an iterative procedure to obtain the solutions.

1. INTRODUCTION

Recovering waste heat from a high temperature gas stream by using an air preheater to preheat incoming combustion air is an effective way of reducing fuel consumption. In industries such as electric power generators, steel and glass manufacturing, air preheaters have been used for years.

Air preheaters may be classified according to the principle of their operation as (a) recuperative and (b) regenerative. In a recuperative design, the heat is transfered directly from the hot gases or steam, on one side of the surface, to air on the other side; whereas in a regenerative air preheater, the heat is transfered inderectly from the hot gases to the air through some intermediate storage medium. Air preheaters operating on the recuperative principle are generally tubular type, although some are plate type.

Experiences indicate that corrosion may occur in air preheaters operating with flue gas when the metal temperature of the tube falls below the sulfuric acid dewpoint temperature. This temperature is the highest temperature at which condensation of sulfuric acid can exist on a cooled surface in equilibrium with a flue gas containing SO_3 and H_2O. Acidic condensate deposited in sections of the flue gas passages operating at low temperature could cause rapid corrosion of the tube materials and blockage of the gas passages with deposits of fly ash. These problems can be avoided if the cold end of the air preheater is allowed to operate a few degrees hotter. This is commonly done by several means: (1) heating the air entering the preheater, (2) recirculating a portion of the hot air from the air preheater outlet back to the forced draft fan inlet.

Information on the metal temperature field must be known as a function of operating parameters of the air preheater in order to avoid acid deposition and corrosion problems. This information on metal temperatures can be obtained by either taking direct measurements or by numerically simulating the heat transfer processes within the air preheater. Measurements of metal temperatures are difficult to make in a large heat exchanger; therefore, except for research purposes it is not practical to rely on such measurements as the source of information. The alternative way is to have a computer program which performs a numerical simulation of the heat transfer processes within the air preheater.

In this thesis, a tubular air preheater arranged in a two-pass counter-crossflow configuration was modelled and a computer program was written. The numerical simulation of the heat transfer problem was based on the ϵ-NTU method [1].

The air preheater is subdivided into two separate passes, each of which can be viewed as a single pass crossflow heat exchanger (see Figure 6.2). The gas flow between these passes was assumed to behave as a one-dimensional adiabatic flow. That is, the temperature of the gas is assumed to remain unchanged throughout the passage which connects both passes.

Moreover, to account for temperature and velocity nonuniformities of gas and air at the inlet of the air preheater, each pass is divided into MxN separate smaller elements (grids). Since inlet gas temperature and velocity variations for one pass and inlet air temperature and velocity variations for the other pass were considered as boundary conditions; an iterative prediction-correction method was applied to find the metal temperatures. Outlet gas and air temperatures and tube metal temperature of each grid are directly computed by using the ϵ-NTU relations. The temperature fields of air, gas and tube metal are calculated using a step by step marching method starting from an appropriate smaller element in the first pass.

The assumption of negligible longitudinal heat conduction along the lengths of the tubes within the air preheater made it possible to use ϵ-NTU method. This was justified by a simple analysis which showed that longitudinal conduction along a tube in crossflow is not important for the conditions of interest.

2. HEAT TRANSFER IN DIRECT-TYPE HEAT EXCHANGERS

2.1 Dimensional and Nondimensional Variables

Heat exchanger design theory deals with various thermo-fluid relations concerning the following two parameters :

- Heat transfer and fluid friction parameters.
- Principal design/operating parameters of the exchanger; such as flow rates, flow distributions, thermo-physical properties of the fluids, specified fluid temperature levels and exchanger effectiveness.

The parameters related to heat transfer characteristics are as follows:

$U =$ *overall heat transfer coefficient, W/K* m^2

$A =$ *heat transfer area on which U is based,* m^2

$C = (m\ c_p) =$ *capacity rate, W/K*

$m =$ *mass flow rate, kg/s*

$c_p =$ *specific heat at constant pressure, J/kg K*

$$\begin{bmatrix} T_{g,in} \\ T_{g,out} \end{bmatrix} = \text{gas (hot-fluid) terminal temperatures, K}$$

$$\begin{bmatrix} T_{a,in} \\ T_{a,out} \end{bmatrix} = \text{air (cold-fluid) terminal temperatures, K}$$

where subscripts a, g show air and gas respectively.

The importance of the parameters listed above is easy to compute, with the exception of U. This term comes from an overall heat transfer rate equation, which combines the convective and conductive mechanisms responsible for the heat transfer from the hot to the cold fluid into a single equation similar to Ohm's law for the steady-state flow of electrical current.

$$\frac{dq}{dA} = U\,(T_g - T_a) \tag{2.1}$$

The term $\frac{dq}{dA}$ stands for heat flux per unit heat transfer area at a section where the temperature difference is $(T_g - T_a)$. The overall heat transfer coefficient of a direct-type tubular air preheater, having three components (air-side convection, gas-side convection, and wall conduction) may be expressed in the following forms;

$$U_g = \frac{1}{\frac{1}{h_g} + \frac{r_g}{k_w}\,ln(r_a/r_g) + \frac{r_g}{r_a}\frac{1}{h_a}} \tag{2.2}$$

$$U_a = \frac{1}{\frac{r_a}{r_g}\frac{1}{h_g} + \frac{r_a}{k_w}\,ln(r_a/r_g) + \frac{1}{h_a}} \tag{2.3}$$

where r_g and r_a are the inside and outside radii of the tubes, respectively, and k_w is the thermal conductivity of the tube wall (W/m K).

Equations (2.2) and (2.3) define U in terms of the gas side heat transfer area A_g and air side heat transfer area A_a, respectively. It is clear that equation (2.4) relates U_a and U_g.

$$U_a A_a = U_g A_g \tag{2.4}$$

The convective heat transfer coefficients h_a and h_g are complex functions of the surface geometry, fluid properties, and flow conditions. They are approximately calculated by experimental correlations.

The ϵ-NTU theory groups heat transfer variables of a heat exchanger into nondimensional parameters. These nondimensional parameters are named and defined as follows

- *heat exchanger effectiveness*

$$\epsilon = \frac{q}{q_{max}} = \frac{C_g\,(T_{g,in} - T_{g,out})}{C_{min}(T_{g,in} - T_{a,in})} = \frac{C_a\,(T_{a,out} - T_{a,in})}{C_{min}(T_{g,in} - T_{a,in})} \tag{2.5}$$

where C_{min} is the smaller of the C_g and C_a magnitudes. The quantity q_{max} is the maximum possible heat transfer rate for the exchanger. This heat transfer rate could, in principle, be achieved in a counterflow heat exchanger of infinite length. In such an exchanger, one of the fluids would experience the maximum possible temperature difference ($T_{g,in} - T_{a,in}$).

- *number of heat transfer units*

$$NTU = \frac{(A\ U)_g}{C_{min}} = \frac{(A\ U)_a}{C_{min}} \tag{2.6}$$

- *capacity rate ratio*

$$C_R = \frac{C_{min}}{C_{max}} \tag{2.7}$$

where C_{min} and C_{max} are, respectively, the smaller and the larger of two magnitudes C_g and C_a.

In general, it is possible to show that the heat exchanger effectiveness is explicitly dependent on:

1. the thermal size of the heat exchanger
2. the fluid flow heat capacity rate ratio
3. the flow arrangement in the heat exchanger

This can be shown with the following equation:

$$\epsilon = \phi \; (NTU, \; C_R, \; flow \; arrangement) \tag{2.8}$$

Effectiveness expressions in this nondimensionalized form have been developed for a variety of heat exchangers [1]. For instance, when a heat exchanger is arranged as a cross-counterflow (single pass), and one fluid is mixed and the other unmixed, the ϵ-NTU relations are given as follows;

1. C_{max} *(mixed)*, C_{min} *(unmixed)*;

$$\epsilon \;=\; (1/C_R) \left\{ 1 - exp \; [1 - exp(- \; NTU)] \right\} \tag{2.9}$$

2. C_{min} *(mixed)*, C_{max} *(unmixed)*;

$$\epsilon \;=\; 1 - exp\left(- \; [\frac{1}{C_R}] \left\{ 1 - exp(- \; C_R \; NTU) \right\} \right) \tag{2.10}$$

Examination of Figure 2.1 demonstrates the asymptotic character of the ϵ versus NTU relation for a given capacity rate ratio in a crossflow heat exchanger where one fluid is mixed, the other unmixed [1].

On the other hand, there is no closed form effectiveness expression for a crossflow exchanger, having both of the fluids unmixed. In this case the effectiveness relation, in terms of nondimensional parameters C_R and NTU, is available in the series form proposed by Mason [2]. Mason's series solution was further developed and suitably arranged for computer programing by Chung [3].

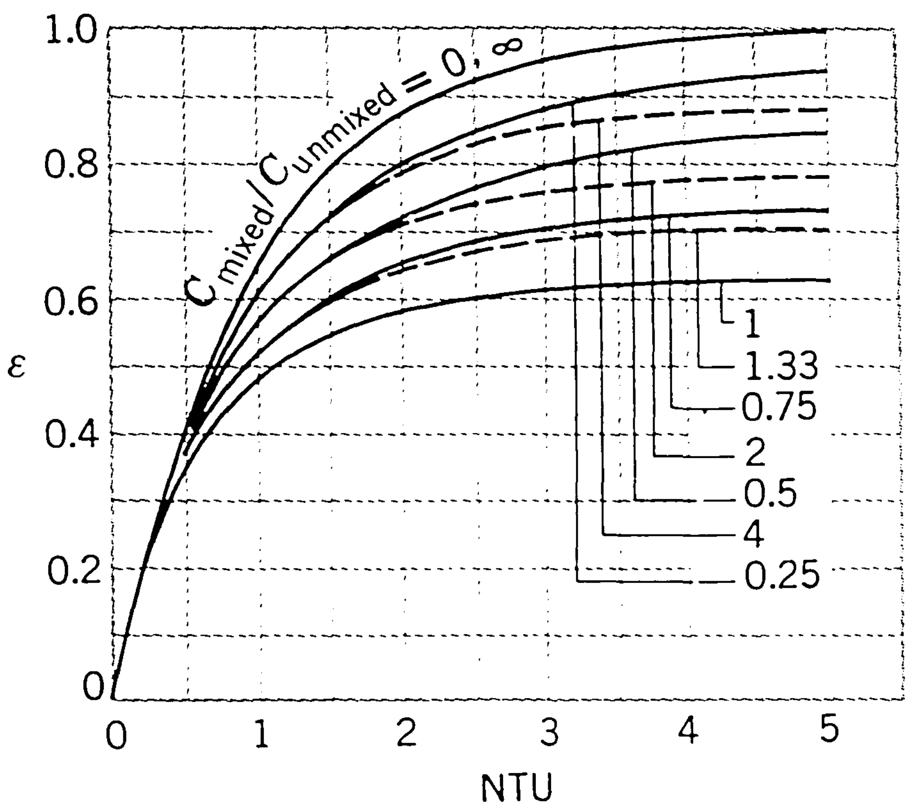

Figure 2.1 Effectiveness of a single-pass crossflow heat exchanger with one of the fluids mixed and the other unmixed [20].

2.2 Assumptions Applied to ϵ-NTU Theory

The ϵ-NTU theory groups heat transfer variables of a heat exchanger into nondimensional parameters. These nondimensional parameters are easily readable and allow a compact graphical presentation. However, The ϵ-NTU theory has certain limitations because of the following idealizations:

- *steady state*
- *constant and uniform velocity profiles at inlet sections*
- *no longitudinal heat conduction in the flow direction;*

  in the solid wall

  in the fluid
- *constant overall heat transfer coefficient*
- *constant fluid specific heats*
- *no heat loss to the surroundings*
- *constant and uniform temperature profiles at inlet sections*
- *no heat generation, no phase change occur in the fluid streams flowing through the exchanger*
- *uniform distribution of heat transfer area throughout exchanger core*

2.3 Longitudinal Heat Conduction Effect on Air Preheater Performance

The ϵ-NTU theory is based on the idealization that there is no longitudinal conduction (in the flow direction), either in the solid wall or in the fluid. Fluids generally have a low thermal conductivity (liquid metals excepted), but the wall conductivity may be quite high for some cases.

Many investigations about this effect have been performed for storage type period-flow heat exchangers [1, 2, 4, 5], and for direct-transfer type heat exchangers such as counterflow heat exchangers [6, 7, 8] and crossflow heat exchangers having plate-fin surfaces [9]. Some of these investigations showed that the deterioration of the exchanger effectiveness due to axial conduction is the greatest when $C_R=1$ [1, 4, 7, 9].

A complete study of this effect on direct-transfer type tubular crossflow heat exchangers does not seem to be available in the literature. However, it is stated that heat exchanger performance deterioration, because of longitudinal conduction, is less significant for tubular heat exchangers than for plate-fin heat exchangers [9].

A simple analysis was made in order to determine the amount of deterioration occuring in the total heat transfer rate. In this study, only one tube was considered and it was assumed that the air temperature was constant. Gas flows through the tube while air flows around the outside of the tube, perpendicular to the gas flow (see Figure 2.2). The design and operating parameters of the air preheater under consideration were the same as those of a real tubular air preheater.

On the basis of these idealizations and design and operating conditions of the air preheater, a set of differential equations describing the heat transfer process for a typical element of the tube (see Figure 2.2) can be expressed as follows:

- *heat exchange between gas and tube wall*

$$C_g \frac{dT_g}{dZ} + \frac{2\pi r_g}{\frac{1}{h_g} + \frac{r_g}{k_w} ln\left(\frac{r_m}{r_g}\right)} (T_g - T_m) = 0 \qquad (2.11)$$

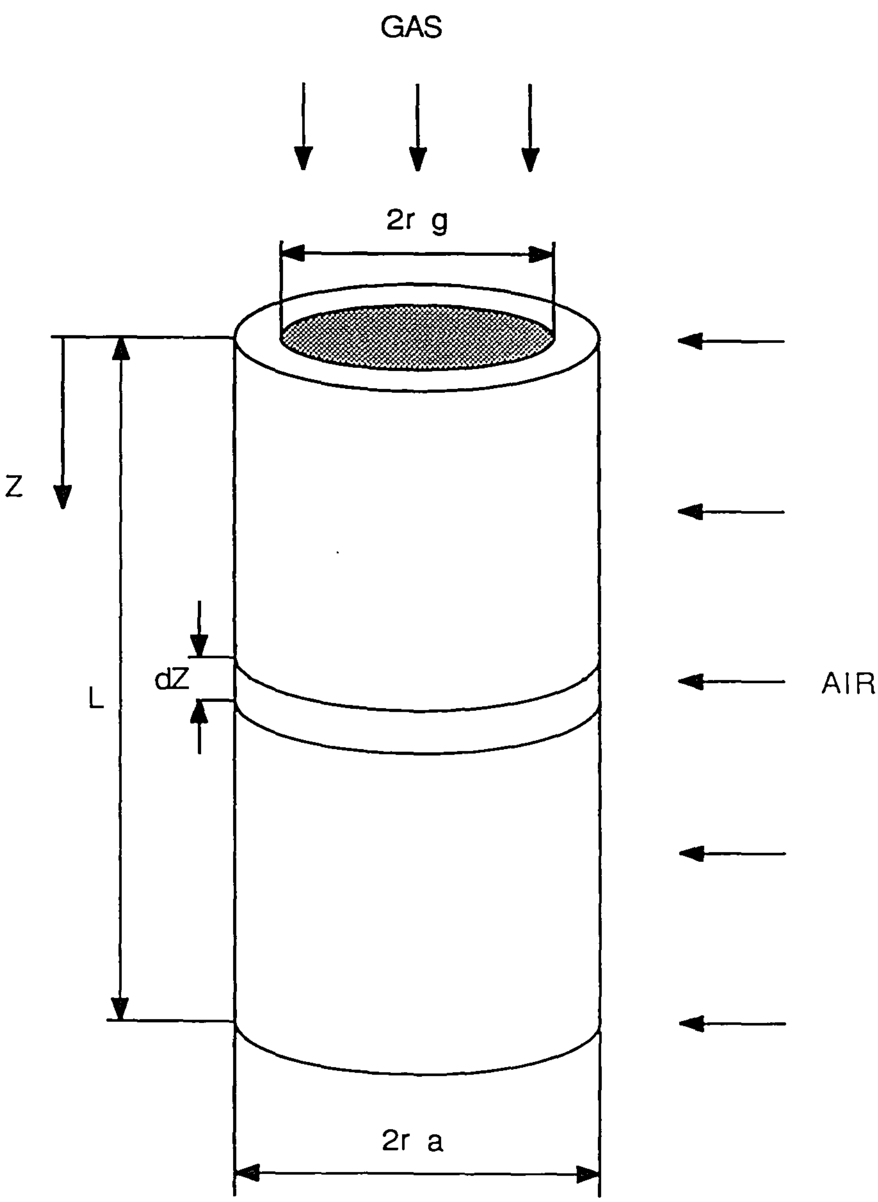

Figure 2.2 The dimensions of one tube of a crossflow tubular heat exchanger. The longitudinal conduction effect was studied using this particular tube (Chapter 2.3).

where $r_m = \frac{r_a + r_g}{2}$

- *energy balance at the wall of the typical element*

$$k_w A_w \frac{d^2 T_m}{dZ^2} + \frac{2\pi r_g}{\frac{1}{h_g} + \frac{r_g}{k_w} ln\left(\frac{r_m}{r_g}\right)}(T_g - T_m) - \frac{2\pi r_a}{\frac{1}{h_a} + \frac{r_a}{k_w} ln\left(\frac{r_a}{r_m}\right)}(T_m - T_a) = 0 \tag{2.12}$$

The boundary conditions are

$$T_a = constant \tag{2.13}$$

$$T_g(0) = T_{g,in} \tag{2.14}$$

$$\frac{dT_m}{dZ}(0) = 0 \tag{2.15}$$

The boundary conditions specify inlet gas temperature and mandate no heat conduction at the inlet of the tube (Z=0).

The system of ordinary differential equations consisting of the equations (2.11) to (2.14) can be written in nondimensional form by introducing the following dimensionless parameters:

- *dimensionless axial coordinate (in the gas flow direction)*

$$z = \frac{Z}{L} \tag{2.16}$$

- *conduction parameter*

$$\lambda_g = \frac{k_w A_w}{L C_g} \tag{2.17}$$

- *dimensionless temperatures*; θ_m, θ_g, and θ_a

$$\theta = \frac{T - T_a}{T_{g,in} - T_a} \tag{2.18}$$

- *number of heat transfer units on gas side*

$$\alpha = \frac{2\pi r_g L / C_g}{\frac{1}{h_g} + \frac{r_g}{k_w} ln\left(\frac{r_m}{r_g}\right)} \tag{2.19}$$

- *number of heat transfer units on air side*

$$\beta = \frac{2\pi r_a L / C_g}{\frac{1}{h_a} + \frac{r_a}{k_w} ln\left(\frac{r_a}{r_m}\right)} \tag{2.19}$$

Governing differential equations (2.11) and (2.12) become

$$\frac{d\theta_g}{dz} + \alpha(\theta_g - \theta_m) = 0 \tag{2.21}$$

$$\lambda_g \frac{d^2\theta_m}{dz^2} + \alpha\theta_g + (\alpha + \beta)\theta_m = 0 \tag{2.22}$$

with the boundary conditions

$$\theta_g(0) = 1 \tag{2.23}$$

$$\frac{d\theta_m}{dz}(0) = 0 \tag{2.24}$$

$$\theta_a = 0 \tag{2.25}$$

The quantity λ_g is the conduction parameter which gives us valuable information about longitudinal conduction effect on total heat transfer rate. When $\lambda_g=0$, we have no longitudinal conduction in the problem. The parameters α and β are the number of heat transfer units on gas side and air side, respectively. The θ's are the nondimensional temperatures ($\theta_a=0$).

The general solutions to eqns. (2.11) and (2.12) are

$$\theta_g=c_1e^{r_1z}+c_2e^{r_2z}+c_3e^{r_3z} \tag{2.26}$$

$$\theta_m=b_1e^{r_1z}+b_2e^{r_2z}+b_3e^{r_3z} \tag{2.27}$$

where the r's represent the roots of the characteristic equation;

$$r^3+\alpha r^2-\frac{(\alpha+\beta)}{\lambda_g}r-\frac{\alpha\beta}{\lambda_g}=0 \tag{2.28}$$

The roots of the above equation were numerically computed by Newton's method and they are in the following ranges;

$$r_1<0, \quad r_2\gg 0, \quad \text{and} \quad r_3\ll 0 \tag{2.29}$$

Since the solution is exponential, the root r_2 causes the solution to go to infinity. Therefore, c_2 and b_2 must have zero values because the temperature profiles don't go infinity in an actual heat exchangers.

The rest of the constants c_1, c_3, b_1, and b_3 may be found from the boundary conditions, eqns. (2.23) and (2.24);

$$c_1 = \frac{r_3(r_3+\alpha)}{r_3(r_3+\alpha) - r_1(r_1+\alpha)} \tag{2.30}$$

$$c_3 = \frac{r_1(r_1+\alpha)}{r_3(r_3+\alpha) - r_1(r_1+\alpha)} \tag{2.31}$$

$$b_1 = \frac{c_1}{\alpha}(r_1+\alpha) \tag{2.32}$$

$$b_3 = \frac{c_3}{\alpha}(r_3+\alpha) \tag{2.33}$$

When there is no longitudinal conduction ($\lambda_g = 0$), the solution of the governing equations is greatly simplified. It is

$$\theta_g = e^{-\alpha\left\{1 - \frac{1}{\alpha+\beta}\right\} z} \tag{2.34}$$

$$\theta_m = \frac{\alpha}{[\alpha+\beta]} e^{-\alpha\left\{1 - \frac{1}{\alpha+\beta}\right\} z} \tag{2.35}$$

The results of this study are presented in Figure 2.3. When comparing nondimensional gas temperatures, one with longitudinal conduction and the other without, we find that they are identical up to 4 decimal places. The same goes for tube wall nondimensional temperatures. Moreover, the difference between the total heat transfer rate of each case is less than 0.0005%. It is quite obvious that longitudinal heat conduction has a negligible effect on heat transfer under normal design and operation conditions.

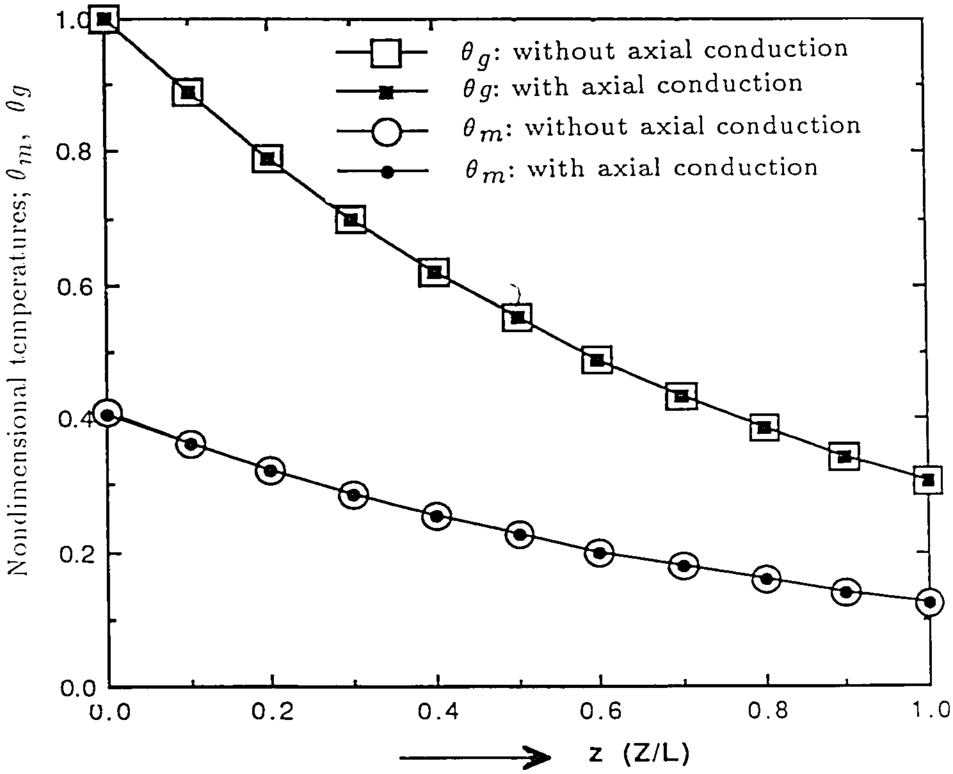

Figure 2.3 Nondimensional temperature profiles along the one tube of the crossflow exchanger; the two with longitudinal heat conduction (λ_g=0.00031), Eqns 2.26 and 2.27, the other two without (λ_g=0.0), Eqns 2.34 and 2.35.

3. CONVECTION CORRELATIONS

3.1 Introduction

The emphasis in this section is placed on forced convection correlations for flows inside circular tubes and over tube bundles and their applicable ranges. The correlations presented here are limited to steady, incompressible flow of constant-property Newtonian fluids. Any effects of natural convection, phase change, mass transfer, chemical reactions, thermal energy sources, viscous dissipation (i.e., internal friction), flow work (i.e., work done by pressure forces), and fluid axial conduction are omitted. Moreover, the tube walls are considered to be smooth, rigid, and stationary.

3.2 Flow Inside Circular Tubes

Laminar, transition, and turbulent flows and heat transfer characteristics of circular tubes have been studied in great detail, as this geometry finds widespread use in practical applications. Different investigators performed extensive experimental and theoretical studies with various fluids. As a result, they formulated relations for the *Nusselt number* vs. the *Reynolds* and *Prandtl numbers* for a wide range of these nondimensional groups.

There are four types of flow in circular tubes, namely, fully developed, hydrodynamically developing, thermally developing and simultaneously developing. Prandtl number is the key parameter in this classification since it is the ratio of the momentum diffusivity ν to the thermal diffusivity α.

In the simultaneously developing flow case, the viscous and thermal effects diffuse simultaneously from the tube wall, commencing at the tube entrance. This happens when Prandtl number is near unity, which includes gases such as flue gas and air.

Constant heat flux is often considered as a thermal boundary condition imposed on a tube wall for gas-to-gas heat exchanger applications. This is because the average heat flux of a row of a tube bank increases until approximately the fifth row, after which there is little change in the turbulence and hence in the average heat flux.

3.2.1 Laminar Flow

Numerous results are available for forced convection laminar flow of a circular tube in the literature. These results have been compiled in a monograph by Shah and London [10] and in an updated review by Shah and Bhatti [11].

For simultaneously developing laminar flow in a circular tube with constant heat flux boundary condition, Heaton, Reynolds, and Kays [12] obtained a solution by an integral method. Their result showed excellent agreement with experimental measurements made for *Prandtl number*=0.7. Their tabulated Nusselt numbers are used for the present analysis (Table 3.1). The *Nusselt number* for fully developed laminar flow in a circular tube is constant (Nu=4.36).

Experimental studies by Kays [14] showed that as long as the values of (x/D) range from 48 to 80 there is no measurable effect on the *Nusselt numbers* when comparing different entry types (*Pr=0.7*) for the laminar flow of a circular tube. However, the behaviour of very short tubes might be different.

Table 3.1 Results of the heat transfer analysis for simultaneously developing laminar flow inside a circular tube (Pr=0.7) [13]

$x^*\left\{Re.Pr/(x/D)\right\}$	Nu_x
0.00010	51.90
0.0010	17.84
0.0025	12.08
0.0050	9.12
0.010	7.14
0.025	5.49
0.050	4.72
0.10	4.41
0.25	4.36

3.2.2 Turbulent Flow

Turbulent circular tube flows have immense technological importance, as they occur frequently under normal operating conditions for a variety of heating and cooling devices.

The observations show that a laminar flow pattern transforms to a chaotic turbulent flow pattern when the *Reynolds number* exceeds a certain critical value called *the critical Reynolds number* Re_{crit}. In the case of a fully developed flow in a circular tube, the lower limit of Re_{crit} is accepted to be 2300, whereas the highest value of the upper limit attained by Pfenninger [11] is 1.001 x 10^5. Although the upper limit of Re_{crit} is undefined, for most practical purposes the flow in the range $2300 \leq Re_D \leq 10^4$ is regarded as a transition flow region. Compact heat exchangers at part loads may operate in the transition region although the design value of Re_D falls above 10^4.

Extensive efforts have been made to obtain empirical correlations that either represent a best fit curve to the experimental data or have the constants in the theoretical equations adjusted to best fit the experimental data. An example of the latter is the correlation given by Petukhov and Popov [14]. Their theoretical calculations for the case of fully developed turbulent flow with constant heat flux boundary condition yielded the following correlation, which is based on the three-layer turbulent boundary-layer model with constants adjusted to match the experimental data:

$$Nu_{fd} = \frac{(f/8) Re_D Pr}{(1+3.4f)+(11.7+1.8Pr^{-\frac{1}{3}})(f/8)^{\frac{1}{2}}(Pr^{\frac{2}{3}}-1)} \quad (3.1)$$

where

$$f = \left\{ \log_{10}[Re_D] - 1.64 \right\}^{-2} \quad (3.2)$$

is the friction factor $\left(f = \frac{\tau_w}{\frac{1}{8}\rho u_m^2} \right)$.

Equation (3.2) is applicable for fully developed turbulent flow in the range

$10^4 \leq Re_D \leq 5 \times 10^5$ and $0.5 < Pr < 2000$ with 1 % error [14]. A simple correlation has also been proposed by Petukhov, Krillov, and Popov [15] as

$$Nu_{fd} = \frac{(f/8)\ Re_D Pr}{1.07 + 12.7 (f/8)^{\frac{1}{2}} (Pr^{\frac{2}{3}} - 1)} \tag{3.3}$$

where f may be obtained from the Moody diagram or, for smooth tubes, from eqn. (3.2) The above correlation (Eqn. 3.3) predicts the results in the range $10^4 < Re_D < 5 \times 10^5$ and $0.5 < Pr < 200$ with 5 to 6 % error [15].

There are numerous heat transfer correlations which have been established for fully developed flow in a circular tube. A compilation of such correlations has been summarized by Kays and Perkins [17], by Shah and Bhatti [11]. One correlation, which is widely used and is attributed to Gnielinski [16], is of the form

$$Nu_{fd} = \frac{(f/8)(Re_D - 1000) Pr}{1 + 12.7 (f/8)^{\frac{1}{2}} (Pr^{\frac{2}{3}} - 1)} \tag{3.4}$$

where, for smooth tubes, the friction factor is given by

$$f = \left\{ 0.79 \ln [Re_D] - 1.64 \right\}^{-2} \tag{3.5}$$

The Gnielinski correlation is a modified version of the second Petukhov et al. correlation (Eqn. 3.3), extending it to the $2300 < Re_D < 5 \times 10^4$ range. For $0.5 \leq Pr \leq 2000$ and $2300 \leq Re_D \leq 5 \times 10^6$, it is in overall best accord with the experimental data; it agrees with the second Petukhov et al. correlation within

−2% and +7.8%. Hence it is selected as the common basis of comparison for all the correlations in [11]. The Gnielinski correlation along with the friction factor given by equation (3.5) was used to calculate *Nusselt numbers* in the present analysis of an air preheater.

All correlations presented so far apply for both uniform surface heat flux and temperature. Properties should be evaluated at an average bulk temperature.

Although entry lengths for turbulent flow are typically short, $10 \leq (x_{fd}/D) \leq 60$, it is often preferred to consider the entry effect for a simultaneously developing flow. Mills [18] carried out extensive experimental investigations to study this effect in a smooth circular tube using air ($Pr=0.7$) as the working fluid, employing the constant heat flux boundary condition. The mean *Nusselt number* Nu_m is expressed for the five entrance configurations shown in Table 3.2 by formulas of the type

$$\frac{Nu_m}{Nu_{fd}} = 1 + \frac{C}{(x/D)^n} \tag{3.6}$$

where Nu_{fd} stands for the fully developed *Nusselt number.* The constants C and n depend on the nature of the inlet (for example, sharp-edged or nozzle) and entry region (thermal or simultaneously developing), as well as on the *Prandtl* and *Reynolds numbers.*

From eqn. (3.6), the mean *Nusselt number* between any two arbitrary points along the tube might be expressed as in the following equation

$$Nu_{m1\text{-}2} = Nu_{fd}\left\{1 + \frac{CD^n}{x_2 - x_1}\left(x_2^{\,1-n} - x_1^{\,1-n}\right)\right\} \tag{3.7}$$

Table 3.2 Ratio of Mean to Fully Developed Turbulent Flow Nusselt Number in the Entrance Region of a Smooth Circular Tube with Various Entrance Configurations for Pr=0.7 [18].

Entrance Configuration	Formula for Nu_m/Nu_∞
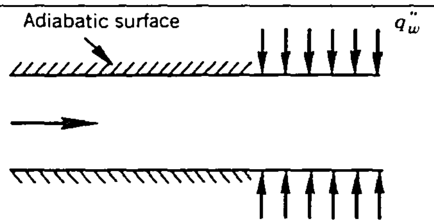 Long calming section	$\frac{Nu_m}{Nu_\infty} = 1 + \frac{0.9756}{(x/D_h)^{0.760}}$
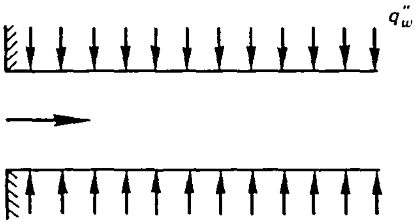 Square entrance	$\frac{Nu_m}{Nu_\infty} = 1 + \frac{2.4254}{(x/D_h)^{0.676}}$
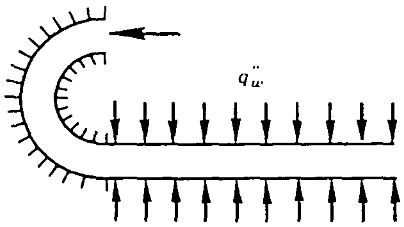 180° Round bend	$\frac{Nu_m}{Nu_\infty} = 1 + \frac{0.9759}{(x/D_h)^{0.700}}$
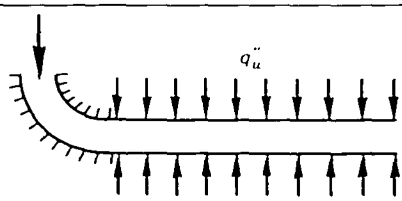 90° Round bend	$\frac{Nu_m}{Nu_\infty} = 1 + \frac{1.0517}{(x/D_h)^{0.629}}$
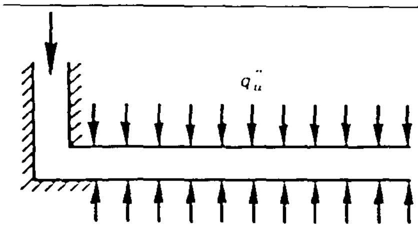 90° Elbow	$\frac{Nu_m}{Nu_\infty} = 1 + \frac{2.0152}{(x/D_h)^{0.614}}$

3.2.3 *The Influence of Surface Roughness*

All the preceding discussion has been based on the assumption of an aerodynamically smooth surface. Circular tube wall roughness has little effect on laminar flow. However, it exerts a strong influence on turbulent flow.

Surface roughness can take many forms. The name of Nikuradse [19] is indelibly associated with the rational analysis of rough surfaces. He performed systematic experiments with sand grains glued onto the interior of circular tubes. The symbol k, a length dimension, is used to describe the roughness element size, k being actually the size of the sieve used by Nikuradse to sift the sand.

The effect of roughness on a turbulent boundary layer is felt mostly right at the wall, and thus a nondimensional expression of roughness size is logically based on the shear velocity u_τ defined as

$$u_\tau = \sqrt{\frac{\tau_w}{\rho}} = u_m\sqrt{\frac{f}{8}} \ . \tag{3.8}$$

This leads to a *roughness Reynolds number* Re_k as a nondimensional measure of surface roughness:

$$Re_k = \frac{u_\tau k}{\nu} \tag{3.9}$$

With this *roughness Reynolds number* Re_k as the parameter, Nikuradse identified the following three flow regimes depending on the variation of f with Re_k and k/r_g:

1. Hydraulically smooth regime, $0 \leq Re_k \leq 5$: $f = f(Re_D)$

2. Transition regime, $5 \leq Re_k \leq 70$: $f = f(k/r_g,\ Re_D)$

3. Completely rough regime, $Re_k > 70$: $f = f(k/r_g)$

The roughness used by Nikuradse in his experiments doesn't represent the type of roughness encountered in commercial circular tube surfaces. To circumvent this difficulty, Schlichting [20] introduced the concept of equivalent sand-grain roughness for roughness elements such as spheres, spherical segments, cones, and short triangles. Moody [21] determined the equivalent sand grain roughness for eight types of commercially available circular tube surfaces. His results, some of which are tabulated in Table 3.3, are very useful in practical applications.

Table 3.3 Equivalent sand roughness for commercial circular tube surfaces [21].

Type of the circular tube	k (μm)
riveted steel	900-9000
reinforced concrete	300-3000
cast iron	240
commercial steel	46

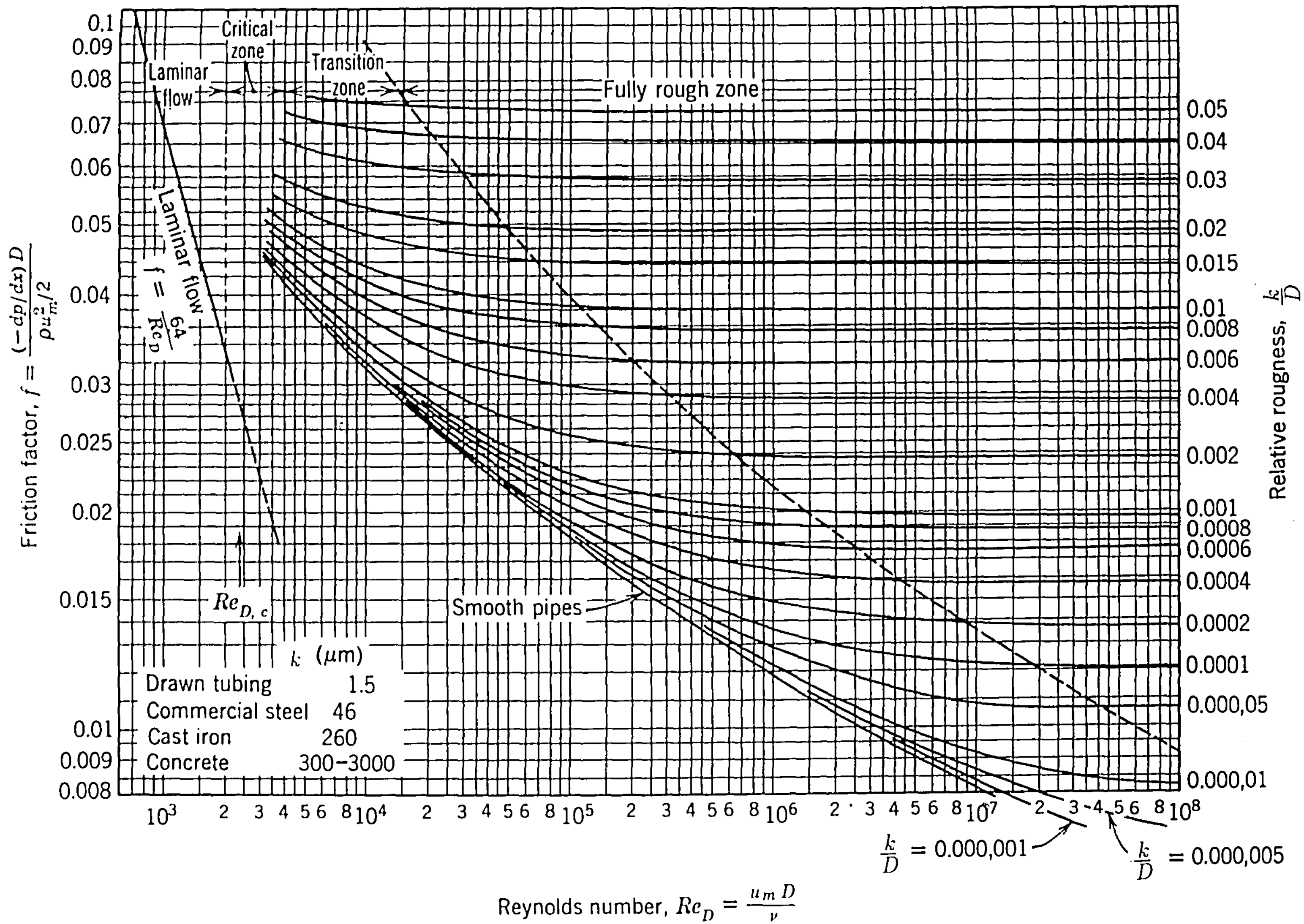

Figure 3.1 Friction Factor for Fully Developed Flow in a Circular Tube [21].

We now turn to the effect of roughness on the heat transfer rate. Two distinct influences of the roughness elements are recognized. First, they increase the tube surface area, and second, they increase the heat transfer coefficient. This latter effect is brought about by the change in the turbulence patterns close to the wall. The following simple correlation, suggested by Norris [22], expresses the effect of roughness for turbulent flow in a circular tube:

$$\frac{Nu}{Nu_s}=\left(\frac{f}{f_s}\right)^n \quad \text{for } \frac{f}{f_s}\leq 4 \tag{3.10}$$

where $n=0.68Pr^{0.215}$ for $1<Pr<6$. For $\frac{f}{f_s}>4$, Norris observed that the *Nusselt number* no longer increases.

Moody's friction factor plot given in Figure 3.1 may be used to determine the effect of surface roughness on the heat transfer rate. For example, consider the following conditions which are some of the operating and design conditions of the air preheater under consideration:

$Re_D=$ 30,000 (turbulent flow in the circular tubes)

Pr=0.7 (flue gas)

$k/D=0.001$ (commercial steel tube with an inside diameter of 0.0146 m)

Using Moody's diagram and Norris's correlation, it was found that

$f_s=0.024$

$f=0.027$

$$\frac{Nu}{Nu_S}=1.077$$

This shows that heat transfer rate increases by 7.7% due to surface roughness for conditions of interest.

3.3 Flow Over Tube Banks

3.3.1 *Banks of Tubes*

In practice, air heaters made from banks of tubes are widely in use. The tubes in a bank are often arranged in staggered or in-line configurations. Fig. 3.2 illustrates these two arrangements and definitive characteristic dimensions of a tube bank

$$a=S_T/D=\text{the relative transverse pitch} \tag{3.11}$$

$$b=S_L/D=\text{the relative longitudinal pitch} \tag{3.12}$$

$$c=S_D/D=\text{the realtive diagonal pitch} \tag{3.13}$$

Flow conditions within the bank are dominated by boundary layer separation effects and by wake interactions, which in turn influence convection heat transfer. The majority of experimental investigations showed that the heat transfer in a tube in a bank is greater than that of a single tube and depends on longitudinal and transverse pitches. From the heat transfer standpoint, the staggered arrangement is more effective [23].

Banks of tubes act as vortex generators, and, depending on the location of the tubes, a corresponding turbulence level is established in each bank. Therefore, heat transfer for tubes in inner rows is considerably higher than heat transfer for tubes in the front rows [23].

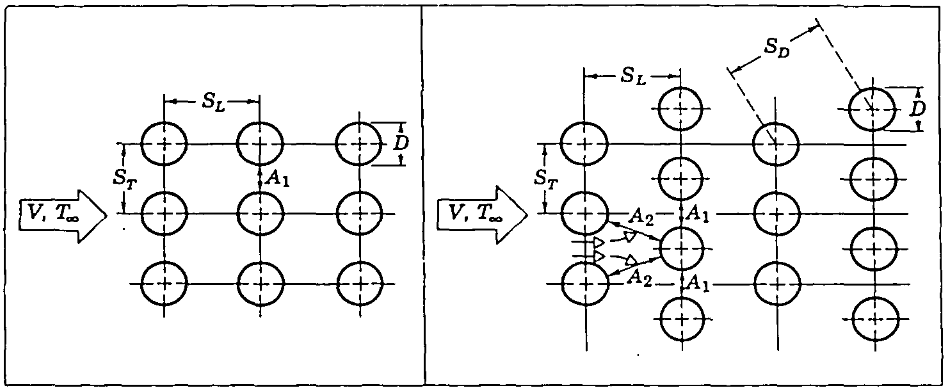

a) b)

Figure 3.2 Tube arrangements in a tube bank; (a) in-line, (b) staggered.

3.3.2 *Mean Heat Transfer from Banks of Tubes*

Heat transfer of a tube in a bank depends mainly on the velocity of the thermal carrier, tube arrangements, properties of the incoming fluid, thermal loading, turbulence level, and direction of heat flux.

Experimental results of heat transfer for banks of tubes in gas flow were generalized according to similarity theory and were expressed by the equation of similarity ($Nu_D = C Re^m{}_{Dmax} Pr^n$). Zukauskas [23] has proposed a correlation of the form

$$Nu_D = C Re^m_{Dmax} Pr^{0.36} (\frac{Pr}{Pr_s})^{0.25} \tag{3.14}$$

This correlation is applicable to both staggered and in-line tube arrengements with $\mp$ 15% error, having the following restrictions

N_L = row number of tube banks > 20

$0.7 < Pr < 500$

$1000 < Re_{Dmax} < 2 \times 10^6$

All properties except Pr_s are evaluated at $T_{a,in}$ (inlet bulk temperature of the fluid). The constants C and m are listed in Table 3.3. Reynolds and Nusselt numbers are defined as follows

$$Re_{Dmax} = \frac{\rho V_{max} D}{\mu} \tag{3.15}$$

$$Nu_D = \frac{h_a D}{k} \tag{3.16}$$

where D is the outside diameter of the tubes ($2r_a$).

Since the *Prandtl number* is almost constant for gases, $\frac{Pr}{Pr_s} \approx 1$. The *Reynolds number* Re_{Dmax} is based on the maximum average fluid velocity occuring within the tube bank. For the in-line arrangement, V_{max} occurs at the transverse plane

A_1 of Figure 3.2a, and from mass conservation for an incompressible fluid:

$$V_{max} = \frac{a}{a-1} V \tag{3.17}$$

Table 3.4 Constants of Equation 3.14 for tube banks in crossflow [23].

CONFIGURATION	Re_{Dmax}	C	m
In-line	$10-10^2$	0.80	0.40
Staggered	$10-10^2$	0.90	0.40
In-line	10^2-10^3	0.52	0.50
Staggered	10^2-10^3	0.52	0.50
In-line $(S_T/S_L<0.7)$*	$10^3-2\text{x}10^5$	0.27	0.63
Staggered $(S_T/S_L<2)$	$10^3-2\text{x}10^5$	$0.35(\frac{S_T}{S_L})^{0.25}$	0.60
Staggered $(S_T/S_L>2)$	$10^3-2\text{x}10^5$	0.40	0.60
In-line	$2\text{x}10^5-2\text{x}10^6$	0.021	0.84
Staggered	$2\text{x}10^5-2\text{x}10^6$	0.022	0.84

* For $S_T/S_L>0.7$, heat transfer is inefficient and in-line tubes should not be used.

For a staggered configuration, the maximum average velocity may occur at either the transverse plane A_1 or the diagonal plane A_2 of Figure 3.2b. It will occur at plane A_1 if the rows are spaced such that

$$2(c-1)<(a-1) \tag{3.18}$$

The factor of 2 results from the bifurcation experienced by the fluid moving from the A_1 to the A_2 planes. Hence V_{max} occurs at A_2 if

$$c=[b^2+(a/2)^2]^{0.5}<\frac{a+1}{2} \tag{3.19}$$

in which case it is given by

$$V_{max}=\frac{a}{2(c-1)}V \tag{3.20}$$

If V_{max} occurs at A_1 for the staggered configuration, it may again be computed from equation 3.14 [24].

Flow around tubes in the first row of a tube bank corresponds to that for a single (isolated) cylinder in crossflow. However, for subsequent rows, the flow depends strongly on the tube bank arrangement (Figure 3.3). In-line tubes beyond the first row are in the turbulent wakes of upstream tubes, and for moderate values of S_L, convection coefficients associated with downstream rows are enhanced by turbulation of the flow. Typically, the convection coefficient of a row increases with increasing row number until approximately the fifth row, after which there is little change in the turbulence and hence in the convection coefficient. However, for small values of S_L, upstream rows, in effect, shield downstream rows from much of the flow, and heat transfer is adversely affected. That is, the preferred flow path is in lanes between the tubes and much of the tube surface is not exposed to the main flow. For this reason, operation of in-line tube banks with $S_T/S_L > 0.7$ (Table 3.4) is undesirable. For the staggered array, however, the path of the main flow is more tortuous and a greater portion of the surface area of the downstream tubes remains in this path. In general, heat transfer enhancement is favored by the more tortuous flow of a staggered arrangement, particularly for small *Reynolds number* ($Re_D < 100$) [24].

From Re_{Dmax} equal to 1000 and above, the heat transfer of the first rows of the tubes decreases further, compared with heat transfer of the inner rows. This is an indication of how turbulence, generated by the first rows of tubes in a bank, affects heat transfer of the inner rows. At Re_{Dmax} equal to 1000, the difference in heat transfer of the first and inner rows amounts to 24%. At Re_{Dmax} equal to 10^5, this difference rises to 70% [23].

3.3.3 *The Influence of Roughness on the Mean Heat Transfer of a Bank*

Heat transfer of smooth tube banks in crossflow has been extensively investigated [23]. However, the effect of surface roughness on the heat transfer rate in those investigations has not been sufficiently studied.

Zukauskas [23] proposed correlations for the calculation of the mean heat transfer coefficient in rough tube banks on the basis of other investigators' experimental results for local heat transfer coefficients. When Re_{Dmax} ranges from 10^3 to 10^5, the correlation is

$$Nu_D = 0.5(a/b)^{0.2}(Re_{Dmax})^{0.65} Pr^{0.36}(k/D)^{0.1} \tag{3.25}$$

and in the Re_{Dmax} range from 10^5 to $2\text{x}10^6$, the correlation is

$$Nu_D = 0.1(a/b)^{0.2}(Re_{Dmax})^{0.8} Pr^{0.4}(k/D)^{0.15} \tag{3.26}$$

The mean heat transfer can be computed from these equations with an accuracy of $\pm 15\%$ for a in the range from 1.25 to 2.0, b from 0.935 to 2.0, and k/D from $6.67\text{x}10^{-3}$ to $40\text{x}10^{-3}$.

In the flow of air over a tube bank, the effect of roughness is manifest at higher Re_{Dmax} ($Re_{Dmax}=5\text{x}10^4$ to $7\text{x}10^4$) for the k/D range from $0.3\text{x}10^{-3}$ to $8\text{x}10^{-3}$ [23]. Since k/D is near $1\text{x}10^{-3}$ and Re_{Dmax} changes from $2\text{x}10^4$ to $5\text{x}10^4$ in the present analysis of the air preheater, the correlations for rough tube banks proposed by Zukuaskas were not used for calculating the mean heat transfer rate. Instead all analysis based on the correlations for smooth tube banks proposed by Zukuaskas [23].

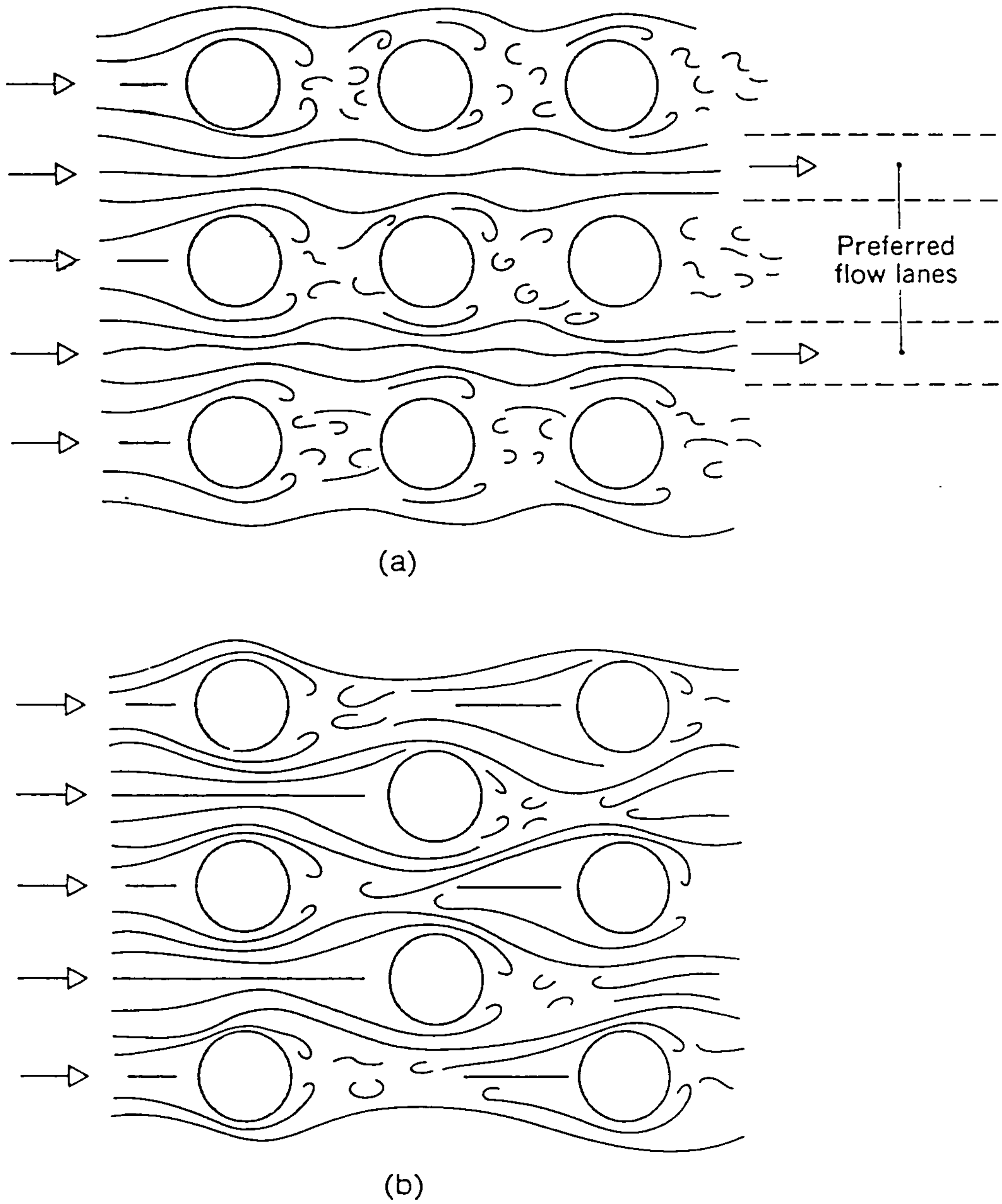

Figure 3.3 Flow conditions in a bank; (a) in-line, (b) staggered.

4. MATHEMATICAL MODEL

4.1 Single-Pass Crossflow Exchanger

The mathematical model is based on one of the two basic heat exchanger theories which has been used extensively; namely the ϵ-NTU method [1]. In the heat exchanger shown in Figure 4.1, flue gas flows through the tubes while air flows over the tube bundle.

The overall heat exchanger is divided into smaller crossflow heat exchanger assemblies in the gas flow direction, i, and in the air flow direction, j (see Figure 4.1). A small element may consist of a number of tubes, depending on its size. For modeling purposes, each small element of the heat exchanger was approximated by a crossflow heat exchanger, with one of the fluids (air) mixed and the other (gas) unmixed. It has also been assumed that the mass flow rates at each row i, and column j, don't change throughout the flow length. That is, both fluids are flowing in closed passages, representing the rows and columns in Figure 4.1. Moreover, these smaller heat exchanger assemblies are considered to have uniform metal temperatures since their dimensions are small compared to the overall heat exchanger.

Using the ϵ-NTU Method [1], outlet gas temperature, outlet air temperature and the tube metal temperature of each element have been calculated. Considering *the ij th* element in Fig. 4.1 and using the equations presented in Chapter 2.1,

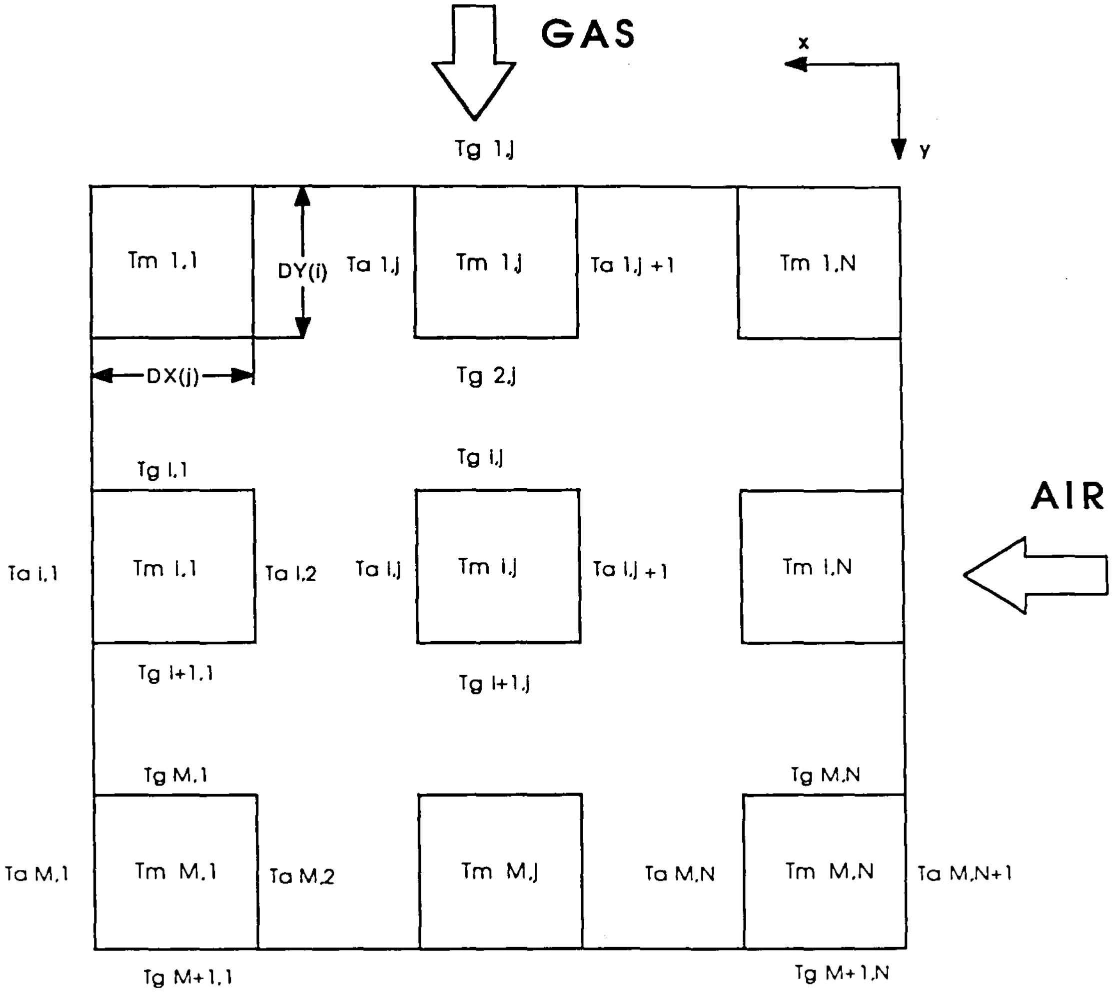

Figure 4.1 Subdivisions of a single-pass crossflow heat exchanger on xy plane.

the capacity rate ratio of the *ij th* element is

$$C_{R\ ij} = \frac{C_{min\ ij}}{C_{max\ ij}}, \tag{4.1}$$

The number of heat transfer units of the *ij th* element is

$$NTU_{\ ij} = \frac{(AU)_{g\ ij}}{C_{min\ ij}}, \tag{4.2}$$

If $C_{max\ ij}$ is mixed and $C_{min\ ij}$ unmixed;

the effectiveness of the *ij th* element becomes

$$\epsilon_{\ ij} = (1/C_{R\ ij})\left\{1 - exp[1 - exp(-NTU_{\ ij})]\right\}, \tag{4.3}$$

The outlet air and gas temperatures of the *ij th* element are

$$T_{a\ ij} = T_{a\ ij+1} - \epsilon_{\ ij} C_{R\ ij} (T_{g\ ij} - T_{a\ ij+1}) \tag{4.4}$$

$$T_{g\ i+1j} = T_{g\ ij} - \epsilon_{\ ij} (T_{g\ ij} - T_{a\ ij+1}). \tag{4.5}$$

If $C_{min\ ij}$ is mixed and $C_{max\ ij}$ unmixed;

the effectiveness of the *ij th* element becomes

$$\epsilon_{\ ij} = 1 - exp\left(-[1/C_{R\ ij}]\left\{1 - exp(-C_{R\ ij} NTU_{\ ij})\right\}\right), \tag{4.6}$$

and the outlet air and gas temperatures of the *ij th* element are

$$T_{a\ ij}=T_{a\ ij+1}-\epsilon_{ij}(T_{g\ ij}-T_{a\ ij+1}) \tag{4.7}$$

$$T_{g\ i+1j}=T_{g\ ij}-\epsilon_{ij}C_{R\ ij}(T_{g\ ij}-T_{a\ ij+1}). \tag{4.8}$$

Total heat transfer rate of the *ij th* element may be computed from

$$Q=(mc_p)_{a\ ij}(T_{a\ ij}-T_{a\ ij+1})=(mc_p)_{g\ ij}(T_{g\ ij}-T_{g\ i+1j}) \tag{4.9}$$

or in terms of the tube metal and average gas temperatures,

$$Q=\frac{A_{g\ ij}\left(\left\{[T_{g\ ij}+T_{g\ ij+1}]/2\right\}-T_{m\ ij}\right)}{\left\{\frac{1}{h_{g\ ij}}+\frac{r_g}{k_w}\ ln(r_m/r_g)\right\}}. \tag{4.10}$$

Equating eqns 4.9 and 4.10, we find the tube metal temperature of the *ij th* element, $T_{m\ ij}$ as

$$T_{m\ ij}=(mc_p)_{a\ ij}\frac{(T_{a\ ij}-T_{a\ ij+1})}{A_{g\ ij}}\left\{\frac{1}{h_{g\ ij}}+\frac{r_g}{k_w}ln(r_m/r_g)\right\}-T_{gavg\ ij} \tag{4.11}$$

where $T_{gavg\ ij}$ is the average gas temperature of the *ij th* element.

Knowing inlet gas and air temperatures, we are able to directly calculate the tube metal temperature and outlet gas and air temperatures of the *ij th* element. Now we should find a computing sequence so that the same calculation can be done for all elements. This may be accomplished with a double do-loop in the computer program, commencing at the right hand-side upper corner element. That element is the (1,*N*) *th* element in Fig. 4.1. In this case, the temperature and velocity profiles at inlet sections of the overall heat exchanger must be known. It is obvious from Figure 4.1 that calculations must proceed column by column or row by row. Having evaluated the temperature fields of the overall heat exchanger, we may calculate the overall effectiveness by equation 2.5, using average inlet and outlet temperatures of the working fluids.

4.2 Verification of the Model

The mathematical model presented in Chapter 4.1 enables us to predict the performance of a single-pass crossflow heat exchanger having both of the fluids unmixed.

The accuracy of the results of the mathematical model depends on the number of subdivisions (elements) used. The use of more subdivisions can produce higher accuracy. Practically, the elements used must be determined according to the accuracy desired.

Using a number of different size matrices, the effectiveness of a single-pass crossflow exchanger having both of the fluids unmixed, for the case of $C_R=0.8103$ and NTU=1.8632, was calculated. The results are presented in Figure 4.2. In this calculation, the following parameters were set to a constant value in order to make a comparison with the analytical solution of the same case ($C_R=0.8103$ and NTU=1.8632) [3];

1. inlet gas temperature and velocity
2. inlet air temperature and velocity

3. physical properties of working fluids

4. overall heat transfer coefficient

It can be seen from Figures 4.2 to 4.5 that as the number of subdivisions increases, the accuracy of the mathematical model results increases as well. When a 10x10 matrix is used, these results are accurate to the 3rd digit for most cases, as compared with the analytical solution [3]. Three digit accuracy is believed to be sufficient for most engineering applications. Thus, a 10x10 matrix arrangement was used throughout this investigation.

In Table 4.1, the comparison between the results of the presented mathematical model and the analytical solution is extended to various cases of capacity rate ratio (C_R) and number of heat transfer units (NTU).

As seen from Table 4.1, the effectiveness of the present computer model deviates by 0.05% from the analytical solution by Chung [3], that is, we have agreement to within three digits for given values of C_R and NTU. Using another approach, Chiou [9] also came up with three digit agreement in the effectiveness by solving the governing heat transfer equations for a crossflow exchanger [2] with the aid of a finite difference mathematical method. But computationally, this is relatively expensive compared to approach used in the present analysis.

4.3 Two-Pass Counter-Crossflow Air Preheater

The objective of this work was to find the metal temperature field of a tubular recuperative air preheater arranged as a two-pass counter-crossflow (see Figure 4.4). The inlet gas and air temperatures of the air preheater and the inlet velocity variations of air and gas are given as boundary conditions.

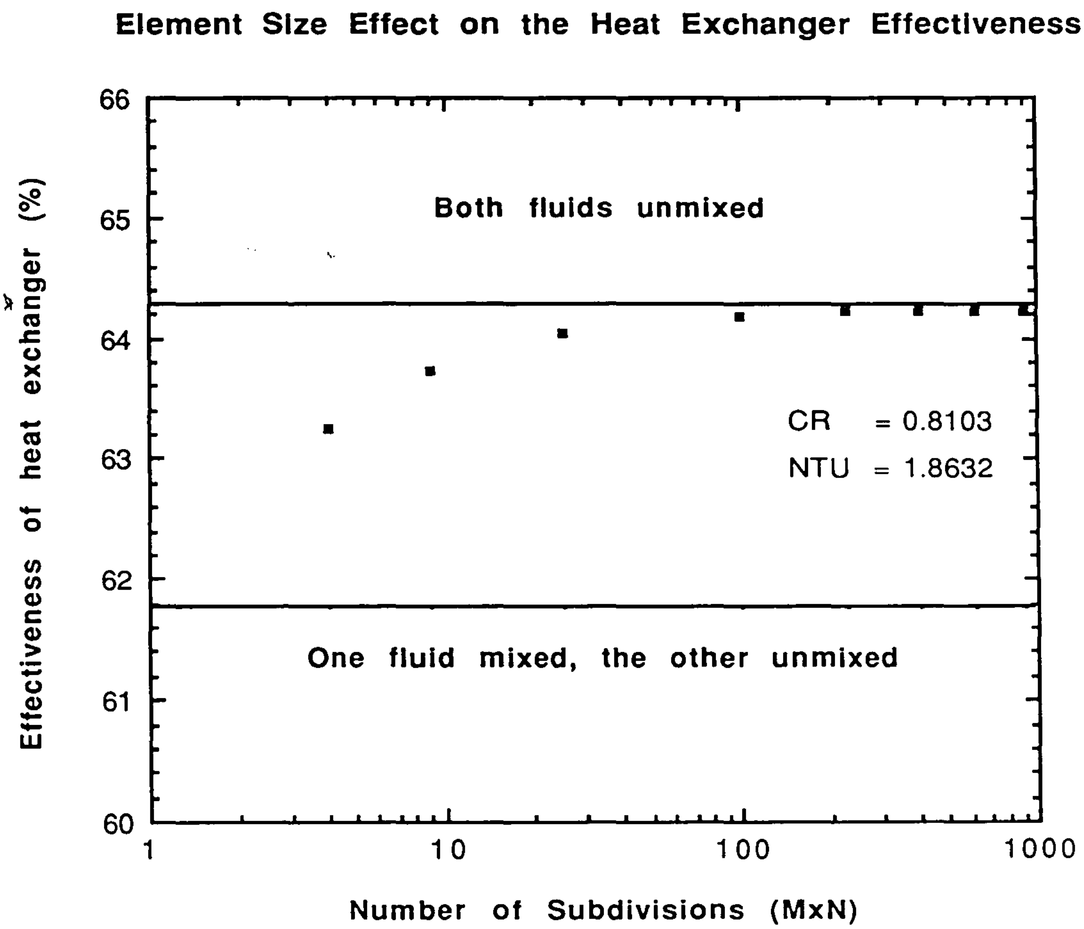

Figure 4.2 The effect of grid size on the heat exchanger effectiveness.

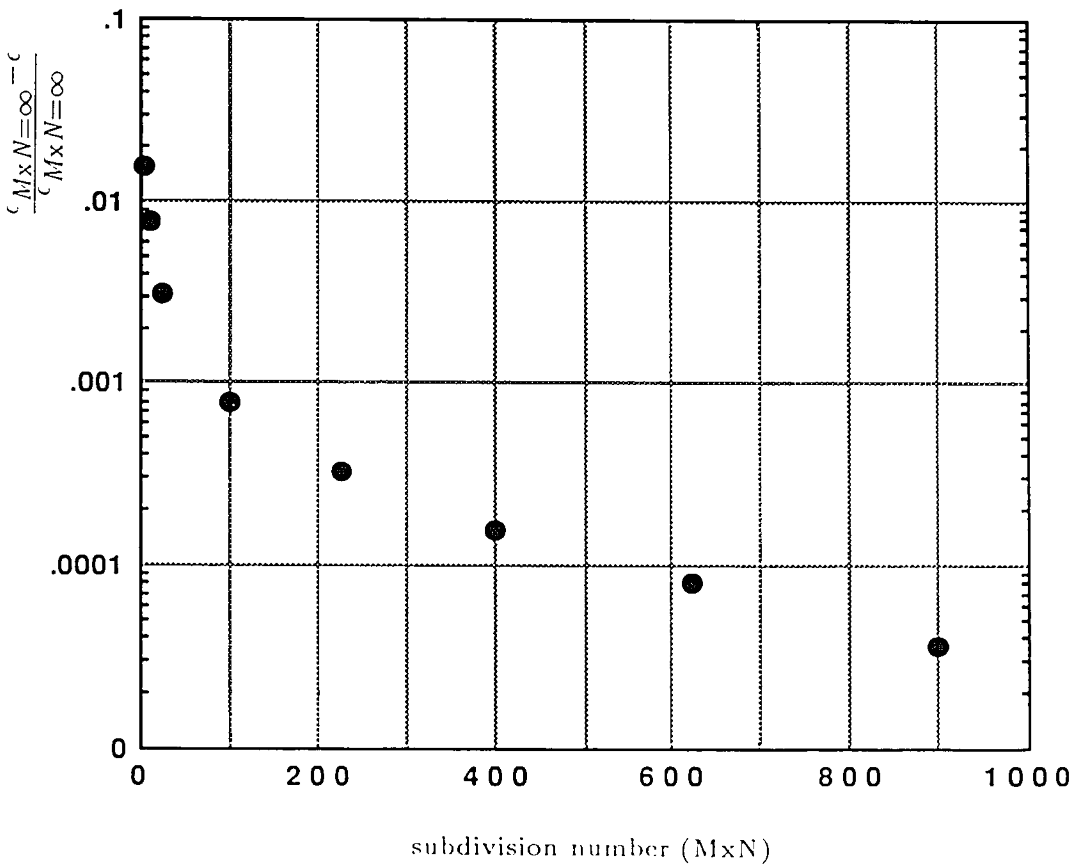

Figure 4.3 The effect of grid size on the accuracy of the mathematical model results for heat exchanger effectiveness.

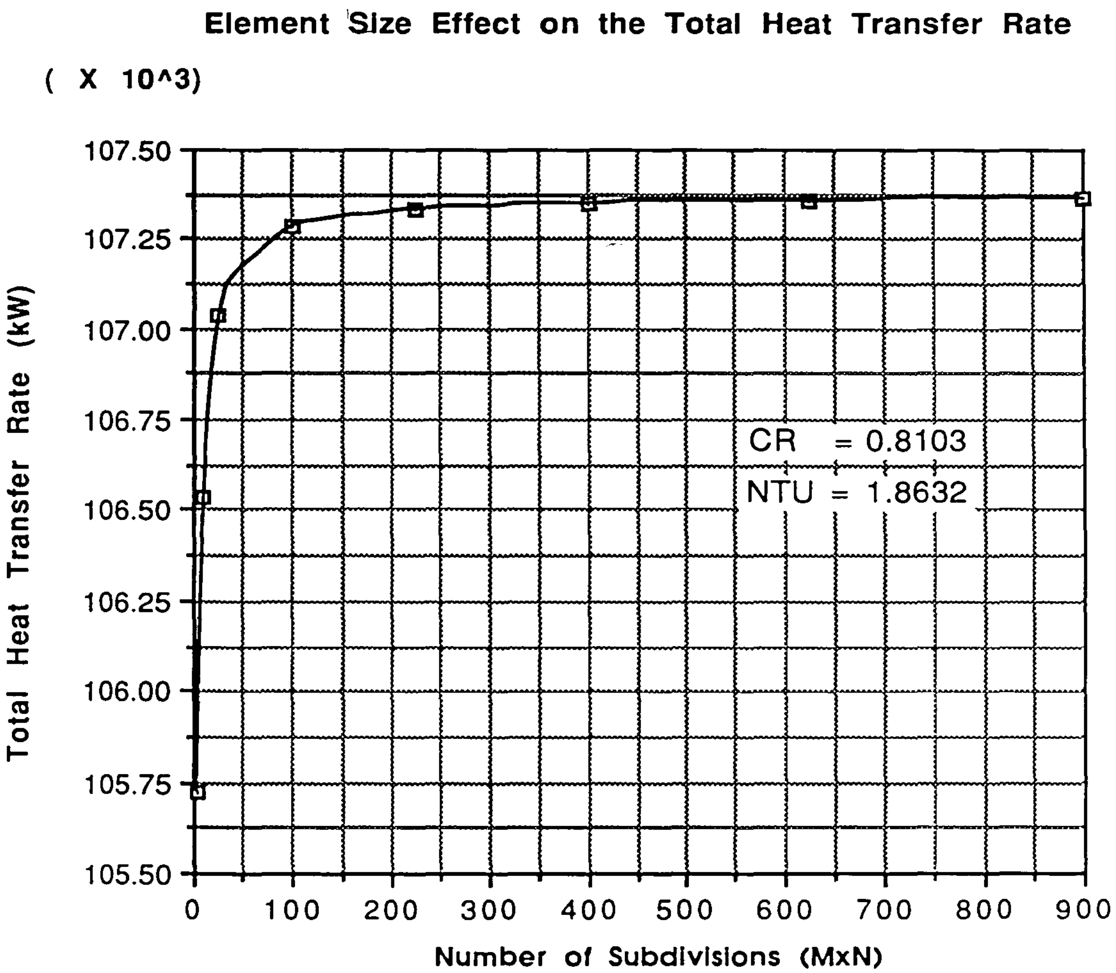

Figure 4.4 The effect grid size on the total heat transfer rate.

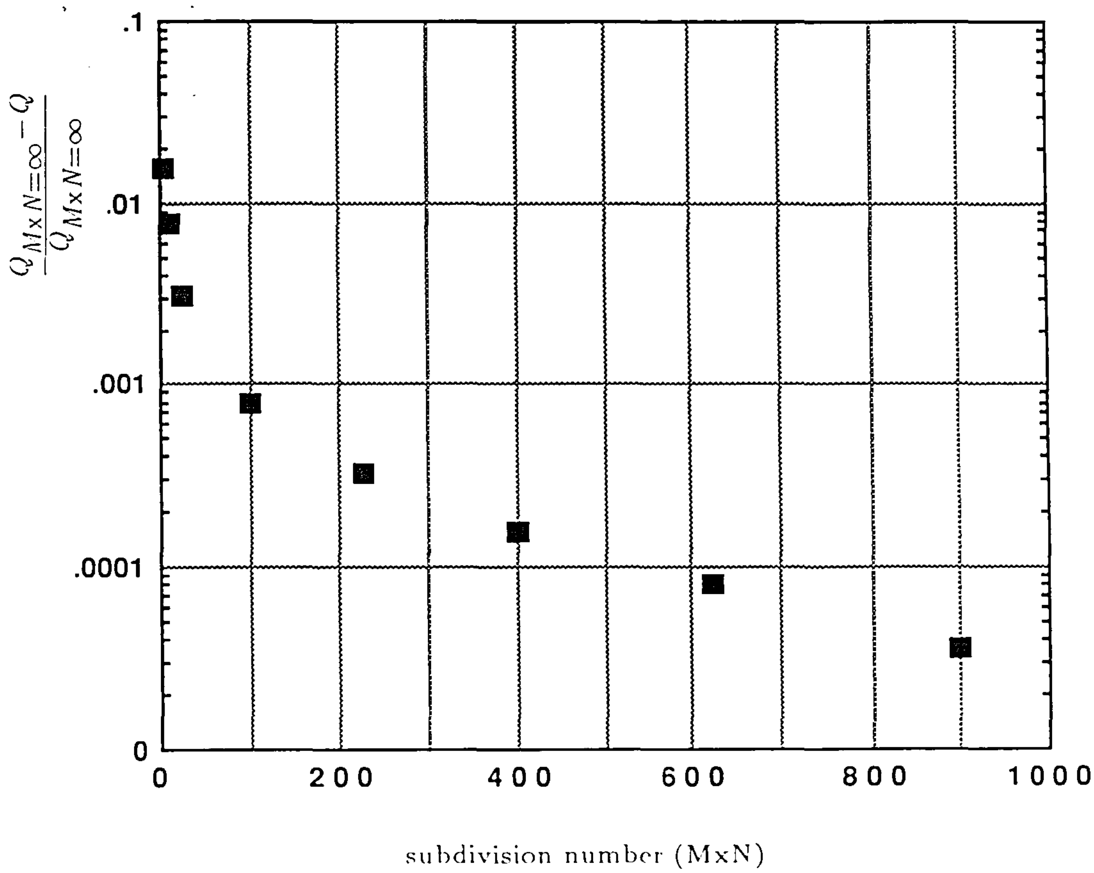

Figure 4.5 The effect of grid size on the accuracy of the mathematical model results for heat transfer rate of the heat exchanger.

Table 4.1 Comparison between the effectiveness of the mathematical model presented in Chapter 4.1 and the analytical solution [3] for a single-pass crossflow exchanger having both fluids unmixed.

	NTU	ϵ	$\epsilon_{analytical}$[3]
C_R=0.70	2.042	0.6884	0.6885
	2.849	0.7548	0.7551
	3.377	0.7850	0.7854
	3.490	0.7905	0.7910
	3.518	0.7919	0.7923
C_R=0.80	1.828	0.6391	0.6392
	2.512	0.7016	0.7019
	2.943	0.7299	0.7303
	2.993	0.7328	0.7332
	3.045	0.7357	0.7361
C_R=0.90	1.677	0.6006	0.6008
	2.278	0.6594	0.6597
	2.647	0.6857	0.6861
	2.687	0.6883	0.6886
	2.725	0.6906	0.6910

To accomplish this goal, we simultaneously employed the mathematical method presented in Chapter 4.1 to both passes of the air preheater using an iterative procedure proposed by Korst [25]. It has also been assumed that there is adiabatic mixing inside the duct which connects the passes of the air preheater. Owing to perfect mixing and no heat loss to the surroundings from the duct, the gas will have a constant temperature throughout the duct (at <2>, <3>, <4> in Figure 4.6). That is, the gas temperature at the inlet of *Pass I* (at <4>) will be the same as the average gas temperature at the outlet of *Pass II* (at <2>).

Consider the sketch of the air preheater in Figure 4.6 and the numbers inside the angle brackets which reference locations in the sketch. The inlet gas temperature of *Pass I* (<4>) is assumed. With this assumed gas temperature entering *Pass I* (<4>), and the known inlet temperature profile of air (<6>), the mathematical model for the single-pass crossflow case may be applied to *Pass I* in order to obtain the temperature profile of air leaving *Pass I* (<7>) and entering *Pass II* (<7>). With the calculated inlet air temperature profile (<7>) and known inlet gas temperature distribution (<1>), the same procedure is applied to *Pass II*. Since the average gas temperature at the outlet of *Pass II* (<2>) is carried out to *Pass I* as the inlet gas temperature (<4>), one iterative calculation has now been completed. The same procedure is followed with the last calculated value of the inlet gas temperature of *Pass I* until convergence to a solution is reached.

A similar iterative procedure was used by Stevens [26] in order to find the effectivenesses of two and three-pass crossflow exchangers.

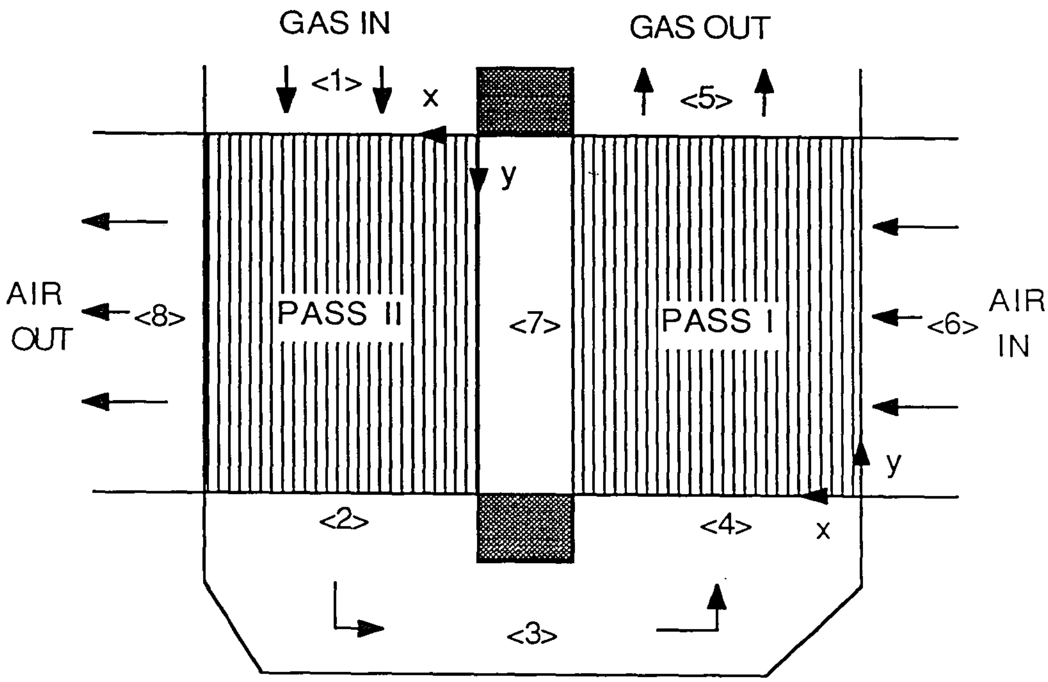

Figure 4.6 The sketch of the tubular recuperative air preheater arranged as a two-pass counter-crossflow.

Since the solution procedure of the computer model is iterative, a convergence criterion is needed. It is assumed that convergence is achieved when the average difference between the total heat transfer rates of the air preheater calculated in two subsequent iterations is within an acceptable error. The average difference in the total heat transfer rate is defined as

$$X = \frac{Q_{new} - Q_{old}}{Q_{new}} \tag{4.12}$$

where the subscripts '*new*' and '*old*' stand for the current and the previous iterations, respectively. When the convergence parameter becomes

$$X \leq 1\text{x}10^{-6} \tag{4.13}$$

the iteration ends. The convergence parameter X decays exponentially after 20 to 40 iterations, depending on the initial guess of the gas temperature at <4> in Figure 4.6 and the capacity rate ratio and the number of heat transfer units of the air preheater. Examination of the criterion, X, showed that convergence to the solution of the problem is reached by the following form of an exponential function,

$$X = exp\{-\text{a (number of iterations)}+\text{b}\} \tag{4.14}$$

where constants a and b change for different operating conditions of the air preheater.

Figure 4.7 shows the representation of *Pass I* of the air preheater. As seen from this figure, *Pass I* is the upside-down mirror image of Figure 4.1 which represents *Pass II* of the air preheater. Thus, the equations represented in Chapter 4.1 are still applicable to *Pass I*.

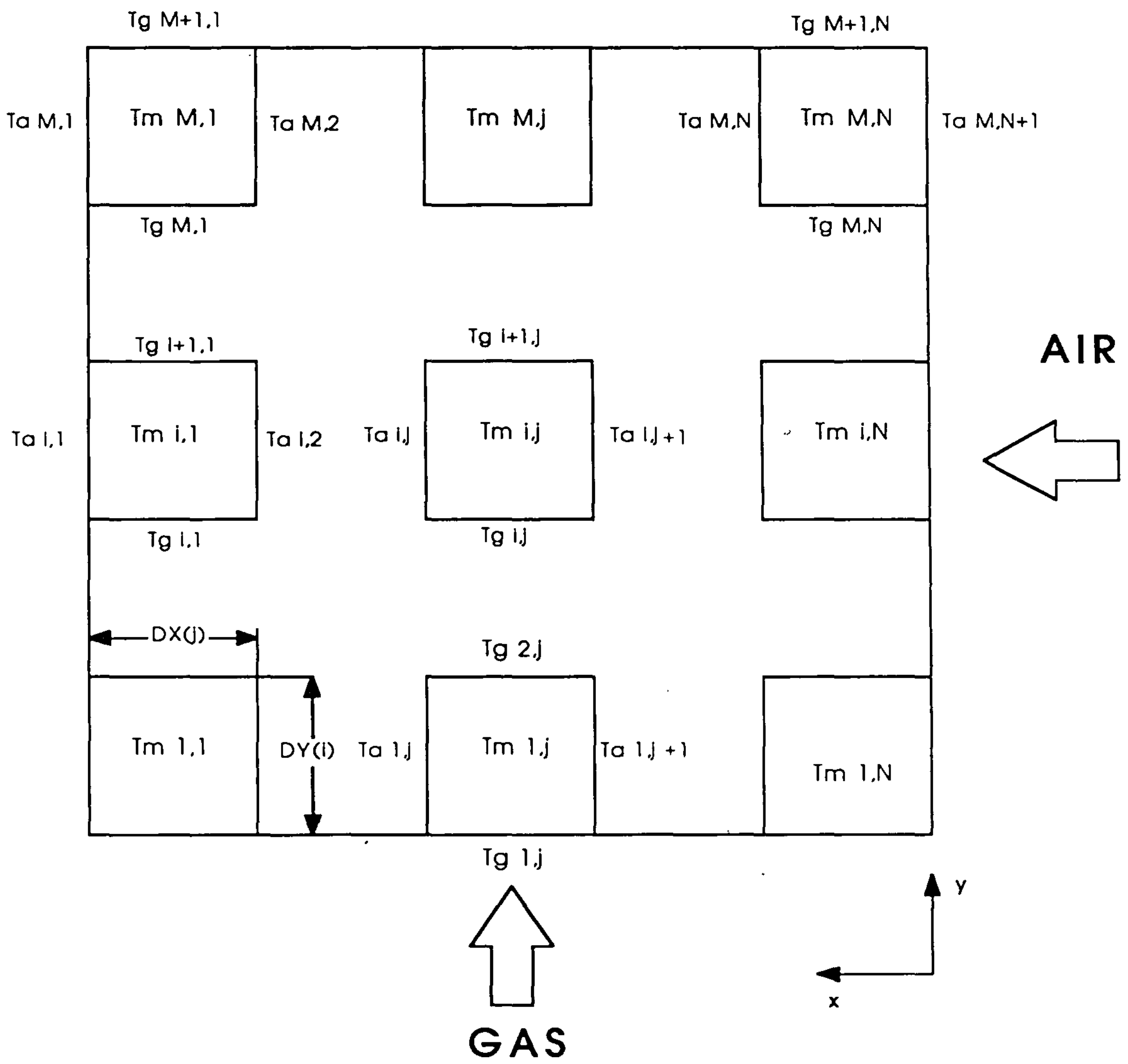

Figure 4.7 Subdivisions of Pass I of the Air Preheater on xy Plane

5. THE EFFECT OF AIR LEAKAGE ON AIR PREHEATER PERFORMANCE

5.1 Air Leakage Model

The tubes in the air preheater are expanded into tube sheets at both ends. To provide for expansion, one tube sheet should be free to move with respect to the casing. Accomplishing this is not possible without air leakage. Due to the difference in pressure between the air and gas streams, some air leaks into the gas stream through the tube sheets at the cold and hot end of the air preheater. The rates of air leakage increase as the air preheater stays in service due to a loosening of the joints and because of acid corrosion.

The air leakage has a negative effect on air preheater performance. An air leakage model has been developed for the two-pass counter-crossflow tubular air preheater in order to predict the effect of the air leakage on the performance of this particular air preheater (see Figure 5.1 and 5.2). It was assumed that air leakage occurs at the inlet and outlet sections of both passes (see Figure 5.1). Also, the leakage calculations are based on average temperature and mass flow rates of the working fluids; therefore, the velocity and temperature profiles remained unchanged at the locations where adiabatic mixing between the main gas flows and leakage flows occur (see Figure 5.1).

The leakage coefficients are defined as follows:

- *cold end leakage coefficient on either pass*

$$\delta_{L,CE}=\frac{m_{L,CE}}{m^e_{gi2}} \tag{5.1}$$

where

$$m_{L,CE}=m_{L,cei}+m_{L,ceo} \tag{5.3}$$

- *hot end leakage coefficient on either pass*

$$\delta_{L,HE}=\frac{m_{L,HE}}{m^e_{gi2}} \tag{5.2}$$

where

$$m_{L,HE}=m_{L,hei}+m_{L,heo} \tag{5.4}$$

The total air leakage of either pass is the sum of the cold and hot end leakage, therefore, the total air leakage coefficients of *Pass I* and *Pass II*, respectively, are

$$\delta_{L1}=\frac{m_{L1}}{m^e_{gi2}}=\delta_{L,CE1}+\delta_{L,HE1} \tag{5.5}$$

$$\delta_{L2}=\frac{m_{L2}}{m^e_{gi2}}=\delta_{L,CE2}+\delta_{L,HE2} \tag{5.6}$$

There are two different leakage flows in opposite directions, at both the cold and hot ends. One of the leakage flows is through the gas-out section and the other is through the gas-in section (see Figure 5.1). The ratio between these two leakages is denoted by R_{CE} and R_{HE} at the cold and hot end, respectively.

$$R_{CE} = \frac{m_{L,ceo}}{m_{L,cei}} \tag{5.7}$$

$$R_{HE} = \frac{m_{L,heo}}{m_{L,hei}} \tag{5.8}$$

Another ratio parameter is defined such that,

$$R_{\delta} = \frac{\delta_{L,CE}}{\delta_{L,HE}} \tag{5.9}$$

The cold and hot end leakage parameters may be represented by these leakage ratio parameters

$$\delta_{L,CE} = \frac{m_{L,cei}}{m^{e}_{gi2}} \left(R_{CE} + 1 \right) \tag{5.10}$$

$$\delta_{L,HE} = \frac{m_{L,hei}}{m^{e}_{gi2}} \left(R_{HE} + 1 \right) \tag{5.11}$$

The preceding definitions of the air leakage coefficients may be used to relate the internal and external mass flow rates. By balancing the mass flow rates at the gas-in section of the air preheater, we obtain

$$m^{i}{}_{g2}=m^{e}{}_{gi2}+m_{L,cei2}+m_{L,hei2} \tag{5.12}$$

From eqns. (5.6) and (5.7), $m_{L,cei2}$ and $m_{L,hei2}$ are as follows

$$m_{L,cei2}=\frac{\delta_{L,CE2}}{(1+R_{CE2})}\ m^{e}{}_{gi2} \tag{5.13}$$

$$m_{L,hei2}=\frac{\delta_{L,HE2}}{(1+R_{HE2})}\ m^{e}{}_{gi2} \tag{5.14}$$

Substituting the quantities $m_{L,cei2}$ and $m_{L,hei2}$ into eqn. (5.8), we get the following relation between the internal and external mass flow rates at the gas-in section of the air preheater.

$$m^{i}{}_{g2}=\left(1+\frac{\delta_{L,CE2}}{1+R_{CE2}}+\frac{\delta_{L,HE2}}{1+R_{HE2}}\right)\ m^{e}{}_{gi2} \tag{5.15}$$

The following relations are obtained in the same way.

$$m^{i}{}_{g1}=\left(1+\delta_{L2}+\frac{\delta_{L,CE1}}{1+R_{CE1}}+\frac{\delta_{L,HE1}}{1+R_{HE1}}\right)\ m^{e}{}_{gi2} \tag{5.16}$$

$$m^{i}{}_{a1}=m^{e}{}_{ai1}-\delta_{L,CE1}m^{e}{}_{gi2} \tag{5.17}$$

$$m^{i}{}_{a2}=m^{e}{}_{ai1}-(\delta_{L1}+\delta_{L,CE2})m^{e}{}_{gi2} \tag{5.18}$$

The relations between the inlet and outlet flow rates are

$$m^{e}{}_{go1}=(1+\delta_{L})\ m^{e}{}_{gi2} \tag{5.19}$$

$$m_{ao2}=m^{e}{}_{ai1}-(1+\delta_L)\ m^{e}{}_{gi2} \tag{5.20}$$

where δ_L ,the air leakage coefficient of the overall air preheater, is the sum of the air leakage coefficients of both passes.

Figures 5.1 and 5.2 illustrate the air leakage model, internal and external temperatures (Fig. 5.2) and mass flow rates (Fig. 5.1). In those Figures, superscript ' i ' and ' e ' are used to denote internal and external quantities, respectively.

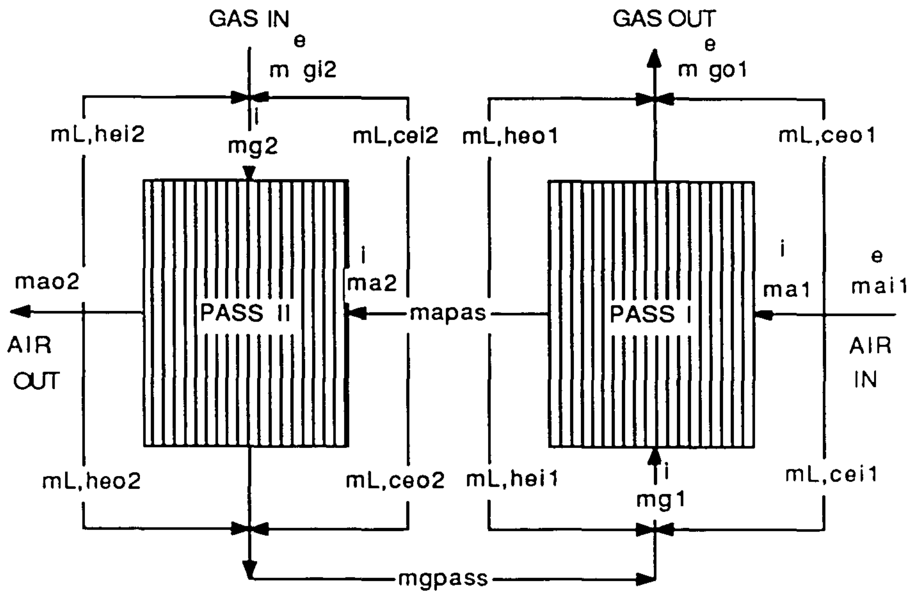

Figure 5.1 Internal and external mass flow rates.

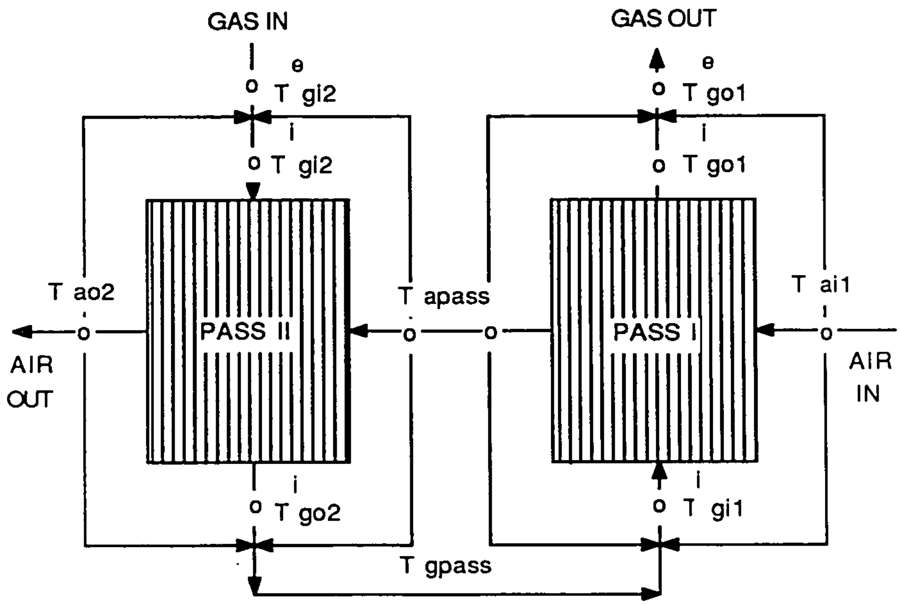

Figure 5.2 Internal and external fluid temperatures.

Internal and external fluid temperature relations can be derived by using conservation of energy and mass. If c_p is constant and $(c_p)_a = (c_p)_g$, then these relations are simplified to

$$T_{ai1} = T^{i}_{ai1} = T^{e}_{ai1} \tag{5.21}$$

$$T_{ao2} = T^{i}_{ao2} = T^{e}_{ao2} \tag{5.22}$$

$$T^{i}_{gi2} = \frac{T^{e}_{gi2} + \frac{\delta_{L,HE2}}{(1+R_{HE2})} T_{ao2} + \frac{\delta_{L,CE2}}{(1+R_{CE2})} T_{apass}}{\sigma} \tag{5.23}$$

where

$$\sigma = \left(1 + \frac{\delta_{L,HE2}}{1+R_{HE2}} + \frac{\delta_{L,CE2}}{1+R_{CE2}}\right) \tag{5.24}$$

$$T_{gpass} = \frac{\sigma T^{i}_{go2} + \frac{\delta_{L,CE2} R_{CE2}}{(1+R_{CE2})} T_{apass} + \frac{\delta_{L,HE2} R_{HE2}}{(1+R_{HE2})} T_{ao2}}{(1+\delta_{L2})} \tag{5.25}$$

$$T^{i}_{gi1} = \frac{(1+\delta_{L2}) T_{gpass} + \frac{\delta_{L,HE1}}{(1+R_{HE1})} T_{apass} + \frac{\delta_{L,CE1}}{(1+R_{CE1})} T_{ai1}}{\eta} \tag{5.26}$$

where

$$\eta = \left(1 + \delta_{L2} + \frac{\delta_{L,HE1}}{1+R_{HE1}} + \frac{\delta_{L,CE1}}{1+R_{CE1}}\right) \tag{5.27}$$

$$T^{e}_{go1} = \frac{\eta T^{i}_{go1} + \frac{\delta_{L,CE1} R_{CE1}}{(1+R_{CE1})} T_{ai1} + \frac{\delta_{L,HE1} R_{HE1}}{(1+R_{HE1})} T_{apass}}{(1+\delta_{L})} \tag{5.28}$$

5.2 Air Preheater Performance With Leakage

The heat transfer effectiveness of the air preheater under consideration is defined as the ratio of the actual heat transfer rate to the thermodynamically maximum possible heat transfer, where the air leakage effect is not considered. If we let c_p be constant throughout the air preheater core for both of the fluids and let the minumum capacity rate be the air capacity rate, then the effectiveness relations are

$$\epsilon_a = \frac{(T_{ao2} - T_{ai1}) - \dfrac{m^e_{gi2}}{m^e_{ai1}}\,\delta_{effect}}{(T^e_{gi2} - T_{ai1})} \tag{5.29}$$

where

$$\delta_{effect} = \left\{\delta_{L,CE1}(T_{ao2} - T_{ai1}) + (\delta_{L,HE1} + \delta_{L,CE2})(T_{ao2} - T_{apass})\right\} \tag{5.30}$$

$$\epsilon_g = \frac{\sigma(T^i_{gi2} - T^i_{go2}) + \eta(T^i_{gi1} - T^i_{go1})}{C_R(T^e_{gi2} - T_{ai1})} \tag{5.31}$$

where C_R is the capacity rate ratio as

$$C_R = \frac{(c_p m)^e_{gi2}}{(c_p m)^e_{ai1}} \tag{5.32}$$

Similar heat transfer effectiveness expressions may be derived for both passes of the air preheater by using the same effectiveness definition.

The air leakage model was added to the computer program which computes the temperature fields within the air preheater. Using the design data of the air preheater (see Appendix A), a number of runs were performed with different air leakage coefficients. At the same time, all other leakage coefficients are kept constant at the following values:

$$R_{\delta 1}=R_{\delta 2}=1.5$$

$$R_{CE1}=R_{CE2}=1.$$

$$R_{HE1}=R_{HE2}=1.$$

The overall air preheater performance decreases with increasing air leakage. This is shown in Figure 5.3 where the effectiveness of both passes are also plotted. Figures 5.4 and 5.5 show the effect of air leakage on outlet gas and air temperatures and mass flow rates, respectively. It is seen that both outlet gas and air temperatures gradually increase as the air leakage increases.

When air leakage is introduced into the present analysis, it becomes difficult to identify the reasons for the changes in temperatures of air, gas, and tube metal due to air leakage, because there are many parameters involved with the heat and mass transfer mechanisms. To illustrate these trends, a table containing those parameters is prepared for two different cases, one with 0% leakage, and the other with 10% leakage (see Table 5.1).

As shown in Table 5.1, the average heat transfer coefficient and total heat transfer rate of *Pass I* are gradually increased as the air leakage increases. This occurs because the gas mass flow rate in *Pass I* increases by 7.5% while the air mass flow rate of *Pass I* decreases by 3.5% due to air leakage. In contrast, the average heat transfer coefficient and total heat transfer rate of *Pass II* are decreased with increasing air leakage due to changes in mass flow rates.

When there is 10% total air leakage, *Pass II* operates with 9.36% lower air mass flow rate, 0.56% lower average heat transfer coefficient, 2.5% higher gas mass flow rate, 2.24% higher inlet air temperature and 0.47% lower inlet gas temperature compared to the no-leakage case. Since less heat is transfered from the gas to air, the gas leaves *Pass II* with a higher temperature and mass. On the other hand, temperatures of air and tube metal within *Pass II* are increased because less air mass flows through *Pass II*, as shown in Figures 5.4 and 5.6. The gas temperatures decrease close to the gas-inlet section of *Pass II* due to the cold and hot end air leakage flows through the gas-inlet section (see Figure 5.4). The internal gas inlet temperature (T^i_{gi1}) and internal gas mass flow rate of *Pass I* increase with inreasing air leakage (see Table 5.1). The increases in the internal gas mass flow rate and internal gas inlet temperature of *Pass I* due to air leakage cause to increase air, gas, and tube metal temperatures in *Pass I* (see Figures 5.4 and 5.6).

Table 5.1 Results of air leakage analysis.

$R_{\delta 1}=R_{\delta 2}=1.5$; $R_{CE1}=R_{CE2}=1.$; $R_{HE1}=R_{HE2}=1.$

	$\delta_L=0\%$	$\delta_L=10\%$	increase, %
U_1, $W/m^2\ K$	29.1625	29.6091	1.53
U_2, $W/m^2\ K$	35.0629	34.8659	-0.56
Q_1, kW	75,986.6653	78,564.2883	3.39
Q_2, kW	62,192.3926	55,557.3250	-10.67
$m^i{}_{a1}$, kg/s	536.000	517.195	-3.51
$m^i{}_{a2}$, kg/s	536.000	485.853	-9.36
$m^i{}_{g1}$, kg/s	626.840	673.853	7.50
$m^i{}_{g2}$, kg/s	626.840	642.511	2.50
$T^i{}_{gi1}$, K	520.103	524.794	0.90
$T^i{}_{go1}$, K	392.052	400.676	2.20
$T^i{}_{gi2}$, K	614.820	611.946	-0.47
$T^i{}_{go2}$, K	520.103	529.427	1.79
T_{ai1}, K	302.600	302.600	0.00
$Tapass$, K	442.801	452.729	2.24
T_{ao2}, K	555.196	563.322	1.46

It should be kept in mind that all preceding discussions are based on the given constant leakage ratio parameters. For different values of leakage ratio parameters ($R_{\delta 1}$, $R_{\delta 2}$, R_{CE1}, R_{HE1}, R_{CE2}, R_{HE2}), the results of the air leakage analysis may change. It is, therefore, very important to know these parameters.

One of the most exasperating problems in air preheater maintenance is the detection, location, and correction of small leaks. Large leaks can be easily located, but small leaks are usually hard to detect and still harder to locate precisely so that they can be repaired. Any leakage model, therefore, will not represent the real effect of air leakages on the performance of the air preheater. We were not able to verify the model with the field data. However, we believe that the presented air leakage model will give approximate information on how the air leakages affect the performance of the air preheater.

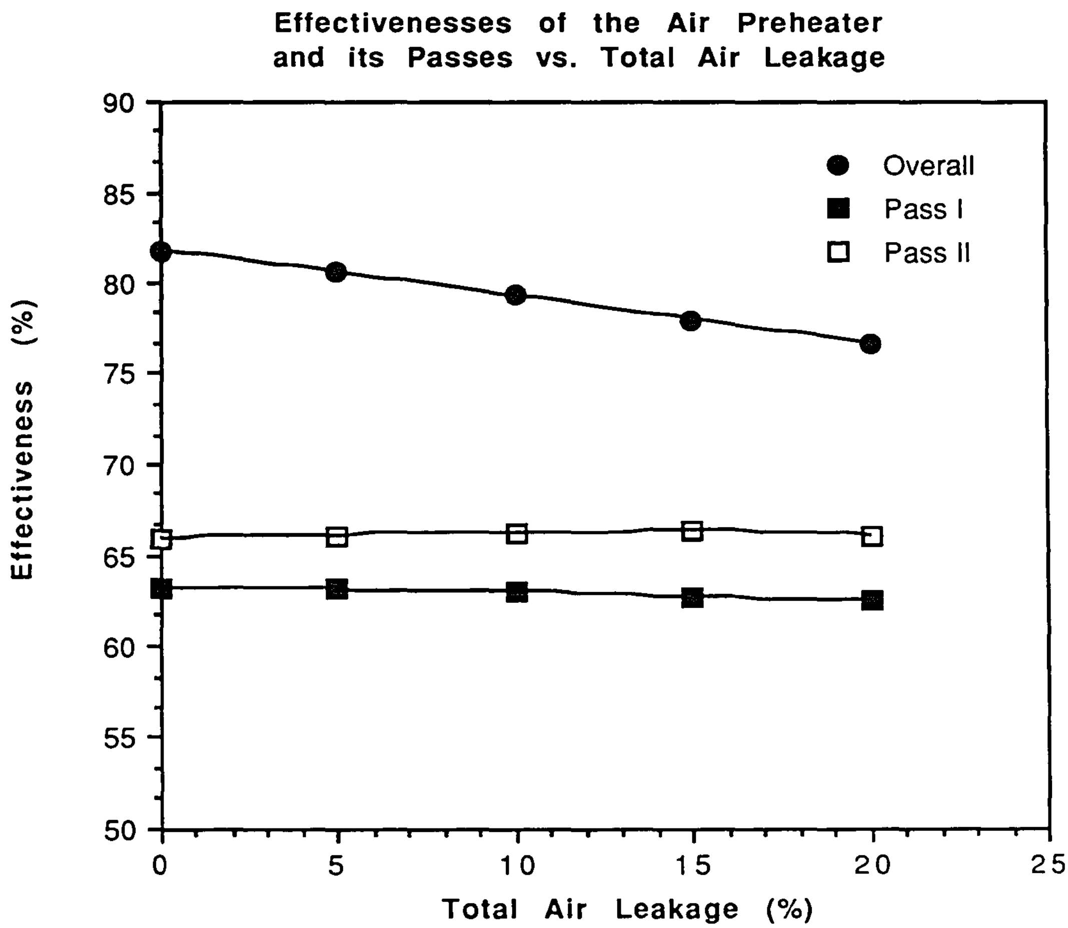

Figure 5.3 The air leakage effect on the air preheater performance.

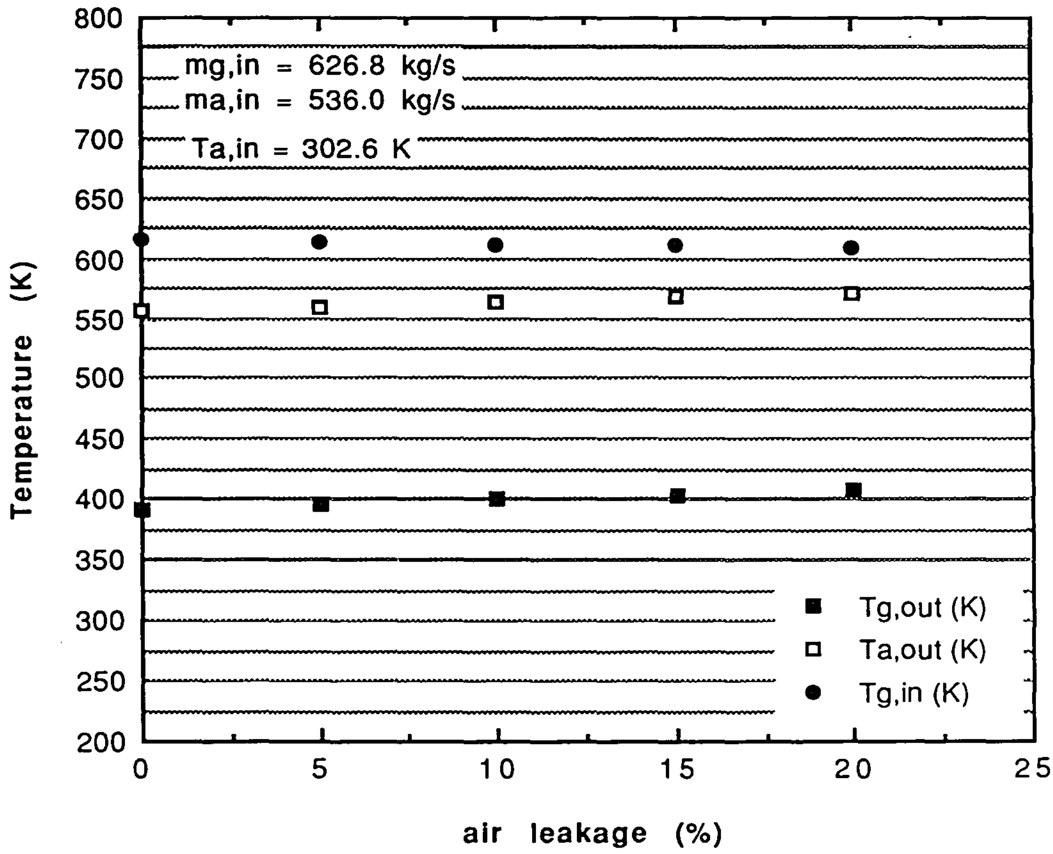

Figure 5.4 The air leakage effect on internal gas inlet (T^{i}_{gi2}), external gas outlet (T^{e}_{go1}), and external air outlet (T_{ao2}) temperatures.

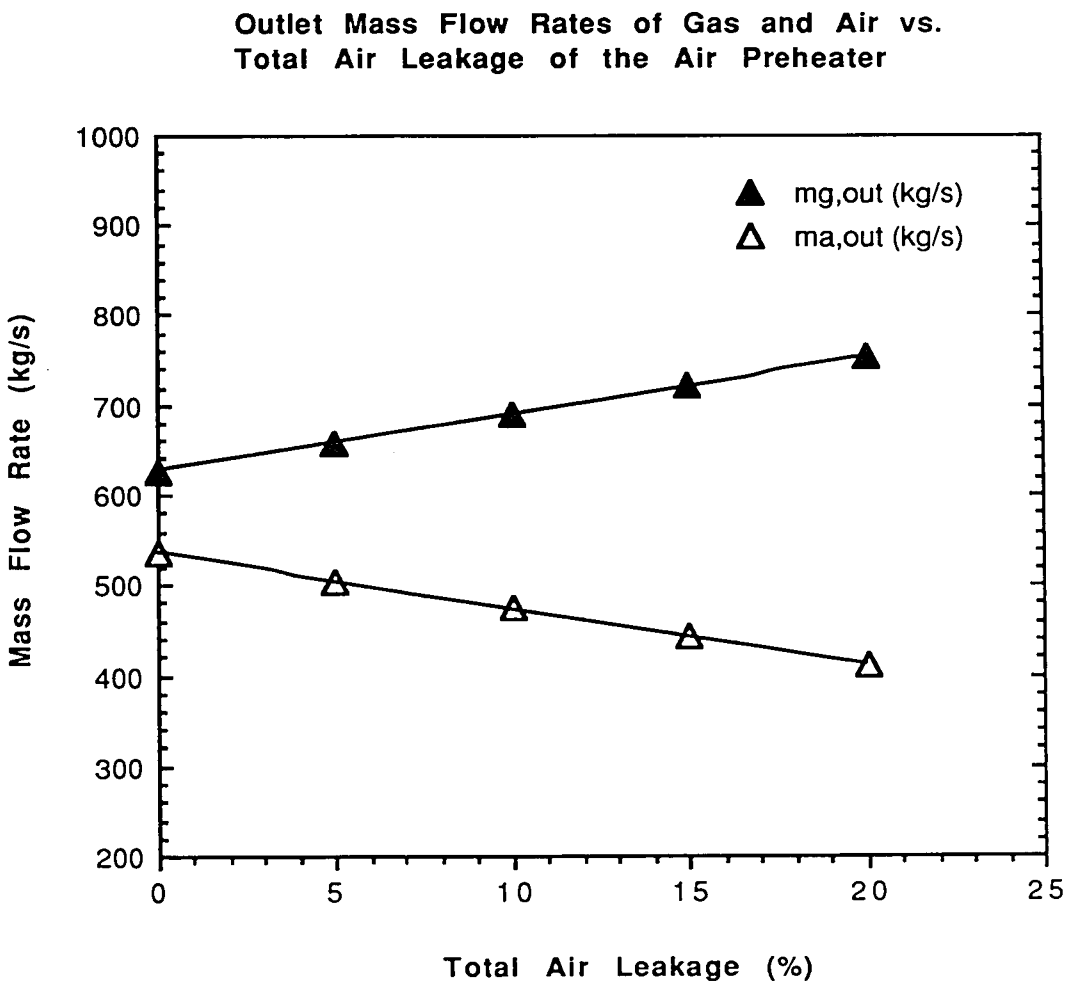

Figure 5.5 The air leakage effect on mass flow rates of the air preheater.

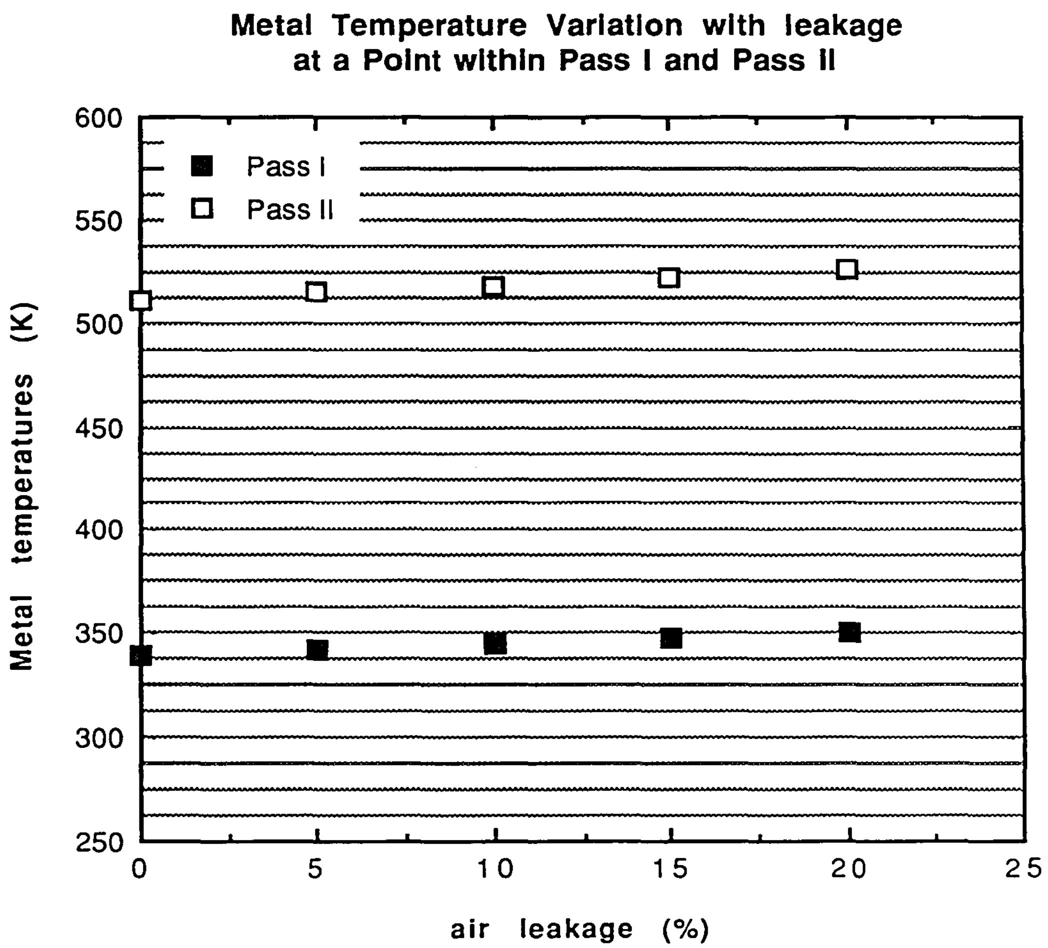

Figure 5.6 Metal temperature variation with leakage at x=.24 m and y=9.21 m within *Pass I* and at x=.31 m and y=.48 m within *Pass II*.

6. COMPUTER ALGORITHM

6.1 Introduction

A large number of tubular air preheaters in coal fired power plants have experienced difficulty with plugging and corrosion. The presence of sulfur trioxide in a flue gas elevates the dew point of the gases. Water vapor condences and forms an acid with the sulfur trioxide and the corrosion of the tubes results in iron sulphate. To protect the tubes from acid deposition and corrosion, we need to keep the metal temperature field of the air preheater above the dew point temperature. This requires that information on the metal temperature field within the air preheater be available as a function of operating parameters.

Information on metal temperature can be obtained either by direct measurements or by numerical simulation. Measurements of metal temperatures are not practical except for research purposes; therefore, numerical simulation of the heat transfer process is the only alternative.

A computer program named TPHMT (Tubular Air Preheater Metal Temperature), developed for a two-pass counter-crossflow tubular air preheater, computes the metal temperature field of the air preheater as a function of operating parameters. The mathematical model, presented in Chapter 4.1, uses an iterative procedure to obtain the solutions.

6.2 General Approach in the TPHMT Code

The computer code TPHMT is made up of the main program and 21 subroutines. A flow chart of the TPHMT code is shown in Figure 6.1.

The code starts by reading the input data and then performs the initial operations including: calculation of internal and external flow rates of gas and air through the air preheater and calculation of dimensional velocity and temperature profiles of gas and air at the inlet of the air preheater.

With the aid of a do-loop, the code performs a cyclical iteration until convergence is achieved. The iteration starts with an assumed inlet gas temperature at *Pass I*. (see Figure 6.2). Using subroutine APHTM which performs all necessary mathematical model calculations of a single-pass crossflow exchanger (Chapter 4.1); the code first calculates the temperature fields of *Pass I* starting from A and ending at C, then the same calculations are done for *Pass II*. This is the first iteration in the code and more reiterations come after that unless the calculated inlet gas temperature of *Pass I* agrees with the assumed one within an acceptable error. When the convergence criterion is satisfied, the code computes the heat transfer performance of each pass and the overall air preheater performance. Finally, it displays the results with the input data in tabular forms. Results of metal temperature distribution within the air preheater are stored in a result file for plotting.

In all cases, convergence to a final steady state solution has been rapid and generally occurs in about 10 iterations. (This correspondes to about 3 seconds of CPU time on a CDC 855 Cyber System.)

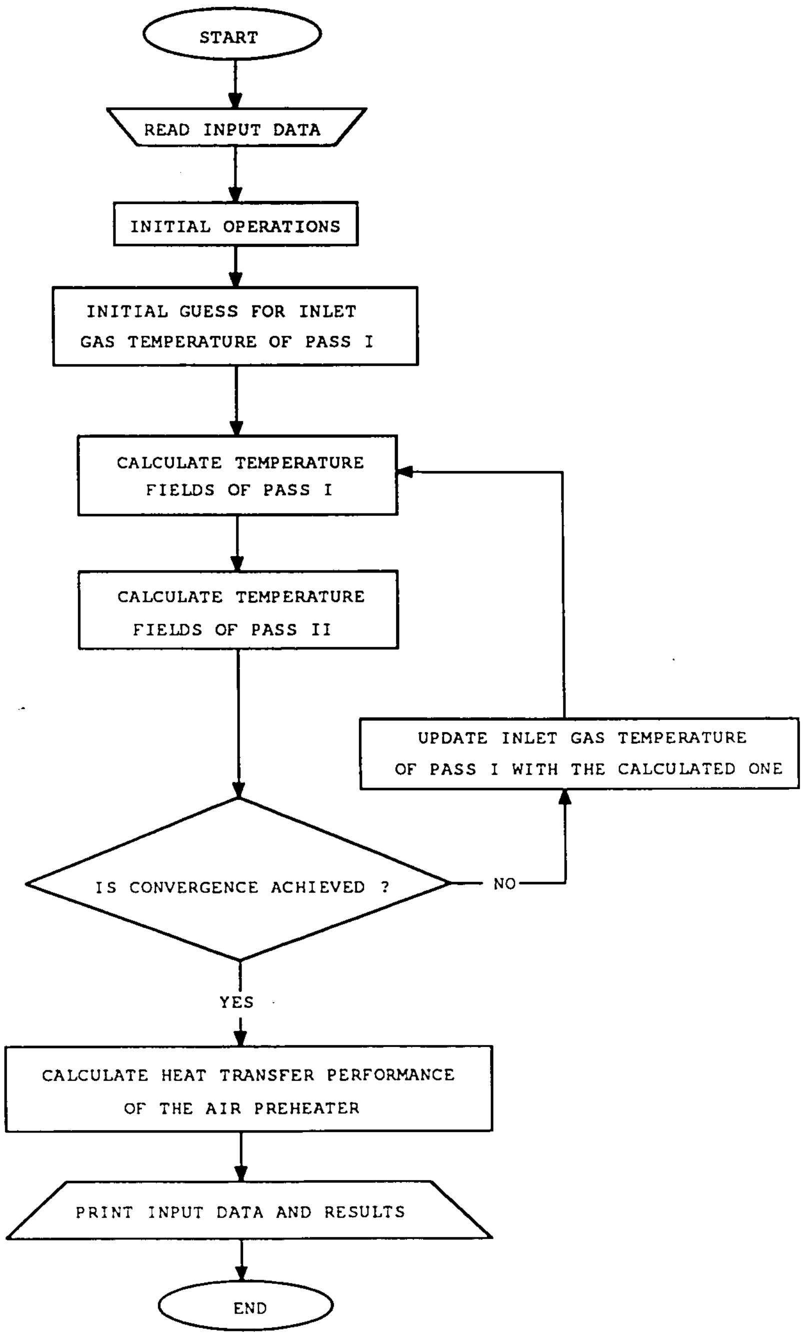

Figure 6.1 Flow chart of computer code TPHMT.

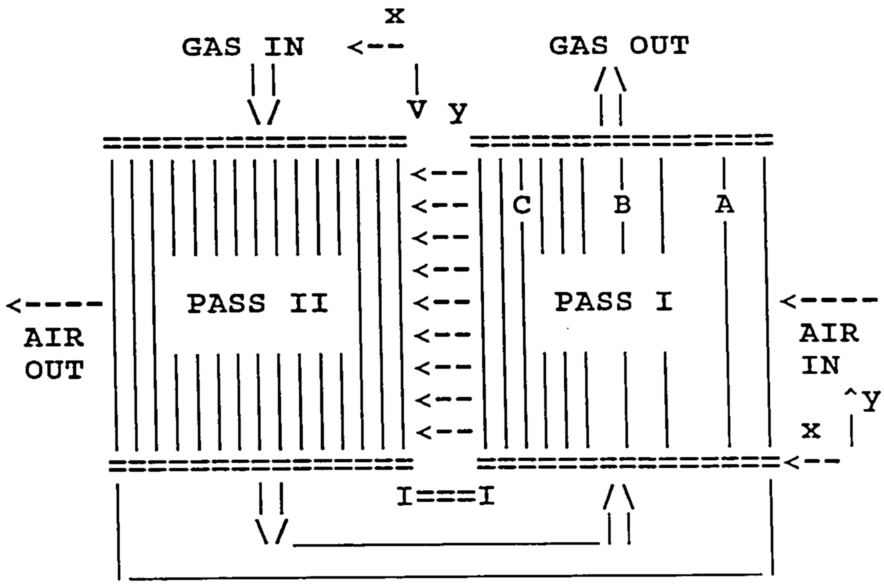

Figure 6.2 The sketch of the tubular air preheater.

6.2.1 *Input Data*

To run the TPHMT code, the user must supply the following data:

– *flow rates of gas and air*

– *average gas and air temperatures at the inlet of the air preheater*

– *air leakage coefficients (if any)*

– *geometry of the air preheater*

– *dimensions of the grids*

– *inlet gas velocity and temperature variations in nondimensional form*

—thermal conductivity of the tube metal

—gas side and air side average pressures

6.2.2 *Possible Applications of the Computer Program*

The TPHMT code is a computational tool which enables the user to analyze the effect of changes in operating parameters and design on the performance of two-pass counter-crossflow tubular air preheaters and on the temperature fields of working fluids and tube metal.

Some of the possible applications include:

1. Analysis of the effects of changes in the inlet air temperature
2. Analysis of the effects of air leakage.
3. Analysis of the effects of design changes
4. Analysis of the effects of flow and temperature stratifications

Concerning the first possible application, inlet air temperature control is typically done by the use of steam coils or by recirculating a portion of the hot air from the air preheater outlet back to the forced draft fan inlet.

For the second possible application, as indicated earlier in Chapter 5.1, the air leakages increases the longer air preheater stays in service. The effects of air leakage on the performance of the air preheater under consideration and on the metal temperature distribution within the tube bundle can be easily analyzed by the TPHMT Code.

As for the third possible application, the effects of any proposed design change in the subject air preheater geometry, such as addition or removal of heat transfer surfaces or a change in its design, can be analyzed by using the TPHMT

Code before actual modifications are made.

Analysis of other parameters, such as stratification in the inlet air/gas velocities and temperatures or variations in unit load, is also possible with the code.

6.3 Results of Sample Calculations

The results presented here were obtained by the TPHMT for a two-pass counter-crossflow tubular air preheater at Allegheny Power Company's Fort Martin Power Plant. This air preheater has three different tube bundle arrangements within *Pass I* as shown in Figure 6.2. The geometry characteristics and operating conditions of the air preheater are summarized in Appendix A. In these calculations, outlet gas and air temperatures and the heat transfer performance of the air preheater as well as the metal temperature distribution were predicted as a function of the following parameters:

- *inlet air temperature*
- *inlet gas temperature*
- *mass flow rate of gas*
- *mass flow rate of air*

Uniform temperature and velocity profiles at the air preheater inlet were assumed in the calculations.

6.3.1 *Effect of Inlet Air Temperature*

The TPHMT Code was run with inlet air temperature varying from 297 to 308.2 K. The effectiveness of the air preheater remains almost constant as shown in Figure 6.3. The temperatures of the gas and air at the outlet of the air preheater all increase as the inlet air temperature is increased, as shown in Figures 6.4 and 6.5. The metal temperatures within *Pass I* decrease sharply as the inlet air temperature decreases (see Figure 6.6), whereas in *Pass II*, the effect of inlet air temperature is small, as shown in Figure 6.7.

6.3.2 *Effect of Inlet Gas Temperature*

The effectiveness of the air preheater increases gradually as the inlet gas temperature is increased (see Figure 6.3). The temperature of the air and gas at the outlet of the air preheater all increase with increasing the inlet air temperature, as shown in Figures 6.4 and 6.5. The metal temperatures within *Pass II* increases sharply as the inlet gas temperature increases (see Figure 6.7), while the metal temperatures within *Pass I* increases gradually (see Figure 6.6).

6.3.3 *Effect of Gas Flow Rate*

Solutions were obtained with the mass flow rate of gas varying from 550 to 690 kg/s. As the mass flow rate of gas is increased, the outlet air and gas temperatures increase as well (see Figures 6.8 and 6.9). The effectiveness and metal temperatures of the air preheater also increase when the mass flow rate of gas is increased (see Figures 6.10 , 6.11, and 6.12)

6.3.4 *Effect of Air Flow Rate*

The mass flow rate of air was varied from 482.4 to 589.6 kg/s. It was seen that the effectiveness of the air preheater (Figure 6.10) and both outlet gas and air temperatures decrease as the mass flow rate of air is increased as shown in

Figure 6.8 and 6.9. The metal temperatures within *Pass I* and *Pass II* increase as the mass flow rate of air is increased, as shown in Figures 6.11 and 6.12.

The metal temperature distributions within *Pass I* and *Pass II* are plotted in Figures 6.13 and 6.14, respectively. These metal temperature distributions are the results of the code when the design operating conditions of the air preheater (Appendix A) are used as input data.

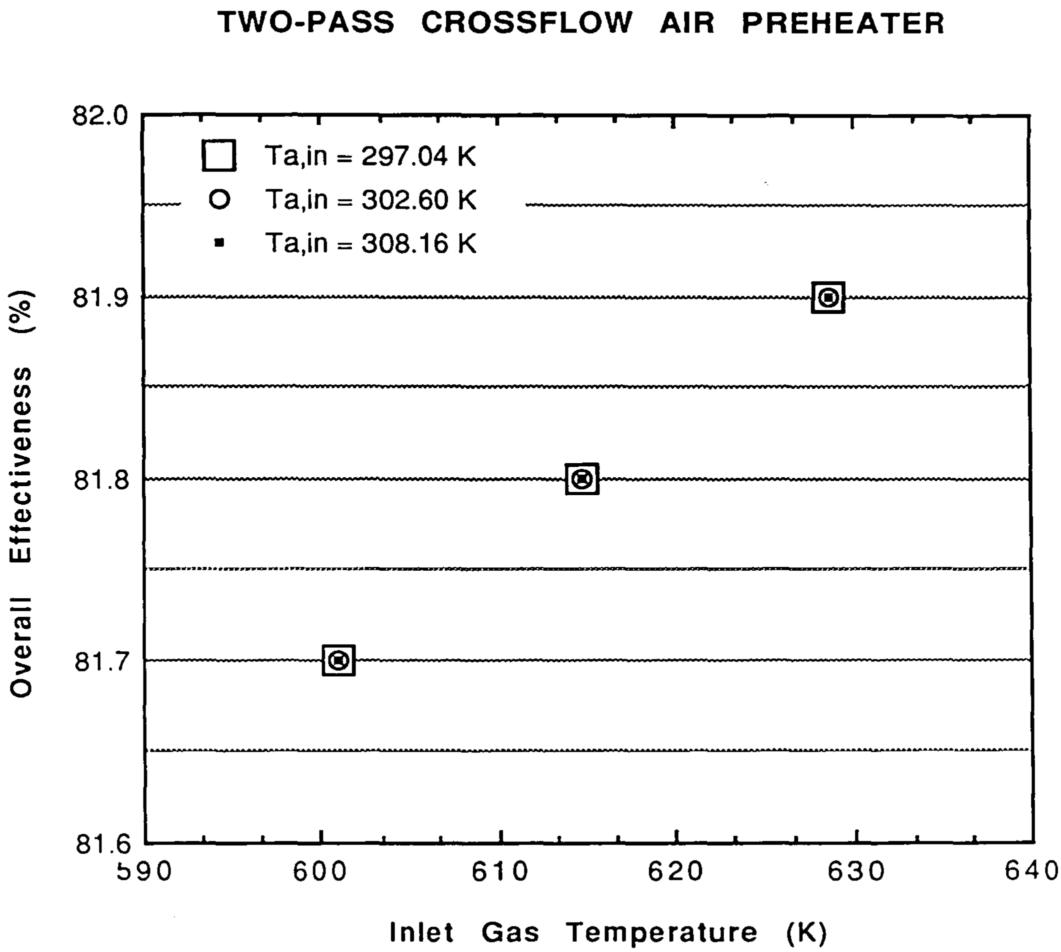

Figure 6.3 The effect of the inlet gas and air temperature on the overall effectiveness of the air preheater.

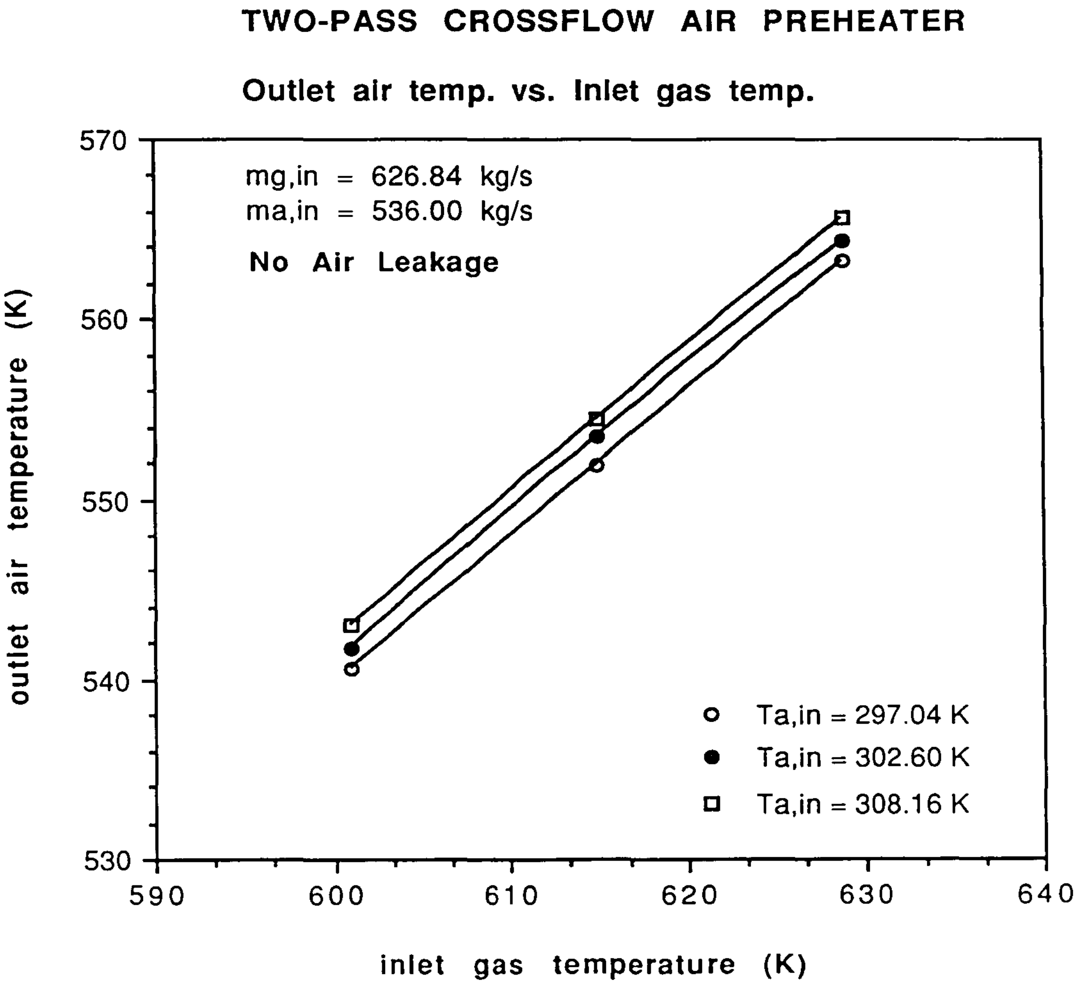

Figure 6.4 The effect of the inlet gas and air temperature on the outlet air temperature of the air preheater.

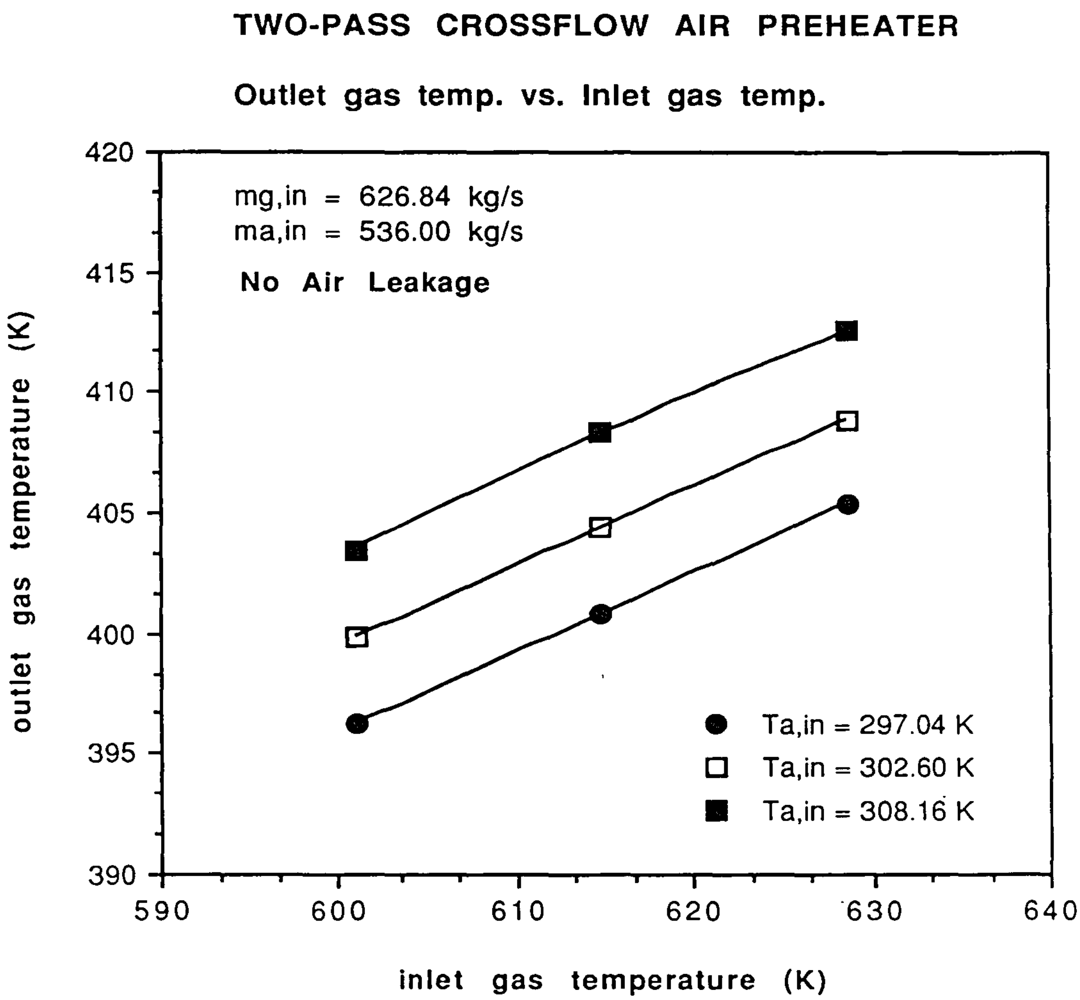

Figure 6.5 The effect of the inlet gas and air temperature on the outlet gas temperature of the air preheater.

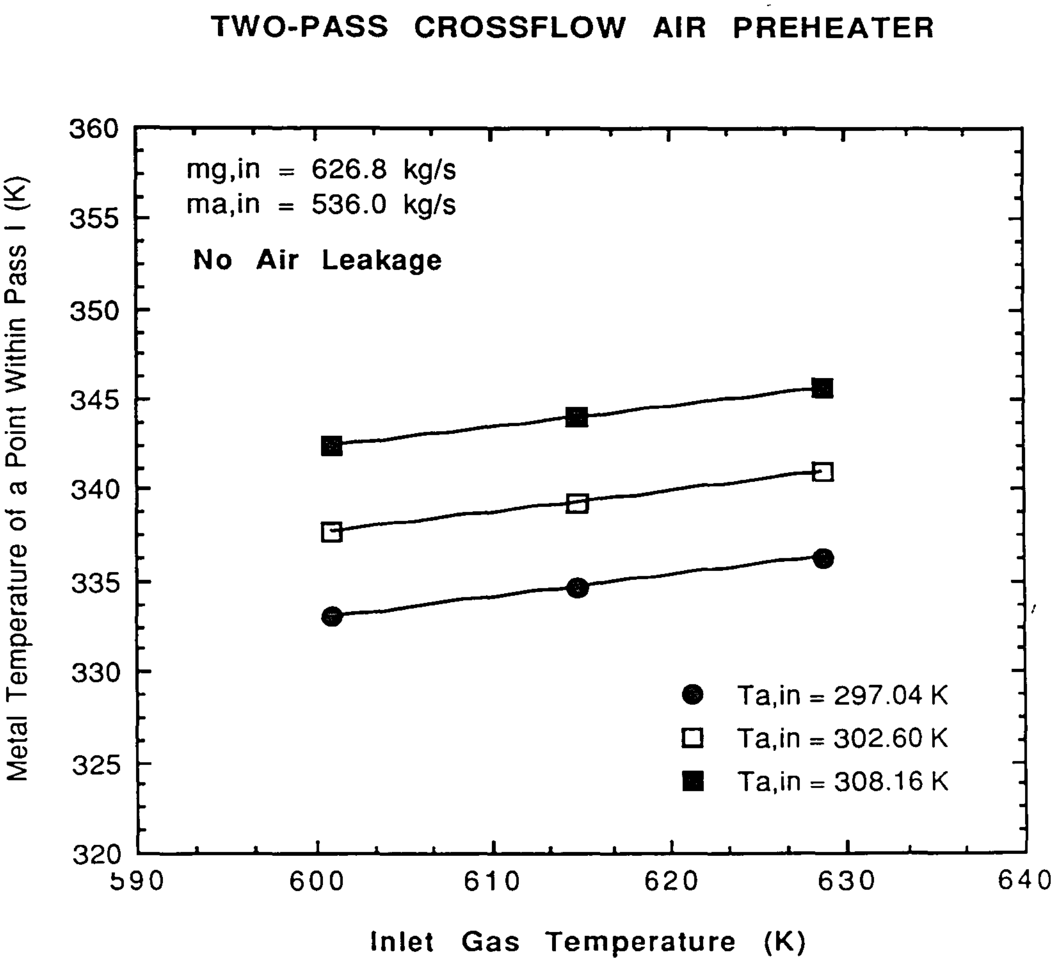

Figure 6.6 Metal temperature variation with the inlet gas and air temperatures of the air preheater at x=.24 m and y=9.21 m within *Pass I*.

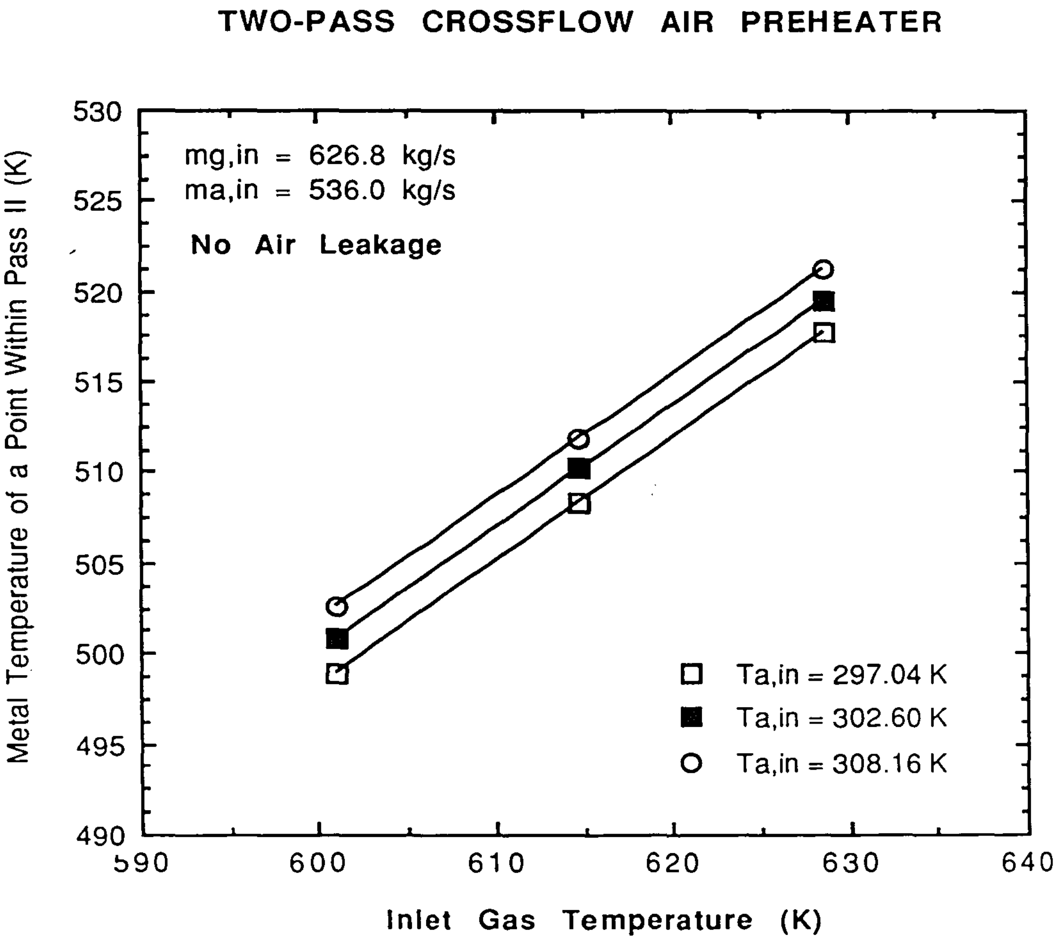

Figure 6.7 Metal temperature variation with the inlet gas and air temperatures of the air preheater at x=.31 m and y=.48 m within *Pass II*.

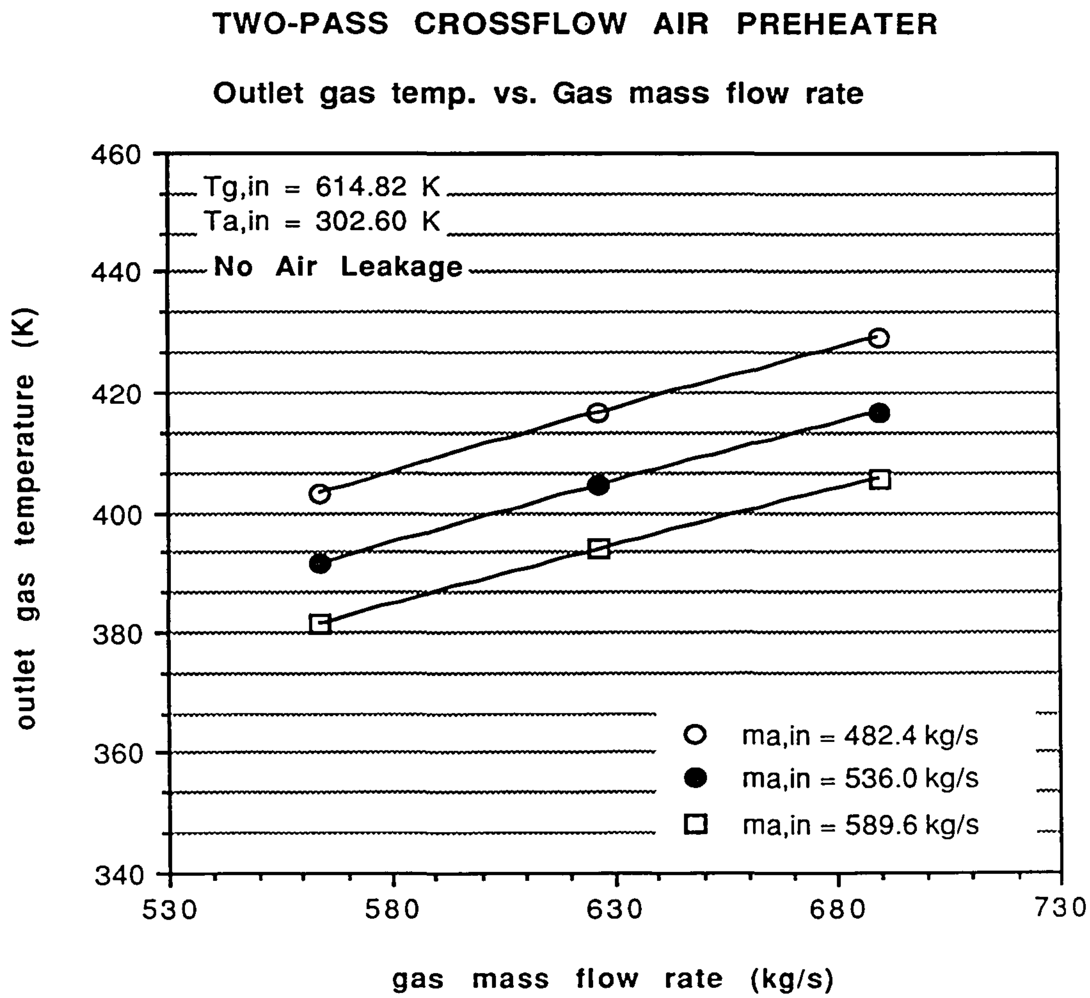

Figure 6.8 The effect of the mass flow rates of gas and air on the outlet gas temperature of the air preheater.

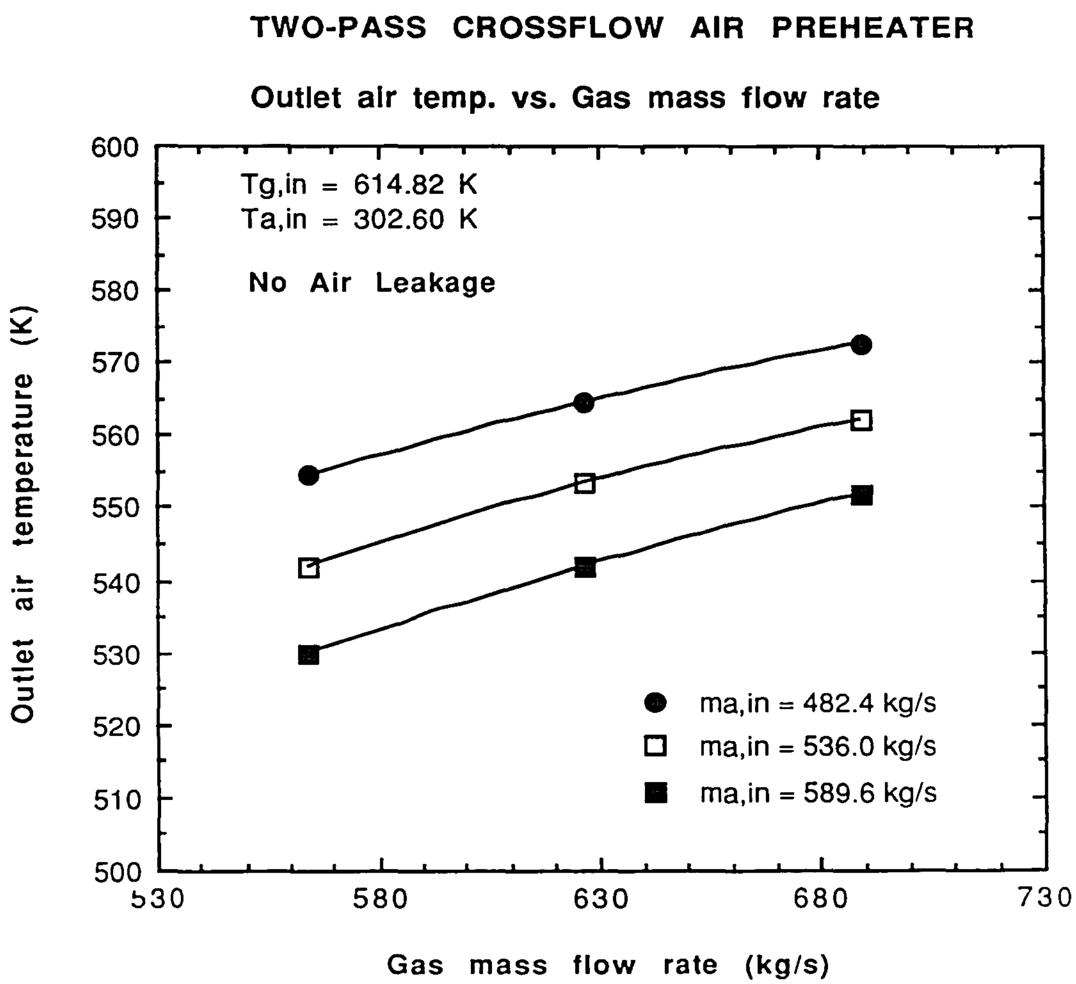

Figure 6.9 The effect of the mass flow rates of gas and air on the outlet air temperature of the air preheater.

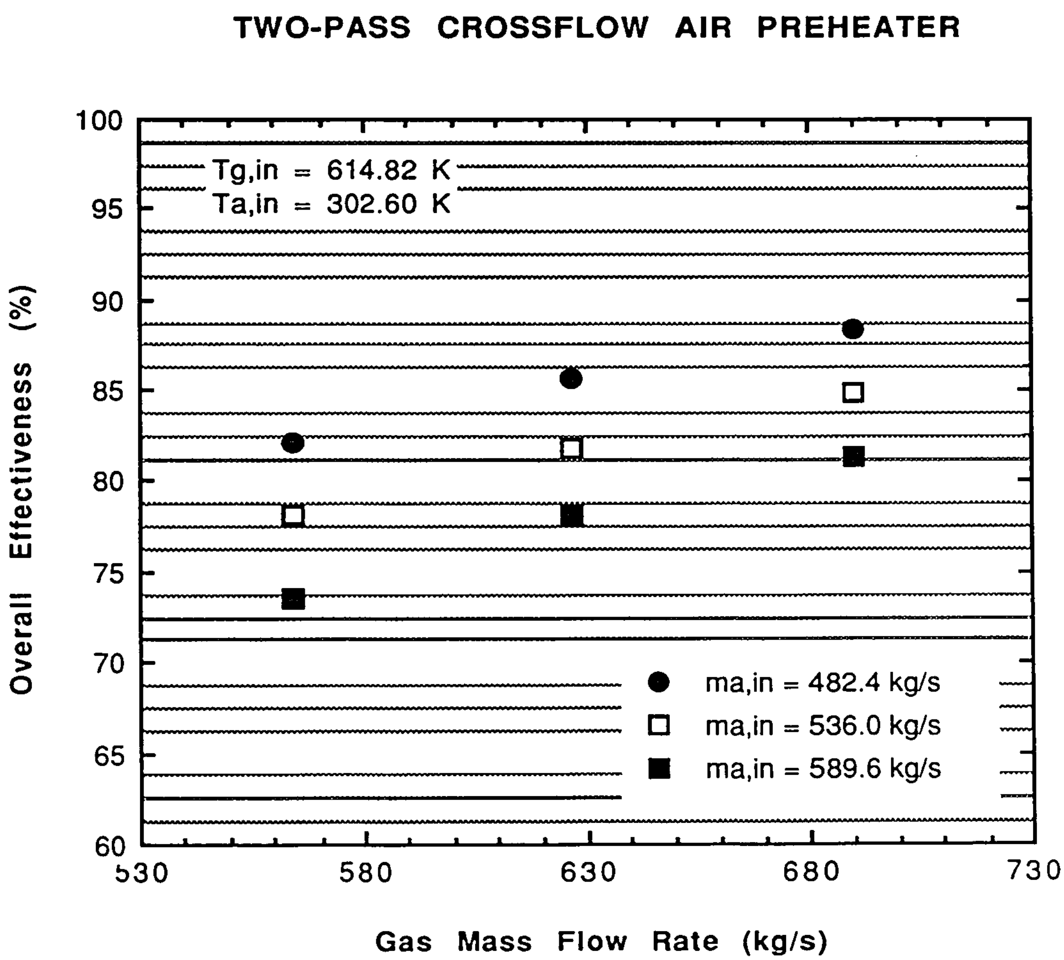

Figure 6.10 The effect of the inlet gas and air mass flow rates on the overall effectiveness of the air preheater.

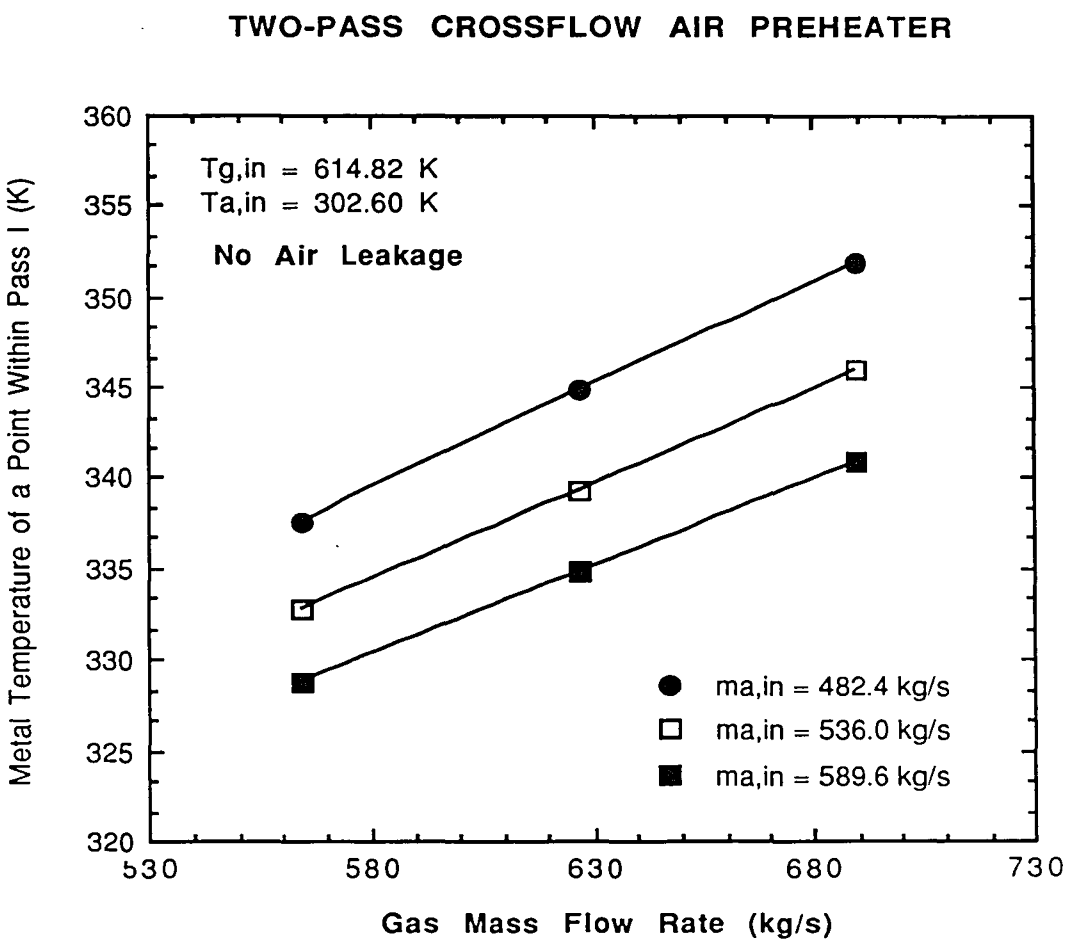

Figure 6.11 Metal temperature variation with the inlet gas and air mass flow rates of the air preheater at x=.24 m and y=9.21 m within *Pass I*.

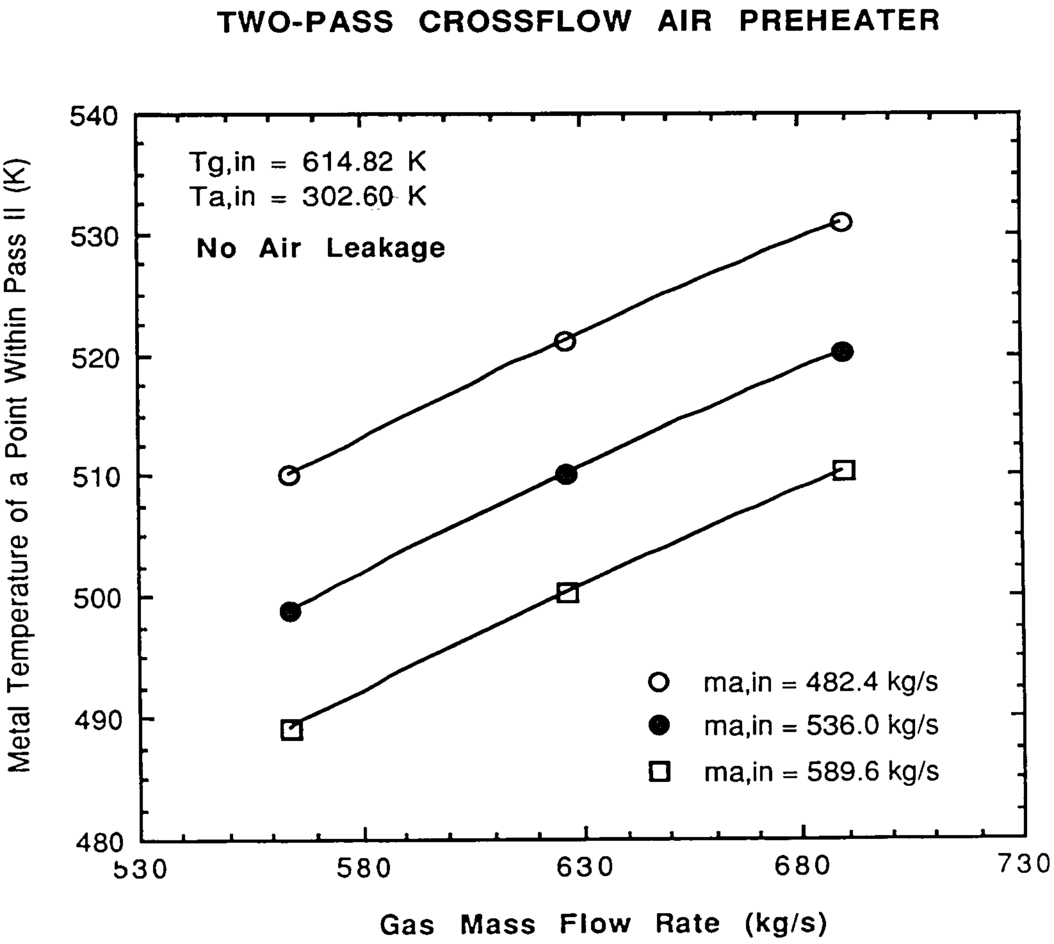

Figure 6.12 Metal temperature variation with the inlet gas and air mass flow rates of the air preheater at x=.31 m and y=.48 m within *Pass II*.

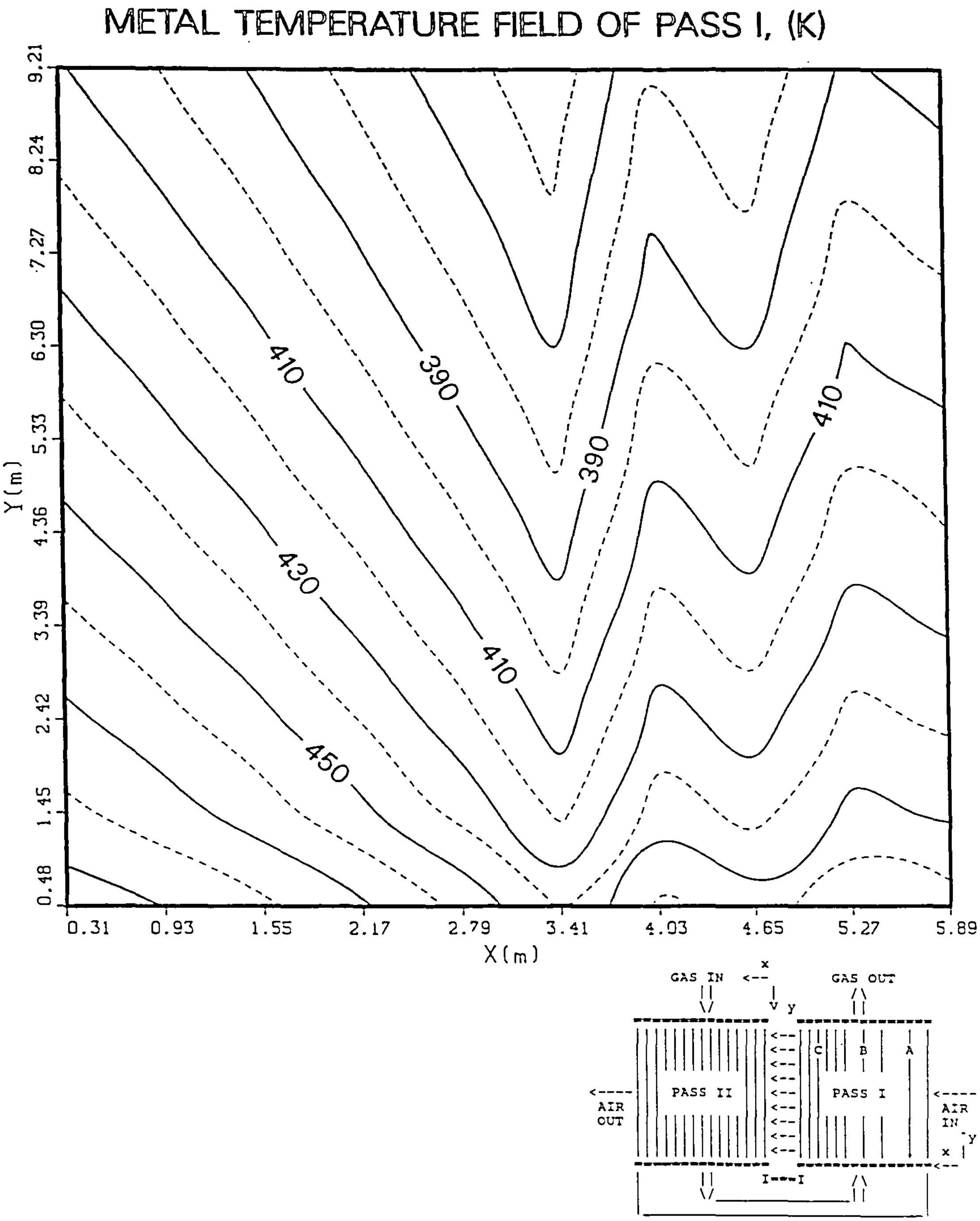

Figure 6.13 Metal temperature distribution within *Pass I* for baseline conditions.

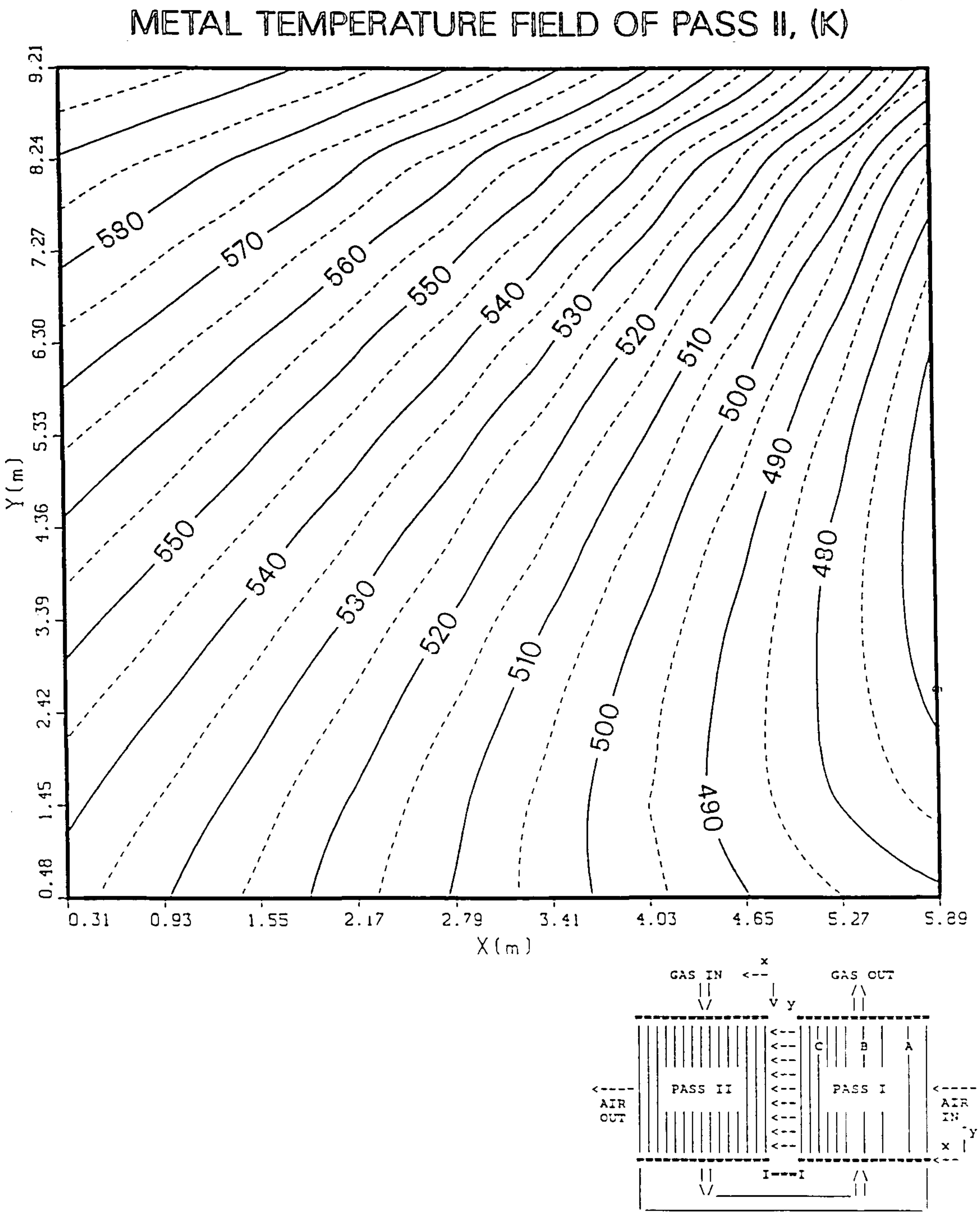

Figure 6.14 Metal temperature distribution within *Pass II* for baseline conditions.

7. SUMMARY AND CONCLUSIONS

A mathematical model has been developed to predict the metal temperature field, both working fluid temperature fields and heat transfer characteristics of crossflow type tubular air preheaters. A computer program applying this mathematical model to a two-pass counter-crossflow tubular air preheater has been created. The effects of air preheater operating parameters on the tube metal temperature and the performance of this particular air preheater are easily evaluated with the aid of the computer program. Prediction of the tube metal temperature field would enable the utility to operate the air preheater at the onset of acid deposition and corrosion.

Based on the results of this study, we have concluded that the presented computer modeling technique can be used

- To analyse the effects of air leakage on the performance of the air preheater.
- To study acid deposition and corrosion phenomena on the tubes.
- To modify air preheater geometries in existing units.
- To design new air preheaters for new units.

Work is continuing at the Energy Research Center to verify this computer modeling technique with field data and apply it to different crossflow arrangements of air preheaters. For example, it is presently being used to study three and four-pass counter-crossflow air preheaters.

8. RECOMMENDATIONS FOR FUTURE WORK

Tubular air Preheaters may be arranged with more than two passes. As long as the passes of the air preheater have a crossflow arrangement, the basic approach used in the computer program (Chapter 6.) will enable us to find the temperature fields and heat transfer characteristics of the air preheater. However, each additional case requires a special version of the code.

Figure 8.1 shows some of these multi-pass crossflow air preheater arrangements with various directions of the working fluids. As seen from these arrangements, some of the passes have different flow directions and boundary conditions. Therefore, the equations and calculation sequence described in Chapter 4.1 should be modified for those passes. There are four possible gas/air flow direction combinations. For each gas/air flow direction combination there are four boundary conditions (see Fig. 8.2) yielding 16 different cases which need to be modelled computationally. A separate subroutine should be written for each of these 16 different cases, if an expansion of the capabilities of the TPHMT code is desired.

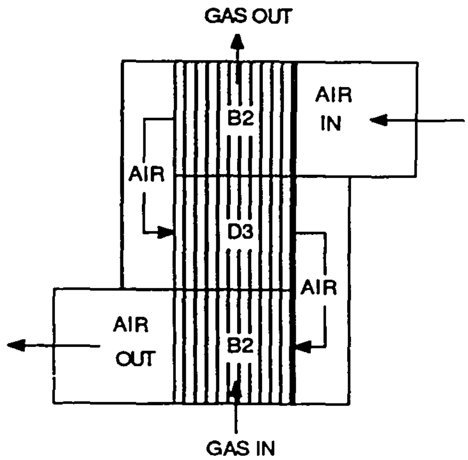

a)

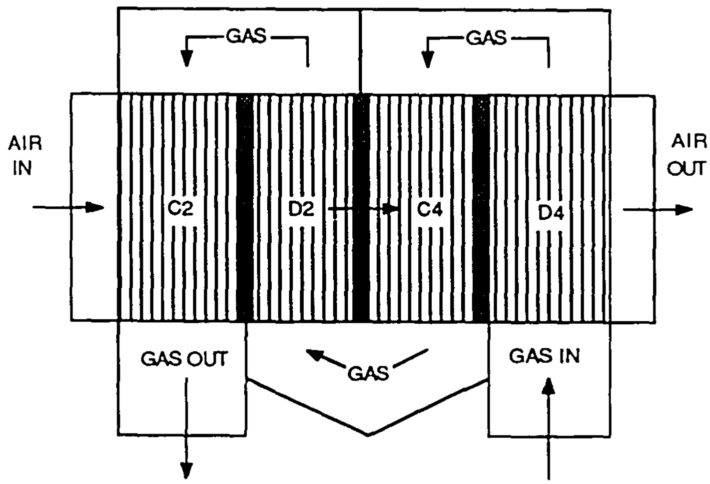

b)

Figure 8.1 Multi-pass crossflow air preheaters; a) three-pass counter-crossflow, b) four-pass counter-crossflow

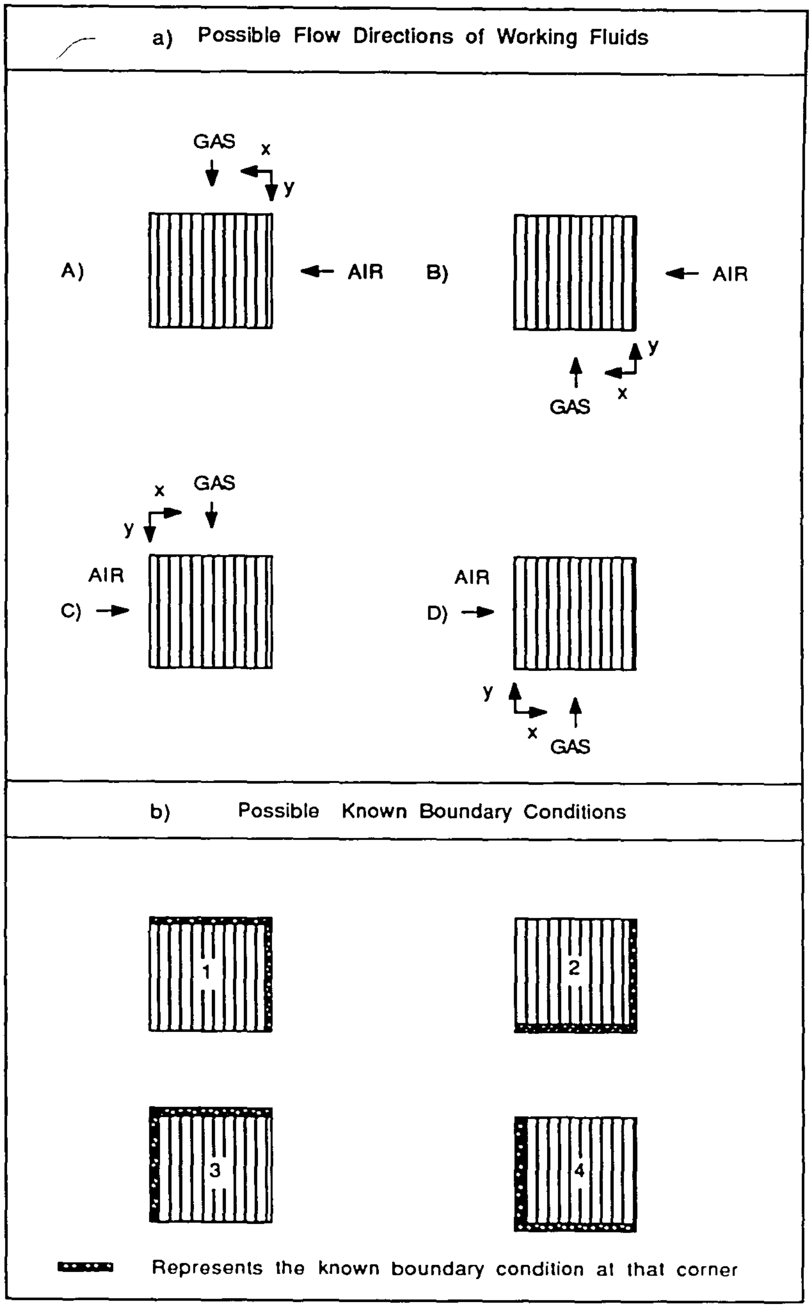

Figure 8.2 a) Possible flow directions, and b) possible given boundary conditions of a single-pass crossflow exchanger.

REFERENCES

[1] Kays, W. and London, A. L., Compact Heat Exchangers, 3rd ed., McGraw, New York, 1984.

[2] Mason, J. L., 'Heat Transfer in Crossflow,' *Proc. Appl. Mechanics*, 2nd U.S. Nat. Congress, 1954, p. 801.

[3] Chung, H. L., 'A New Simplified Formula for Crossflow Heat Exchanger Effectiveness,' *ASME Journal of Heat Transfer*, Vol. 109, 1987,pp. 521-22.

[4] Bankhe, G. D. and Howard, C. P., 'The Effect of Longitudinal Heat Conduction on Periodic-Flow Heat Exchanger Performance,' *Trans. ASME*, *Journal of Engineering for Power*, Vol. 86, Series A, 1964, pp. 105-120.

[5] Schultz, B. H., 'Regenerators with Longitudinal Heat Conduction,' *IME-ASME General Discussion on Heat Transfer*, London, England, 1951, pp. 440-43.

[6] Hahnemann, H. W., 'Approximate Calculation of Thermal Ratios in Heat Exchangers Including Heat Conduction in Direction of Flow,' *National Gas Turbine Establishment Memorandum*, No. M36, 1948.

[7] Kroeger, P. G., 'Performance Deterioration in High Effectiveness Heat Exchanger Due to Axial Heat Conduction Effects,' 1966 *Cryogenic Engineering Conference*, Boulder, Colo.

[8] Landau, H. G. and Hlinka, J. W., 'Steady State Temperature Distribution in a Counterflow Heat Exchanger Including Longitudinal Conduction in the Wall,' *ASME paper, No.* 60-*WA*-236, 1960.

[9] Chiou, J. P., 'Thermal Performance Deterioration in Crossflow Heat

Exchanger Due to Longitudinal Heat Conduction in the Wall,' *ASME 76-WA/HT-8, paper presented at ASME Winter Annual Meeting*, 1976.

[10] Shah, R. K. and A. L. London, 'Laminar Flow Forced Convection in Ducts,' Supplement 1 to *Advances in Heat Transfer*, Academic Press, New York, 1978.

[11] Shah, R. K. and M. S. Bhatti, in S. Kakac, R. K. Shah, and W. Aung, Eds., *Handbook of Single-Phase Convective Heat Transfer*, Wiley-Interscience, New York, 1987.

[12] Heaton, H. S., W. C. Reynolds, and W. M. Kays, 'Heat Transfer in Annular Passages. Simultaneous Development of Velocity and Temperature Field in Laminar Flow,' *Int. J. Heat Mass Transfer*, Vol. 7, 1964, pp. 763-781.

[13] Kays, W., 'Numerical Solutions for Laminar-Flow Heat Transfer in Circular Tubes,' *Trans. ASME*, Vol. 77, 1955, pp. 1265-1274.

[14] Petukhov, B. S. and V. N. Popov, 'Theoretical Calculation of Heat Exchange and Frictional Resistance in Turbulent Flow in Tubes of an Incompressible Fluid with Variable Physical Properties,' *High Temperature* ,Vol. 1, No. 1, 1963, pp. 69-83.

[15] Petukhov, B. S., in T. F. Irvine and J. P. Hartnett, Eds., *Advances in Heat Transfer*, Vol. 6, Academic Press, New York, 1970.

[16] Gnielinski, V., *Int. Chem. Eng.*, Vol. 16, p. 359, 1976.

[17] Kays, W. and H. C. Perkins, 'Forced Convection, Internal Flow in Ducts,' *Handbook of Heat Transfer, Fundamentals*, 2nd ed., ed. W. M. Rohsenow, J. P. Hartnett, and E. N. Ganic, Chapter 7, McGraw, New York, 1985.

[18] Mills, A. F., 'Experimental Investigation of Turbulent Heat Transfer in

the Entrance Region of a Circular Conduit,' *J. Mech. Eng. Sci.*, Vol. 4, 1962, pp. 63-77.

[19] Nikuradse, J. : Forsch. Arb. Ing.—Wes., no. 361, 1933; English transl., *NACA TM* 1292.

[20] Schlichting, H., Experimentelle Untersuchungen Zum Rauhigkeitsproblem, Ing.—Arch., Vol. 7, pp. 1-34, 1936; English transl. *Proc ASME*, 1936.

[21] Moody, L. F., 'Friction Factors for Pipe Flow,' *Trans. ASME*, Vol. 66, 1944, pp. 671-684.

[22] Norris, R. H., 'Some Simple Approximate Heat Transfer Correlations for Turbulent Flow in Ducts with Rough Surfaces,' *Augmentation of Convective Heat and Mass Transfer*, *ASME*, New York, Dec. 1970.

[23] Zukuaskas, A. A., *Heat Transfer in Tube Banks in Crossflow*, Hemisphere Publishing Corp., New York, 1988.

[24] Incropera, F. P. and D. P. Dewitt, *Fundamentals of Heat Mass Transfer*, 3rd ed., John Wiley & Sons, New York, 1990.

[25] Korst, H. H., 'Mean Temperature Difference in Multi-Pass Crossflow Heat Exchangers,' *Proceedings of the First U.S. National Congress of Applied Mechanics*, *ASME*, New York, 1952, pp. 949-55.

[26] Stevens, R. A., J. Fernandez, and J. R. Woolf, 'Mean-Temperature Difference in One, Two and Three-Pass Crossflow Exchangers,' *Trans. ASME*, Vol. 79, 1957, pp. 287-97.

APPENDIX A

An example Output of the TPHMT Code for the Design Operating Conditions of the Air Preheater at Allegheny Power Company's Fort Martin Power Plant

```
TTTTTTT  PPPPPP  H     H  M       M  TTTTTTT
   T     P    P  H     H  M M   M M     T
   T     PPPPPP  HHHHHHH  M   MM  M     T
   T     P       H     H  M       M     T
   T     P       H     H  M       M     T
```

A TWO DIMENSIONAL HEAT TRANSFER MODEL FOR A TWO-PASS CROSSFLOW AIR PREHEATER

VERSION 1.1

by

ALI YILMAZ

```
                      x
          GAS IN   <--         GAS OUT
            ||        |           /\
            \/        V y         ||
     ===============     ===============
     |||||||||||||||<--|||||| | |  | |
     |||||||||||||||<--||C||| B |  A |
     |||||||||||||||<--|||||| | |  | |
     |||         |||<--|||         | |
<----||| PASS II |||<--||| PASS I  | |<----
 AIR |||         |||<--|||         | | AIR
 OUT |||||||||||||||<--|||||| | |  | | IN
     |||||||||||||||<--|||||| | |  | |   ^y
     |||||||||||||||<--|||||| | |  | | x |
     ===============     ===============<--
     |      ||     I===I      /\       |
     |      \/________________||       |
     |_________________________________|
```

ENERGY RESEARCH CENTER
200 PACKARD LABORATORY, BLD. 19
LEHIGH UNIVERSITY
BETHLEHEM, PA 18015
PHONE : (215) 758-4090

INLET GAS VELOCITY PROFILE AT PASS II, m/s vs. x, m

Vg ->	7.97	7.97	7.97	7.97	7.97	7.97	7.97	7.97	7.97	7.97
x ->	5.91	5.29	4.67	4.04	3.42	2.80	2.18	1.56	.93	.31

INLET AIR VELOCITY PROFILE AT PASS I, m/s vs. y, m

Va ->	1.96	1.96	1.96	1.96	1.96	1.96	1.96	1.96	1.96	1.96
y ->	.48	1.45	2.42	3.39	4.36	5.33	6.30	7.27	8.24	9.21

FLOW RATES AND AVERAGE TEMPERATURES OF GAS AND AIR
AT INLET AND OUTLET SECTIONS OF EACH PASS

APH TOTAL AIR LEAKAGE, % = 0.00

Mg,in = 626.8 kg/s Mg,out = 626.8 kg/s
Tg,in = 614.8 K Tg,out = 388.3 K

```
                                 x
                       GAS IN <--       GAS OUT
                         ||      |        /\
                         \/      V y      ||
                  ===============   ===============
                  |||||||||||||||<--|||||| | |  | |
                  |||||||||||||||<--||C||| B |  A |
Ma,o= 536.0 kg/s  |||||||||||||||<--|||||| | |  | |  Ma,in= 536.0 kg/s
Ta,o= 554.0 K     ||| PASS II |||<--||| PASS I  | |  Ta,in= 297.0 K
            <-----||| ------- |||<--||| ------- | |<----
              AIR ||| E2=65.9 |||<--||| E1=65.1 | | AIR
              OUT |||||||||||||||<--|||||| | |  | | IN
                  |||||||||||||||<--|||||| | |  | |   ¬ y
                  |||||||||||||||<--|||||| | |  | | x |
                  ===============   ===============<--
                  |      ||     I===I     /\      |
                  |      \/_______________||      |
                  |_______________________________|
```

Tg,pass = 518.4 K

E overall= 82.5 %

AIR LEAKAGE ANALYSIS

INTERNAL AND EXTERNAL AVERAGE MASS FLOW RATES AND TEMPERATURES

EXTERNAL GAS INLET FLOW RATE OF PASS II,	kg/s	=	626.840
INTERNAL GAS FLOW RATE OF PASS II,	kg/s	=	626.840
PASSAGE GAS FLOW RATE,	kg/s	=	626.840
INTERNAL GAS FLOW RATE OF PASS I,	kg/s	=	626.840
EXTERNAL GAS OUTLET FLOW RATE OF PASS I,	kg/s	=	626.840
EXTERNAL AIR INLET FLOW RATE OF PASS I,	kg/s	=	536.000
INTERNAL AIR FLOW RATE OF PASS I,	kg/s	=	536.000
PASSAGE AIR FLOW RATE,	kg/s	=	536.000
INTERNAL AIR FLOW RATE OF PASS II,	kg/s	=	536.000
AIR OUTLET FLOW RATE OF PASS II,	kg/s	=	536.000
EXTERNAL GAS INLET TEMPERATURE OF PASS II,	K	=	614.820
INTERNAL GAS INLET TEMPERATURE OF PASS II,	K	=	614.820
INTERNAL GAS OUTLET TEMPERATURE OF PASS II,	K	=	518.373
PASSAGE GAS TEMPERATURE,	K	=	518.373
INTERNAL GAS INLET TEMPERATURE OF PASS I,	K	=	518.373
INTERNAL GAS OUTLET TEMPERATURE OF PASS I,	K	=	388.287
EXTERNAL GAS OUTLET TEMPERATURE OF PASS I,	K	=	388.287
AIR INLET TEMPERATURE OF PASS I,	K	=	297.040
PASSAGE AIR TEMPERATURE,	K	=	439.571
AIR OUTLET TEMPERATURE OF PASS II,	K	=	554.049
TAPH TOTAL AIR LEAKAGE	%	=	0.000
TOTAL AIR LEAKAGE OF PASS I,	%	=	0.000
HOT END AIR LEAKAGE OF PASS I,	%	=	0.000
COLD END AIR LEAKAGE OF PASS I,	%	=	0.000
TOTAL AIR LEAKAGE OF PASS II,	%	=	0.000
HOT END AIR LEAKAGE OF PASS II,	%	=	0.000
COLD END AIR LEAKAGE OF PASS II,	%	=	0.000

PASS I

PART "A"

SOME OF THE INLET PARAMETERS USED IN THE TPHMT CODE, AND THEIR VALUES

****

GAS SIDE AVG. PRESSURE, N/m¬2	=	97591.5000
AIR SIDE AVG. PRESSURE, N/m¬2	=	105053.8000
DEPTH OF THE HEAT EXCHANGER (in the z direction),m	=	22.8600
WIDTH OF THE HEAT EXCHANGER (in the x direction),m	=	.9525
LENGTH OF THE HEAT EXCHANGER(in the y direction),m	=	9.6933
INSIDE DIAMETERS OF TUBES, m	=	.0416
OUTSIDE DIAMETERS OF TUBES, m	=	.0508
THERMAL CONDUCTIVITY OF TUBE METAL, W/m-K	=	63.9000
GAS SIDE HEAT TRANSFER AREA PER UNIT CORE VOLUME m¬2/m¬3	=	9.0271
TRANSVERSE PITCH OF THE TUBE BANK, m	=	.2432
LONGITUDINAL PITCH OF THE TUBE BANK, m	=	.0595
INDICATES HOW TUBES ARE ARRANGED IN THE HEAT EXCHANGER (0-INLINE, 1-STAGGERED)	=	0

****

PART "B"

SOME OF THE INLET PARAMETERS USED IN THE TPHMT CODE, AND THEIR VALUES

****

GAS SIDE AVG. PRESSURE, N/m¬2	=	97591.5000
AIR SIDE AVG. PRESSURE, N/m¬2	=	105053.8000
DEPTH OF THE HEAT EXCHANGER (in the z direction),m	=	22.8600
WIDTH OF THE HEAT EXCHANGER (in the x direction),m	=	1.1938
LENGTH OF THE HEAT EXCHANGER(in the y direction),m	=	9.6933
INSIDE DIAMETERS OF TUBES, m	=	.0416
OUTSIDE DIAMETERS OF TUBES, m	=	.0508
THERMAL CONDUCTIVITY OF TUBE METAL, W/m-K	=	63.9000
GAS SIDE HEAT TRANSFER AREA PER UNIT CORE VOLUME m¬2/m¬3	=	13.3129
TRANSVERSE PITCH OF THE TUBE BANK, m	=	.1645
LONGITUDINAL PITCH OF THE TUBE BANK, m	=	.0597
INDICATES HOW TUBES ARE ARRANGED IN THE HEAT EXCHANGER (0-INLINE, 1-STAGGERED)	=	0

****

PART "C"

SOME OF THE INLET PARAMETERS USED IN THE TPHMT
CODE, AND THEIR VALUES

```
************************************************************************

GAS SIDE AVG. PRESSURE, N/m-2                           =    97591.5000
AIR SIDE AVG. PRESSURE, N/m-2                           =   105053.8000
DEPTH OF THE HEAT EXCHANGER (in the z direction),m      =       22.8600
WIDTH OF THE HEAT EXCHANGER (in the x direction),m      =        4.7625
LENGTH OF THE HEAT EXCHANGER(in the y direction),m      =        9.6933
INSIDE DIAMETERS OF TUBES, m                            =         .0416
OUTSIDE DIAMETERS OF TUBES, m                           =         .0508
THERMAL CONDUCTIVITY OF TUBE METAL, W/m-K               =       63.9000
GAS SIDE HEAT TRANSFER AREA PER UNIT CORE VOLUME
                                          m-2/m-3       =       25.7886
TRANSVERSE PITCH OF THE TUBE BANK, m                    =         .0819
LONGITUDINAL PITCH OF THE TUBE BANK, m                  =         .0618
INDICATES HOW TUBES ARE ARRANGED IN THE HEAT
EXCHANGER (0-INLINE, 1-STAGGERED)                       =        0

************************************************************************
```

PASS II

SOME OF THE INLET PARAMETERS USED IN THE TPHMT
CODE, AND THEIR VALUES

```
************************************************************************

GAS SIDE AVG. PRESSURE, N/m-2                           =    97591.5000
AIR SIDE AVG. PRESSURE, N/m-2                           =   105053.8000
DEPTH OF THE HEAT EXCHANGER (in the z direction),m      =       22.8600
WIDTH OF THE HEAT EXCHANGER (in the x direction),m      =        6.2230
LENGTH OF THE HEAT EXCHANGER(in the y direction),m      =        9.6933
INSIDE DIAMETERS OF TUBES, m                            =         .0416
OUTSIDE DIAMETERS OF TUBES, m                           =         .0508
THERMAL CONDUCTIVITY OF TUBE METAL, W/m-K               =       63.9000
GAS SIDE HEAT TRANSFER AREA PER UNIT CORE VOLUME
                                          m-2/m-3       =       25.8877
TRANSVERSE PITCH OF THE TUBE BANK, m                    =         .0819
LONGITUDINAL PITCH OF THE TUBE BANK, m                  =         .0622
INDICATES HOW TUBES ARE ARRANGED IN THE HEAT
EXCHANGER (0-INLINE, 1-STAGGERED)                       =        0

************************************************************************
```

RESULTS

PART "A"

```
****************************************************************
TOTAL HEAT TRANSFER RATE,         (kW)        =      5959.1931
CAPACITY RATE OF AIR,             (W/K)       =    536341.6277
CAPACITY RATE OF GAS,             (W/K)       =     37386.6393
CAPACITY RATE RATIO,              (nondim.)   =          .0697
NUMBER OF TRANSFER UNITS          (nondim.)   =         1.3249
EFFECTIVENESS OF HEAT EXCHANGER               =          .7202
AVG. OVERALL HEAT TRANSFER COEF.  (W/m-2-K)   =        25.9969
TOTAL GAS-SIDE HEAT TRANSFER AREA(m-2)        =      1905.2965
VOL. OF HEAT EXCHANGER CORE       (m-3)       =       211.0634
****************************************************************
```

PART "B"

```
****************************************************************
TOTAL HEAT TRANSFER RATE,         (kW)        =     10608.4277
CAPACITY RATE OF AIR,             (W/K)       =    537420.4742
CAPACITY RATE OF GAS,             (W/K)       =     69156.0561
CAPACITY RATE RATIO,              (nondim.)   =          .1287
NUMBER OF TRANSFER UNITS          (nondim.)   =         1.4014
EFFECTIVENESS OF HEAT EXCHANGER               =          .7297
AVG. OVERALL HEAT TRANSFER COEF.  (W/m-2-K)   =        27.5193
TOTAL GAS-SIDE HEAT TRANSFER AREA(m-2)        =      3521.7034
VOL. OF HEAT EXCHANGER CORE       (m-3)       =       264.5328
****************************************************************
```

PART "C"

```
****************************************************************
TOTAL HEAT TRANSFER RATE,         (kW)        =     60626.8690
CAPACITY RATE OF AIR,             (W/K)       =    543295.1872
CAPACITY RATE OF GAS,             (W/K)       =    537016.9623
CAPACITY RATE RATIO,              (nondim.)   =          .9884
NUMBER OF TRANSFER UNITS          (nondim.)   =         1.7023
EFFECTIVENESS OF HEAT EXCHANGER               =          .5927
AVG. OVERALL HEAT TRANSFER COEF.  (W/m-2-K)   =        33.5903
TOTAL GAS-SIDE HEAT TRANSFER AREA(m-2)        =     27215.0922
VOL. OF HEAT EXCHANGER CORE       (m-3)       =      1055.3168
****************************************************************
```

PASS I

****

TOTAL HEAT TRANSFER RATE,	(kW)	=	77194.4898
CAPACITY RATE OF AIR,	(W/K)	=	539019.0964
CAPACITY RATE OF GAS,	(W/K)	=	643559.6577
CAPACITY RATE RATIO,	(nondim.)	=	.8376
NUMBER OF TRANSFER UNITS	(nondim.)	=	1.7583
EFFECTIVENESS OF HEAT EXCHANGER		=	.6506
AVG. OVERALL HEAT TRANSFER COEF.	(W/m-2-K)	=	29.0355
TOTAL GAS-SIDE HEAT TRANSFER AREA	(m-2)	=	32642.0920
VOL. OF HEAT EXCHANGER CORE	(m-3)	=	1530.9130

****

PASS II

****

TOTAL HEAT TRANSFER RATE,	(kW)	=	63319.0963
CAPACITY RATE OF AIR,	(W/K)	=	554239.3802
CAPACITY RATE OF GAS,	(W/K)	=	655317.3345
CAPACITY RATE RATIO,	(nondim.)	=	.8458
NUMBER OF TRANSFER UNITS	(nondim.)	=	2.2542
EFFECTIVENESS OF HEAT EXCHANGER		=	.6587
AVG. OVERALL HEAT TRANSFER COEF.	(W/m-2-K)	=	34.9984
TOTAL GAS-SIDE HEAT TRANSFER AREA	(m-2)	=	35697.7251
VOL. OF HEAT EXCHANGER CORE	(m-3)	=	1378.9473

****

AIR PREHEATER
(overall)

****

TOTAL HEAT TRANSFER RATE,	(kW)	=	140513.5861
EFFECTIVENESS OF HEAT EXCHANGER		=	.8248
AVG. OVERALL HEAT TRANSFER COEF.	(W/m-2-K)	=	32.0169
TOTAL GAS-SIDE HEAT TRANSFER AREA	(m-2)	=	68339.8172
VOL. OF HEAT EXCHANGER CORE	(m-3)	=	2909.8603

****

2-Dimensional Representation of Pass I
on xy plane

```
           DX(j)
          |<------>|                 Tg 1,j
        ----------------------------------------------------------
          |        | -          |          |              |         |
          |        | |          |          |              |         |
          | Tm 1,1 |DY(i) Ta 1,j| Tm 1,j   | Ta 1,j+1     | Tm 1,N  |
          |        | |          |          |              |         |
          |        | V          |          |              |         |
          |------------         ------------         -----------|
          |                                                         |
          |                                                         |
          |                                                         |
          |                                                         |
          | Tg i,1                Tg i,j                            |
          |----------          -------------          ----------|
          |        |          |          |            |         |
          |        |          |          |            |         |
Ta i,1    | Tm i,1 |    Ta i,j| Tm i,j   | Ta i,j+1   | Tm i,N  |  <--- AIR
          |        |          |          |            |         |
          |        |          |          |            |         |
          |---------           ------------          ----------|
          | Tg i+1,1            Tg i+1,j                          |
          |                                                       |
          |                                                       |
          |                                                       |
          | Tg M,1                                      Tg M,N    |
          |----------          -------------          ----------|
          |        |          |          |            |         |
          |        |          |          |            |         |
Ta M,1    | Tm M,1 | Ta M,2   | Tm M,j   |    Ta M,N  | Tm M,N  | Ta M,N+1
          |        |          |          |            |         |
          |        |          |          |            |         |
        ----------------------------------------------------------
            Tg M+1,1                                    Tg M+1,N

                               GAS                       y -
                               /\                          |
                               ||                    x <--
```

i, j	1	2	3	4	5	6	7	8	9	10

Dimensions of the Smaller Heat Exchanger Assemblies, m

DX(j)	.79	.79	.79	.79	.79	.79	.60	.60	.48	.48
DY(i)	.97	.97	.97	.97	.97	.97	.97	.97	.97	.97

Coordinates of the Smaller Heat Exchanger Assemblies, m

X(j)	6.51	5.72	4.92	4.13	3.34	2.54	1.85	1.25	.71	.24
Y(i)	9.21	8.24	7.27	6.30	5.33	4.36	3.39	2.42	1.45	.48

TEMPERATURE FIELD OF PASS I :

FLUE GAS TEMPERATURE VARIATION IN THE EXCHANGER: Tg(i,j), K

i \ j	1	2	3	4	5	6	7	8	9	10
1	439.3	427.6	414.6	400.2	384.3	367.1	368.8	362.0	361.3	357.6
2	447.6	436.3	423.6	409.3	393.3	375.5	377.3	370.3	369.7	365.8
3	456.0	445.3	433.1	419.1	403.1	385.0	386.9	379.7	379.2	375.2
4	464.5	454.5	443.0	429.5	413.8	395.6	397.5	390.4	389.8	385.9
5	473.0	463.9	453.2	440.5	425.4	407.5	409.4	402.4	402.0	398.0
6	481.4	473.4	463.8	452.2	438.0	420.8	422.8	416.0	415.6	411.9
7	489.7	483.0	474.7	464.4	451.7	435.8	437.7	431.5	431.2	427.7
8	497.7	492.4	485.7	477.3	466.5	452.7	454.3	448.9	448.7	445.7
9	505.3	501.6	496.8	490.6	482.5	471.7	473.0	468.7	468.6	466.3
10	512.4	510.4	507.8	504.4	499.6	493.0	493.9	491.3	491.3	489.8
11	518.4	518.4	518.4	518.4	518.4	518.4	518.4	518.4	518.4	518.4

AIR TEMPERATURE VARIATION IN THE EXCHANGER: Ta(i,j), K

i \ j	1	2	3	4	5	6	7	8	9	10	11
1	399.7	386.2	371.9	357.1	342.1	327.4	313.5	308.1	302.8	299.9	297.0
2	407.4	393.6	378.9	363.3	347.3	331.2	315.6	309.6	303.5	300.3	297.0
3	415.5	401.6	386.4	370.2	353.1	335.5	318.1	311.2	304.4	300.7	297.0
4	424.0	410.1	394.6	377.7	359.6	340.4	320.8	313.2	305.5	301.3	297.0
5	433.0	419.1	403.5	386.0	366.8	346.0	323.9	315.4	306.6	301.9	297.0
6	442.3	428.7	413.0	395.1	374.9	352.3	327.5	317.9	307.9	302.5	297.0
7	452.0	438.8	423.3	405.1	383.9	359.4	331.5	320.7	309.5	303.3	297.0
8	462.0	449.5	434.4	416.1	394.0	367.6	336.1	324.1	311.2	304.3	297.0
9	472.6	461.0	446.5	428.3	405.6	377.1	341.5	328.0	313.3	305.3	297.0
10	487.2	477.4	464.3	447.0	423.9	392.7	350.3	334.4	316.7	307.1	297.0

METAL TEMPERATURE VARIATION IN THE EXCHANGER: Tm(i,j), K

i \ j	1	2	3	4	5	6	7	8	9	10
1	417.3	404.4	390.4	375.5	359.8	343.7	345.2	338.9	338.1	334.7
2	425.3	412.4	398.3	383.0	366.7	349.5	351.2	344.4	343.6	339.9
3	433.6	420.9	406.8	391.2	374.3	356.1	357.8	350.6	349.9	345.9
4	442.2	429.8	415.8	400.1	382.6	363.4	365.3	357.7	357.0	352.8
5	451.0	439.1	425.4	409.7	391.8	371.7	373.8	365.8	365.1	360.8
6	460.0	448.7	435.5	420.0	402.0	381.1	383.3	375.1	374.4	369.9
7	469.1	458.7	446.2	431.2	413.2	391.7	394.1	385.6	385.1	380.4
8	478.3	468.9	457.4	443.1	425.6	403.8	406.3	397.7	397.3	392.5
9	487.6	479.5	469.3	456.2	439.4	417.8	420.4	411.9	411.6	406.9
10	499.9	494.0	486.1	475.4	460.8	440.6	443.2	435.3	435.2	430.8

2-Dimensional Representation of Pass II
on xy plane

```
                                   GAS                      x <--
                                    |                           |
                                    V                         y V

         DX(j)
        |<------>|                Tg 1,j
        -----------------------------------------------------------
        |        | -           |          |                |          |
        |        | |           |          |                |          |
        | Tm 1,1 |DY(i) Ta 1,j | Tm 1,j   | Ta 1,j+1       | Tm 1,N   |
        |        | |           |          |                |          |
        |        | V           |          |                |          |
        |------------          ------------                -----------|
        |                                                             |
        |                                                             |
        |                                                             |
        | Tg i,1                 Tg i,j                                |
        |----------            ------------                -----------|
        |        |             |          |                |          |
        |        |             |          |                |          |
Ta i,1  | Tm i,1 |       Ta i,j| Tm i,j   | Ta i,j+1       | Tm i,N   | <--- AIR
        |        |             |          |                |          |
        |        |             |          |                |          |
        |---------             ------------                -----------|
        | Tg i+1,1            Tg i+1,j                                 |
        |                                                             |
        |                                                             |
        | Tg M,1                                             Tg M,N    |
        |----------           -------------                -----------|
        |        |             |          |                |          |
        |        |             |          |                |          |
Ta M,1  | Tm M,1 | Ta M,2      | Tm M,j   |       Ta M,N   | Tm M,N   | Ta M,N+1
        |        |             |          |                |          |
        |        |             |          |                |          |
        -----------------------------------------------------------
          Tg M+1,1                                           Tg M+1,N
```

i, j	1	2	3	4	5	6	7	8	9	10

Dimensions of the Smaller Heat Exchanger Assemblies, m

DX(j)	.62	.62	.62	.62	.62	.62	.62	.62	.62	.62
DY(i)	.97	.97	.97	.97	.97	.97	.97	.97	.97	.97

Coordinates of the Smaller Heat Exchanger Assemblies, m

X(j)	5.91	5.29	4.67	4.04	3.42	2.80	2.18	1.56	.93	.31
Y(i)	.48	1.45	2.42	3.39	4.36	5.33	6.30	7.27	8.24	9.21

TEMPERATURE FIELD OF PASS II :

FLUE GAS TEMPERATURE VARIATION IN THE EXCHANGER: Tg(i,j), K

i \ j	1	2	3	4	5	6	7	8	9	10
1	614.8	614.8	614.8	614.8	614.8	614.8	614.8	614.8	614.8	614.8
2	609.9	608.7	607.3	605.5	603.2	600.4	596.8	592.2	586.3	578.7
3	603.9	601.7	598.9	595.5	591.5	586.5	580.3	572.8	563.4	551.7
4	597.5	594.2	590.3	585.6	580.0	573.4	565.4	555.9	544.3	530.4
5	590.7	586.5	581.6	575.9	569.2	561.3	552.1	541.3	528.7	513.7
6	583.8	578.9	573.2	566.7	559.1	550.4	540.5	529.1	516.0	501.0
7	577.0	571.4	565.1	558.0	549.9	540.8	530.5	519.0	506.2	491.8
8	570.2	564.2	557.5	550.0	541.6	532.4	522.2	511.0	498.8	485.6
9	563.8	557.5	550.5	542.8	534.4	525.3	515.5	504.9	493.7	481.9
10	557.7	551.2	544.2	536.5	528.3	519.6	510.3	500.7	490.6	480.4
11	552.2	545.7	538.7	531.3	523.5	515.4	507.0	498.5	489.9	481.5

AIR TEMPERATURE VARIATION IN THE EXCHANGER: Ta(i,j), K

i \ j	1	2	3	4	5	6	7	8	9	10	11
1	590.3	584.5	577.3	568.5	557.5	543.7	526.6	505.1	478.0	443.6	399.7
2	577.8	570.8	562.4	552.5	540.7	526.8	510.2	490.6	467.4	439.9	407.4
3	569.3	561.7	552.9	542.7	530.9	517.4	501.9	484.1	463.9	441.1	415.5
4	561.4	553.5	544.4	534.2	522.8	509.9	495.6	479.9	462.6	443.9	424.0
5	554.2	546.1	537.0	527.1	516.1	504.2	491.3	477.5	462.9	448.0	433.0
6	547.6	539.5	530.7	521.1	510.8	499.9	488.5	476.7	464.8	453.2	442.3
7	541.7	533.8	525.3	516.3	506.9	497.2	487.3	477.5	468.0	459.3	452.0
8	536.6	529.0	521.0	512.7	504.3	495.8	487.5	479.5	472.4	466.4	462.0
9	532.3	525.1	517.8	510.3	502.9	495.7	489.0	482.9	477.9	474.3	472.6
10	529.3	522.8	516.3	509.9	503.8	498.2	493.3	489.4	486.8	485.9	487.2

METAL TEMPERATURE VARIATION IN THE EXCHANGER: Tm(i,j), K

i \ j	1	2	3	4	5	6	7	8	9	10
1	600.4	596.9	592.7	587.3	580.7	572.3	561.7	548.3	531.0	508.4
2	589.8	584.9	579.0	572.0	563.6	553.5	541.3	526.7	509.0	487.4
3	582.0	576.2	569.5	561.7	552.5	541.8	529.4	514.9	497.9	478.2
4	574.4	568.0	560.7	552.4	542.8	532.0	519.6	505.7	490.0	472.5
5	567.1	560.2	552.6	544.0	534.4	523.7	511.8	498.8	484.6	469.4
6	560.1	553.1	545.2	536.6	527.1	516.9	505.8	494.0	481.5	468.6
7	553.7	546.5	538.7	530.3	521.2	511.6	501.4	490.9	480.3	469.7
8	547.9	540.7	533.1	525.0	516.5	507.7	498.7	489.6	480.8	472.4
9	542.7	535.7	528.4	520.8	513.1	505.2	497.4	489.9	482.8	476.6
10	538.5	531.9	525.2	518.4	511.6	504.9	498.6	492.9	488.0	484.2

VITA

Ali Yilmaz was born in Akcakoca, Turkiye on September 1, 1967 to Kazim and Emine Yilmaz.

He attended Akcakoca High School and graduated with an honors degree in 1984. He continued his education in Mechanical Engineering at Istanbul Technical University, graduating in the top 2% of his class in July, 1988.

He started his graduate studies at Lehigh University with a scholarship granted by the Turkish Ministry of Education. He continued his graduate studies with the aid of a research assistantship, obtaining a Master of Science Degree in Mechanical Engineering in December, 1991.

END

OF

TITLE